Highlighting strain-induced thermoelastic effect in mesoscopic liquids

Eni Kume

Thèse de doctorat

NNT : 2021UPASP099

université PARIS-SACLAY

Highlighting strain-induced thermoelastic effect in mesoscopic liquids

Mise en évidence de l'effet thermoélastique induit par déformation de cisaillement dans les liquides mésoscopiques

Thèse de doctorat de l'université Paris-Saclay

École doctorale n° 564 : physique en Île-de-France (PIF)
Spécialité de doctorat : Physique
Unité de recherche : Université Paris-Saclay, CEA, CNRS, LLB, 91191, Gif-sur-Yvette, France
Référent : Faculté des sciences d'Orsay

Thèse présentée et soutenue à Paris-Saclay, le 08/10/2021, par

Eni KUME

Composition du Jury

Laurence RAMOS Directeur de Recherche, Université de Montpellier	Présidente
Günter REITER Professeur, Albert-Ludwig-University of Freiburg	Rapporteur & Examinateur
Kostya TRACHENKO Professeur, Queen Mary University of London	Rapporteur & Examinateur
Jean-Pascal RUEFF Directeur de Recherche, S.O.L.E.I.L.	Examinateur

Direction de la thèse

Laurence NOIREZ Directeur de Recherche, Laboratoire Léon Brillouin (CEA – CNRS)	Directrice de thèse
Marie-Claire BELLISSENT-FUNEL Directeur de Recherche, Laboratoire Léon Brillouin (CEA – CNRS)	Invitée
Patrick BARONI Ingénieur IEHC-CNRS, Laboratoire Léon Brillouin (CEA – CNRS)	Invité

Στους γονείς μου, οι οποίοι μου πρόσφεραν με αγώνα ό,τι εκείνοι στερήθηκαν

Acknowledgements

« Η Ιθάκη σου έδωσε το ωραίο ταξίδι. Χωρίς αυτήν δεν θα ‘βγαινες στον δρόμο, αλλά δεν έχει να σου δώσει πια. Κι αν φτωχική την βρεις, η Ιθάκη δεν σε γέλασε. Έτσι σοφός που έγινες, με τόση πείρα, ήδη θα το κατάλαβες οι Ιθάκες τι σημαίνουν.» - Konstantinos Petrou Kavafis (1863-1933).

The present manuscript is the result of personal efforts and of continuous professional and emotional aid from many people during the three years of my stay at Laboratoire Léon Brillouin.

First, I would like to wholeheartedly thank my supervisor Dr Laurence Noirez, Director of Research at CNRS, for her guidance and support throughout my scientific study and her trust by accepting me as a PhD student. I am grateful to her, not only for the proposal of the subject realized in this thesis, but also for her devotion to the subject during these three years. It is due to this devotion, the countless hours that she spent to discuss with me in daily basis, which gradually led to the fruition of the present work.

Further, I would like to warmly thank Mr. Patrick Baroni for his vast technical expertise. His contributions were critical for the realization and treatment of the thermal experiments. His continuous support ranges from repairing malfunctioned devices to sharing through conversations of his engineer knowledge and as well as discussing the scientific aspects of our work.

I would like to thank Dr Alessio Zaccone, Professor at Department of Physics "A. Pontremoli", University of Milan, and University of Cambridge, for the collaboration and his theoretical interpretation of the thermal relaxation time, which enabled further understanding of the present work.

Furthermore, I would like to thank Dr Jean-Pascal Rueff, Director of Research at CNRS and responsible of the GALAXIES beamline at synchrotron SOLEIL and Dr James Ablett that made possible the study of wetted surfaces with the use of inelastic X-ray scattering, as well as their essential help on data treatment and discussion on the results.

Moreover, I would like to thank Dr Marie-Claire Bellissent-Funel, Dr Philippe Bourges and Dr Dalila Bounoua for their interest on the inelastic measurements and the time that they shared with me for helpful discussions on the subject.

I am pleased to thank the Jury members, Dr Laurence Ramos for having accepted to chair my defence, Prof. Dr G. Reiter and Prof. Dr K. Trachenko for having referred my manuscript, whose comments where enlightening, and Dr J.P. Rueff for having examined my PhD and in particular the inelastic part.

I am thankful to Dr Eric Eliot, Director of LLB and Dr Grégory Chaboussant, deputy-director of LLB for their help and for assuring a pleasant stay at the laboratory for me. Moreover, I would like to thank Ms Emiljana Jorgji for her help and advices. I would like to thank Mr Olivier Sineau, Ms Anne-Sophie Lippmann and Ms Aurore Verdier for their help on various administrative problems, as well as Mr Rémy Lautie and Mr Gaston Exil for the IT support.

Further, I would like to thank the European commission for the funding, as my thesis is part of the European project “MaMi – Magnetics and Microhydrodynamics”. I am grateful to the

participants of this project for the introduction to new scientific fields, especially on magnetism and microfluidics even during the period of the COVID-19 pandemic.

Lastly, I would like to thank my family, who either in person or online, they provided me continuous emotional support, especially on the difficult final months of the PhD.

Table of Contents

General Introduction

The liquid state is the most common on the surface of the Earth, it plays an essential role there, but it is also the least understood state of matter. The mesoscopic scale is certainly the scale at which the limits of our understanding are most visible. That these are spectacular shear-induced phase transitions [1], shear band appearances [2], flow instabilities or surface instabilities but also subtle interfacial contributions (liquid / solid or liquid / liquid), the nature of the substrate, these effects call into question cause a simple conception of the liquid state and point out the directions to be taken. Understanding the mesoscopic scale is essential, it is also the scale of microfluidics and physiological fluids, therefore of the living chain.

The liquid nature did not allow of in-detail understanding, in contrary to solids and gasses. Due to lack of periodicity between liquid molecules, a similar theoretical study as for solids was excluded, making the fluidic approach of Maxwell (1876) [3] dominant. In this frame of dissipative systems, based on the fluctuation-dissipation theory, liquids dissipate any form of mechanical energy to their thermal molecular oscillations [4]. Later, Frenkel [5] proposed that liquids should support shear waves if the dynamics of the external excitation is faster than the molecular relaxation time, defining the Maxwell relaxation time as the time between two jumps of a particle from one equilibrium position to the new one. Thus, the critical frequency $\omega_F = 1/\tau_M$, is the inverse of a molecular relaxation time. For smaller frequencies ($\omega < \omega_F$), the liquid behaves in a dissipative manner, while for $\omega > \omega_F$, shear wave propagation leads to a solid-like response. The experimental verification of the theory arrived many years later with the technological advances, like large facilities [6, 7, 8, 9, 10].

However, there is a wide range of materials exhibiting at the macroscopic scale, an intermediate response between viscous liquid and elastic response such as polymers, gels, micellar solutions, etc. Molecular theories have been proposed [11, 12, 13, 14, 15, 16, 17], inspired by the initial Maxwell model, where the characteristic relaxation time is not more that of a particle but that associated with the relaxation of the macromolecule (in terms of Rouse or reptation time depending on the length of the chain considered). This scheme, which is conventionally adopted in polymer rheology, has recently been called into question with the identification of low-frequency shear elasticity at the mesoscopic scale, in particular in polymer melts [18, 19], [20, 21, 22, 23, 24, 25]. Indeed, the existence of "static" elasticity shows that a description in terms of relaxation time is not relevant, but that elastic correlations should be taken into account, in other words the emergence of a solid-like behaviour at the mesoscopic scale.

Various experimental reports have elucidated "static" solid-like behaviour of liquids. These studies were conducted for liquids and polymer melts at different scale, from nanometre [26, 27], micrometre [18, 19], to sub-millimetre [20, 21, 22, 23]. In these studies, the mechanical excitation is in nearly equilibrium conditions, in the low frequency domain (Hz), many orders slower than the molecular dynamics (GHz – THz for small molecules). In these conditions, the liquid did not flow, but exhibited resistance, leading to measurable shear elasticity. As this observation was detected on a series of (relatively large) system sizes, the effect cannot be described as a boundary-induced only, but as a bulk property. This notion is contrary to the conventional viscoelastic description, where shear elasticity is zero in liquids at low frequency (in agreement with the Frenkel theory) and shows long-range correlations between the liquid molecules. Therefore, the viscoelastic response is not universal but can be strengthened by improving the fluid / surface boundary conditions and by the scale at which the fluid response is measured. Mesoscopic shear elasticity concerns both simple liquids (Van der Waals and H-bond liquids), complex fluids (polymer melts, molecular glass formers, ionic liquids) and physiological fluids [18, 19, 20, 21, 22, 23, 26, 27]. Low-frequency elasticity shows the

existence of long-range elastic correlations between liquid molecules at the mesoscopic scale. At this scale, the behavior of liquids is no longer that of "bulk" although the dynamics concern a large number of molecules. There is therefore a strong need to review the theoretical models to take account of experimental reality.

And indeed, from a theoretical point of view, Frenkel's theory has recently been revised. Trachenko et al showed that the propagation of shear waves in liquids is possible but, over a reduced distance 1 / k, defined by the propagation time of the wave in the considered medium (τ.c where τ is Maxwell's time and c is the speed of sound) [28], while based on non-affine lattice dynamics, the scale dependence of shear elasticity in liquids has been also recently established [29]. Finally, a phonon theory of liquids based on Frenkel's theory was proposed [30], while a linear low-frequency vibrational density of state for liquids was shown [31].

Due to the mesoscopic shear elasticity, fluids resist flow below an elastic threshold, the resistance of which depends on the scale considered. The immediate consequence is that a thermoelastic coupling becomes possible, calling into question the hypothesis of an instantaneous dissipation via the rapid lifetime of thermal fluctuations and justifying the search for another property of the solid: thermoelasticity. This is the objective of this experimental thesis.

From a thermal point of view and without external heat source, molecular simulations predict an increase in temperature by viscous friction at the wall in nano-confined liquids under shear and pressure [32, 33]. The wall effect on different thermodynamic parameters has been extensively studied in confined liquids [34, 35, 36, 37, 38, 39, 40, 41, 42, 43] while at the macroscopic scale, the approach conventional theory (Maxwell) predicts an increase in temperature by viscous friction generated during oscillating shear at very high strain amplitude and under non-adiabatic conditions for molten polymers [44]. To our knowledge, there is no experimental data validating the temperature simulations.

In this thesis, based on the recent identification of finite shear elasticity in sub-millimetre scale, we elucidate another solid-like property which is the thermoelastic coupling to the mechanical excitation. We present an in-detail thermal study of mesoscopically-confined liquids under low frequency oscillatory shear strain and step shear strain. We will highlight that a mechanical deformation can produce a thermal response without external heat source. The results might be counter intuitive based on the conventional frame, where a shear deformation should dissipate immediately on the molecular relaxation for slow dynamics (zero-shear elasticity limit), but reinforce the assumption of a finite shear elasticity, and this solid-like properties existing in mesoscopic liquids. Indeed, the coupling between thermodynamics (thermal response) with the mechanical excitation (mechanical response), is familiar in the context of solids as thermoelasticity. We highlight that an elastic in nature, oscillating thermal response is recorded, sharing the same frequency (with a phase shift) upon applying a mechanical shear excitation for various liquids (polypropylene glycol (PPG), glycerol, water). The liquid behaves as a dynamic thermoelastic medium. We study the evolution of the thermal effect as a function of the amplitude and frequency of the shear excitation and show the emergence of both cold and hot shear waves of several tens of micrometres widths. For higher frequency and/or strain values, we observe the generation of thermal harmonics associated with non-linear effects. The gap dependence of the thermal effect is studied, showing a correlation with the scale size, which might be reminiscent of the scale dependence of shear elasticity. We show that the relaxation of the thermal effect shows a similar behaviour to its dielectric response [45]. Finally, since thermoelastic (solid-like) properties of liquids are highlighted, it becomes of interest to probe the liquid/surface interface in the frame of solid-liquid interaction utilized in the thermal measurement system. We study the effect of glycerol on an α-alumina (α-Al_2O_3) phonon dynamics with the help of inelastic x-ray scattering (IXS) performed in S.O.L.E.I.L..

This thesis divides in five chapters. Chapter one describes the thermoelastic effect of solids and discusses several experimental and theoretical advances evidencing shear elasticity in (confined) liquids. In chapter two, we explain the experimental setup, parameters considered and treatment procedure. In chapter three, we study the thermo-mechanical coupling of glycerol, water and mostly PPG. We study the response of the fluids in a wide range of strain values (200% - 4000%) and frequencies (0.5 – 5 rad/s), for different gap thicknesses (100 – 1000μm). Next, the stability of the thermal effect is confirmed, and the respective mechanical response is shown. In chapter four, we study the thermal and mechanical response of liquid glycerol to a step shear strain of various amplitudes (400% – 9500%) and scale (100 – 240μm). Then, we highlight a subsequent thermal relaxation. In chapter five, we highlight the impact of liquid film on the dynamics of the solid substrate (α-Al2O3) by performing IXS scattering.

Chapter 1 Elasticity

Elasticity describes the ability of solids to resist flow under deformation and to return in their initial state as the deformation is removed. In this chapter, we present the basic concepts of mechanical analysis and its parameters and briefly review the connection of mechanical response to the thermodynamics of a periodic system. Mechanical analysis is part of Continuous Medium Physics, which aims to establish the constitutive laws between physical quantities by considering average quantities and a thermodynamic equilibrium assumption.

We will point out that the common state of the art does not allow (static) elastic characteristics of liquids and does not consider a dimensional effect. We show how recent theoretical and experimental reports challenge the purely viscous description of fluids when the scale is reduced down to several tens microns.

We will briefly define the basic laws and theories utilized for the experimental setup to understand the concept of the thermal measurements. All of the above will stand as the driving force for the interpretation and understanding of the studied thermal effects presented in this manuscript.

1.1 Stress and strain

By definition, stress is defined as the rate of the force applied in a surface over the surface, while the surface becomes infinitesimal. Mathematically, it is defined as the traction or stress vector ***t(n)*** as follows [46, 47, 48, 49]:

$$\boldsymbol{t}(\boldsymbol{n}) \equiv \lim_{\delta A \to 0} \frac{\delta \boldsymbol{F}}{\delta A}$$

where, $\delta \boldsymbol{F}$ is the applied force which could vary from being parallel to being perpendicular to the surface, δA is the surface area (Figure 1.1a). As the unit normal vector **n** of the plane P is $\boldsymbol{n} = n_1\boldsymbol{e}_1 + n_2\boldsymbol{e}_2 + n_3\boldsymbol{e}_3$, the traction vector can be written as:

$$\boldsymbol{t} = t_1\boldsymbol{e}_1 + t_2\boldsymbol{e}_2 + t_3\boldsymbol{e}_3 = t_i\boldsymbol{e}_i$$

and then we get $t_j(-\boldsymbol{n}) = -t_j(\boldsymbol{n})$, which is called Cauchy's Lemma and is basically another demonstration of Newton's third law [49]. It is an assumption with great importance for continuum mechanics.

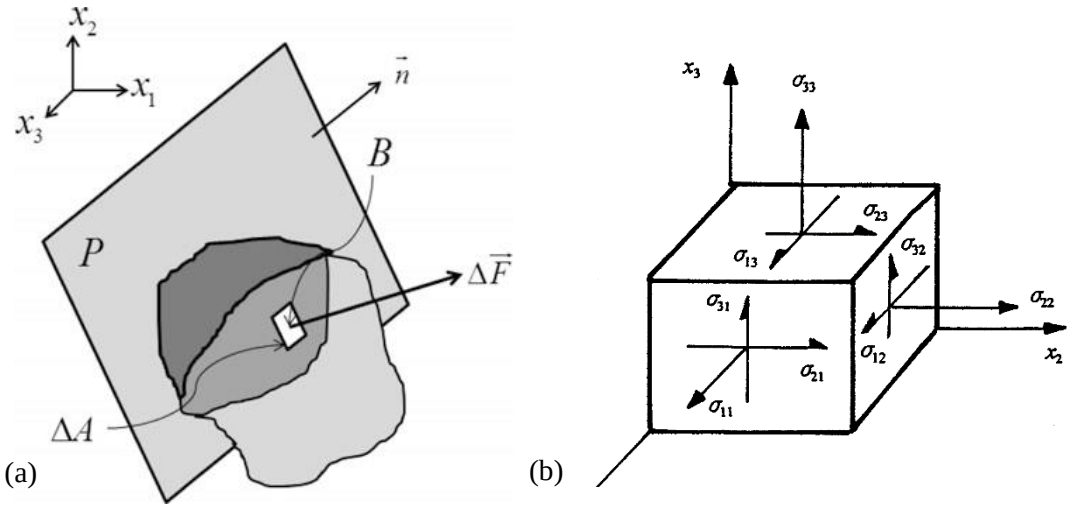

Figure 1.1: a) Stress at the point B. **b)** Three-dimensional general stress. Figures taken from *[49]*.

In three dimensions, we define the stress components on a material as seen in Figure 1.1b, meaning that the stress vector is written as:

$$\boldsymbol{t}(\boldsymbol{e_i}) = \sigma_{ij}\boldsymbol{e_j}$$

where, σ_{ij} is Cauchy's stress tensor component. The components σ_{kk}, which are perpendicular to the surfaces are called normal stresses, while the remaining components are called shear stresses. All the stresses on the medium define the stress tensor:

$$[\sigma_{ij}] = \begin{bmatrix} \sigma_{11} & \sigma_{12} & \sigma_{13} \\ \sigma_{21} & \sigma_{22} & \sigma_{23} \\ \sigma_{31} & \sigma_{32} & \sigma_{33} \end{bmatrix}$$

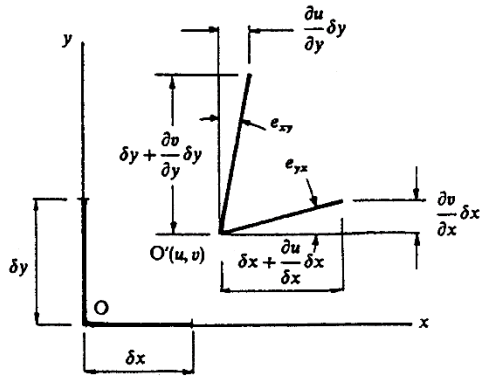

Figure 1.2: Displacement in the x – y plane. Figure taken from *[46]*.

Strain is a quantity that describes the intensity of the deformation u_i [48]. In the one-dimensional case, it is the change of the length of a unit to the unit when it tends to be infinitesimal. For a three-dimensional material for small strains, we may define the strain tensor [46, 47, 48, 49],

$$[\varepsilon_{ij}] = \begin{bmatrix} \varepsilon_{11} & \varepsilon_{12} & \varepsilon_{13} \\ \varepsilon_{21} & \varepsilon_{22} & \varepsilon_{23} \\ \varepsilon_{31} & \varepsilon_{32} & \varepsilon_{33} \end{bmatrix}$$

where, $\varepsilon_{ij} = \frac{1}{2}\left(\frac{\partial u_i}{\partial x_j} - \frac{\partial u_j}{\partial x_i}\right)$. The ε_{kk}components are called normal or volumetric strain, which deform a material through expansion or compression, while the remaining components are named shear strain ones. Thus for the Figure 1.2, the shear strain tensor is $\varepsilon_{xy} = \frac{1}{2}\gamma_{xy} = \frac{1}{2}\left(\frac{\partial u}{\partial y} - \frac{\partial v}{\partial x}\right)$, where γ_{xy} is the engineering shear strain. In this thesis, the studied liquids will be subjected to simple shear, which is pure shear plus rotation.

Stress and strain play fundamental role in the description of the mechanical state of a material and their relationship is for decades of great interest not only from physical perspective, but also from engineering point of view. The study of stress-strain behaviour is extended in various field, from metals [50], solid surfaces [51], amorphous solids [52, 53, 54], glassy polymers [55], elastomers [56], fatigue of polymers composites [57], nanoscale studies of polymers [58], to even biological tissues [59, 60]. In a next section, we will introduce the basic equations of elastic, viscous and viscoelastic materials.

1.2 Conservation laws

In the previous sector, we defined the stress, deformation, and strain in a medium. However, the above parameters are not able to completely define the material's state. To describe mechanical and thermodynamic state of a material, conservation laws are needed [49]. Some conservation laws of interest to describe the mechanical and thermodynamic state of a material are:

a) The conservation of momentum, which is basically the second law of Newton, meaning that the rate of change of momentum should be equal to the external forces [49]. For a continuum body, we can write the Cauchy's equation of motion

$$\sigma_{ji,j} + \rho f_i = \rho \frac{dv_i}{dt}$$

Where, f_i are the external forces, ρ the density, and $v_i = du_i/dt$ the velocity vector.

b) The conservation of energy, which is the first law of thermodynamics states that in a close system, the change of the internal energy of the system is related to the heat exchanged between the environment and the system and the work done on it. It is written as:

$$dU = dQ + dW$$

For an adiabatic case, there is no heat exchange ($dQ = 0$), meaning that the internal energy change is only due to work to or from the system ($dU = dW$). From [61], we can write the equation in a time derivative form:

$$\frac{dU}{dt} = \frac{dQ}{dt} + \frac{dW}{dt}$$

thus, making possible the comparison of the rates of internal energy, heat and work.

c) The second law of thermodynamics states that the entropy change in a closed system is described by:

$$dS \geq \frac{dQ}{T}$$

- The equality of the equation dS=dQ/T means that the process is reversible to its initial state after the perturbation and if the process is also adiabatic then it is called an isentropic process. An isentropic process is seen as ideal, and an approximation is considered.

- In real systems (macroscopic level), any thermodynamic process respects the inequality and is described as an irreversible process.

Other conservation laws such as the conservation of mass and electric charge are not discussed here. Conservation laws are fundamental for the understanding of the physical world.

1.3 Thermoelastic theory in solid systems

In the previous sections, we defined stress, strain and fundamental conservation laws. Now, we couple these mechanical parameters to thermodynamic properties in the case of an elastic solid. Atoms in a solid material occupy certain equilibrium positions, from which they oscillate due to thermal energy. If an external force is applied, the deformation results to change of their equilibrium positions, as long as the excitation is present and thus it alters their in-between interaction. What follows is temperature change of the material, as described from the thermoelastic theory, which associates temperature changes of a solid due to strain load and vice-versa [49, 62, 63]. Starting point is the first law of thermodynamics per volume:

$$du = dq + dw$$

with $dq = Tds$, where T is the temperature and s the entropy of the system, while $dw = \sigma_{ij} d\varepsilon_{ij}$ is the work done on the material due to the external strain, leading to storage of the energy due to the deformation [63]. After a series of calculations by defining, the Gibbs free energy $g = u - Ts - \sigma_{ij}\varepsilon_{ij}$ and describing the entropy as a function of $s = s(T, \sigma_{ij})$, we get the main result of the thermoelastic stress analysis (TSA) [62, 63]:

$$\Delta T = -T_0 \frac{\alpha}{\rho C_\sigma} \Delta\sigma_{kk}$$

where, T_0 the reference temperature, α the thermal expansion coefficient, $\rho C_\sigma = (\frac{\partial q}{\partial T})_\sigma$, with C_σ the specific heat at constant stress or pressure, ρ the density which is not constant since $\frac{\Delta\rho}{\rho} = \varepsilon_{kk}$, with ε_{kk} the volumetric strain tensor, while $\Delta\sigma_{kk}$ are the normal (principal) stresses of the medium.

The thermal expansion coefficient is defined as $\frac{\partial \varepsilon_{ij}}{\partial T} = \alpha_{ij}$ for the anisotropic case, while for an isotopic material is $\alpha_{ij} = a\delta_{ij}$. Depending on the nature of the load (compressive or extensive), the temperature change could result to cooling or heating. The fundamental result of the equation is that relates the temperature change of the medium to the microscopic state of the material due to external deformation. Specifically, the temperature change is related with changes of the volume and thus can be expressed in terms of normal stresses $\Delta\sigma_{kk}$, making the volumetric strain ε_{kk}, the parameter that couples mechanics with thermodynamics. Since, for small deformations, the stress-strain relation is a linear one, it results to a linear relation of strain with temperature. The connection of volumetric strain is not apparent in the final equation but can be seen indirectly at the density change and thermal expansion coefficient definition. Another equation that describes all the stresses in the medium shows the coupling of volumetric strain clearly is:

$$\sigma_{ij} = \frac{\nu E}{(1+\nu)(1-2\nu)} \varepsilon_{kk}\delta_{ij} + \frac{E}{1+\nu}\varepsilon_{ij} - \frac{\alpha E}{(1-2\nu)} \Delta T \delta_{ij}$$

where, *E* is the Young modulus and ν is the Poisson ratio.

The thermoelastic equations hold for the adiabatic case, where $dq = 0$. In an experimental point of view, for the process to be considered adiabatic, it should be related with the heat conductivity of a material, of its environment and the time scale of the considered process.

1.4 Propagation of Mechanical waves in a medium

There are two types of mechanical waves that propagate in a medium. The longitudinal waves and the transverse waves (Figure 1.3). In the longitudinal waves, the displacement of the atoms or molecules of the medium is parallel with the direction of the propagation of the wave. Since the longitudinal waves are related with pressure changes in the medium, they are often referred also as compressional waves. The longitudinal waves propagate in every state of a medium, from solids to gasses.

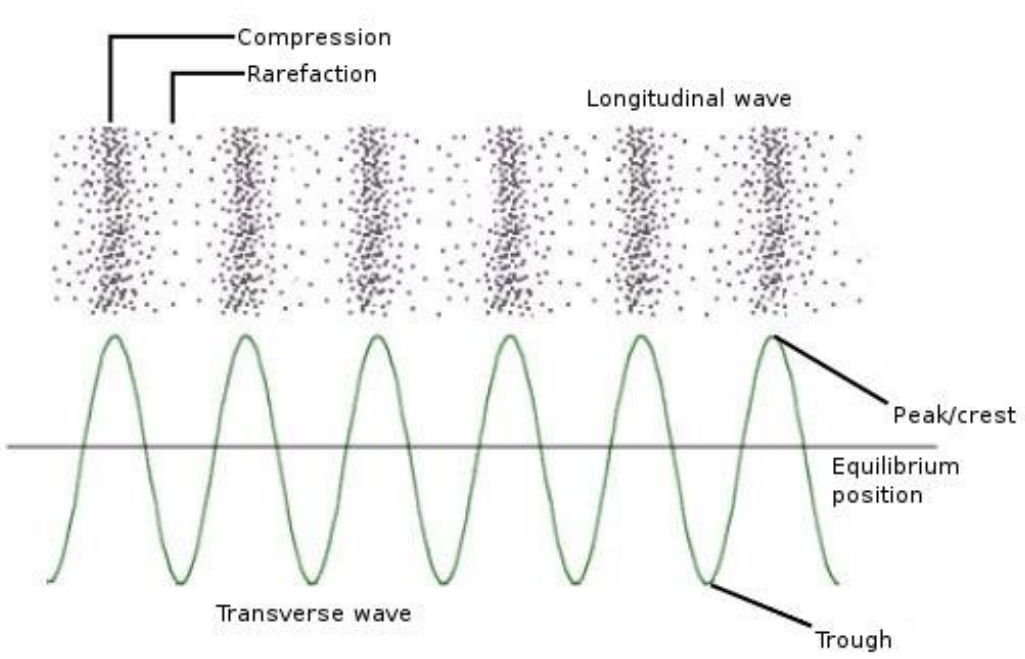

Figure 1.3: Mechanical waves in a medium. Figure taken from *[64]*.

In transverse waves, the displacement of the atoms/molecules is perpendicular to the direction of the propagation of the wave. Transverse waves are not supposed to propagate in every state of the medium. They are known to propagate in solids, due to the ability of the solid atoms to respond under a shear deformation, thus they are also known as shear waves. This ability is highlighted in the elastic model, where stress and strain are related via a linear relationship. For liquids, Maxwell's viscoelastic model does not foresee any ability of shear wave propagation for slow dynamic excitation due to the liquids inability to resist to shear deformation, as seen by the stress – shear rate relation of viscous materials.

1.5 Viscoelastic model

For the viscoelastic model, both elastic and viscous aspects of a material are considered. The behaviour in an elastic (solid) material is described mechanically by the spring analogy (Hookean spring) (Figure 1.4) and written as [65, 49]:

$$\sigma = k\varepsilon$$

The equation shows that the stress-strain relation is linear, defined by the spring constant k. In the elastic case, the main reason of deformation comes from the molecular stretching, causing the molecule to deviate from its equilibrium position as long as the force is acted and leads for the strain energy taken from the system to be stored. Thus, the unload of the energy will result to a return in an initial state.

Figure 1.4: Elastic (Hookean) spring and viscous (Newtonian) dashpot. Figure taken from *[65]*.

For the viscous material, the stress is proportional with the shear rate $\dot{\varepsilon}$:

$$\sigma = \eta\dot{\varepsilon}$$

Where, η is the viscosity, which describes the resistance of a material to flow. The viscous model is applied for fluids like gasses or liquids, where molecular interaction is not considered, and the energy dissipates into the molecular fluctuations. In the linear case, the fluids are called Newtonians, while a deviation from linearity leads to non-Newtonian fluids.

Figure 1.5: Maxwell's viscoelastic model. Figure taken from *[65]*.

Introduction to the notion of relaxation times:

The simplest viscoelastic model that can be considered is the Maxwell model (Figure 1.5). It contains of an elastic spring and a viscous dashpot in series. For this in series mechanical circuit, the stress in the spring and dashpot is the same, while the overall strain is the sum of the strains of the components, in analogy of an electrical circuit. These relations lead to the basic Maxwell equation [49, 65]:

$$k\dot{\varepsilon} = \dot{\sigma} + \frac{\eta}{k}\sigma \qquad (1.1)$$

During stress relaxation, any excitation is removed, meaning that the above equation can be solved over time and gives:

$$\sigma(t) = \sigma(0)e^{-t/\tau_{rel}}$$

Where, $\tau_{rel} = \eta/k$ is the Maxwell's relaxation time and it is a characteristic time of a material. Mathematically, it provides the time needed for the stress to be reduced by 66.7%, but physically it acts as a timescale where the system has relaxed and is referred as a characteristic time that shows the dynamics of the molecules of the material (Frenkel model). Maxwell relaxation time is of the order of 10^{-8} – 10^{-12}s for liquids [66].

The fast relaxation dynamics of fluids leads to athermal theories. As seen above the provided energy to the fluidic system should dissipate, while for solids, the provided mechanical energy is stored due to their elastic properties.

There is a variety of different models that describe viscoelasticity, like the generalized Maxwell model [47], the Kelvin – Voigt model [47, 48] and the Oldroyd – B model [67], but will not be discussed here.

The viscoelastic behaviour of diluted polymer solutions was proposed by Rouse [12] and then advanced by Zimm neglecting interchain interactions [13]. On the model, a polymer chain was considered as a succession of N beads connected with elastic springs. The consideration of the model leads to a generalized Maxwell equation, which is defined by a distribution of relaxation times. The slowest of these relaxation times is called Rouse time $\tau_{Rouse} \sim N^2$. This model holds as long as the polymer chains are not long. As the previous theories are dedicated for dilute solutions, new theories were needed for concentrated solution or polymers melts. The breakthrough was possible with theoretical works of de Gennes [14] with the introduction of the reptation time and later Edwards [15, 16].

The simultaneous progress in instrumentation with the contribution of Weissenberg has enabled the creation of tools about 50 years ago, named rheometers, together with a discipline, schools of rheology with specific conferences and journals. The conventional rheology protocol is established and generalized. The general principle is the following one:

In the ideal viscoelastic conditions, the shear stress response of a fluid to a periodic sin shear strain wave is given by the equation:

$$\sigma(t) = \sigma_0 \sin(\omega t + \delta\varphi)$$

Where, $\delta\varphi$ is the phase shift and $\sigma(t)$ the shear stress. The phase is the parameter that characterizes the response of a material. When $\delta\varphi = 0$, the response is a solid-like one (Figure 1.6, top graph), for $\delta\varphi = \pi/2$ it is purely viscous (Figure 1.6, bottom graph), while for intermediate values ($\delta\varphi \sim \pi/4$), the response is a viscoelastic one.

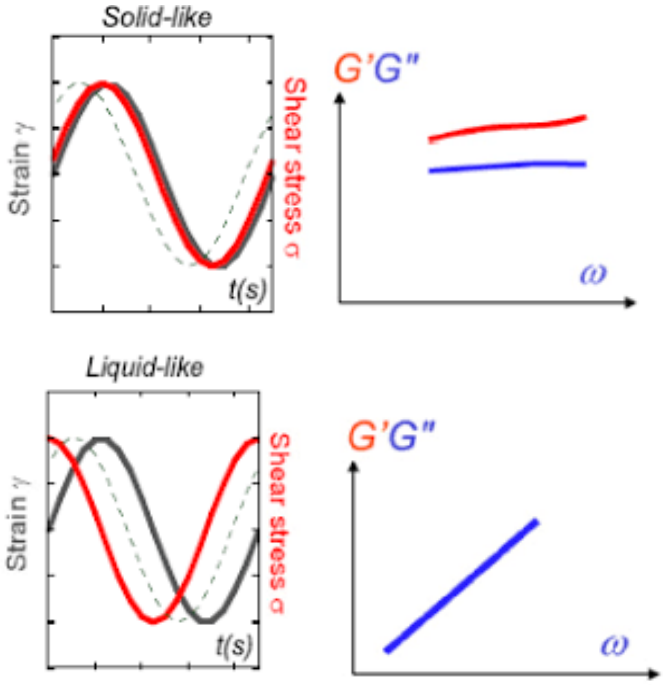

Figure 1.6: Solid like response (top graphs). The stress and strain signals are in-phase, while the elastic modulus is frequency independent and greater than the viscous one. Viscous response (bottom graphs). The strain and stress are π/2 out of phase. The viscous modulus scales with frequency, while the elastic low frequency modulus is zero. Figures taken from *[22]*.

From the previous dynamic evolution equations of strain and stress, we define the complex shear modulus:

$$G^* = \frac{\sigma(t)}{\gamma(t)} = G' + iG''$$

with $G' = (\sigma_0/\gamma_0)cos\delta\varphi$, the elastic modulus, while $G'' = (\sigma_0/\gamma_0)sin\delta\varphi$, the viscous modulus. Thus, the stress is written as [68]:

$$\sigma(t) = \gamma_0 G' sin\omega t + \gamma_0 G'' cos\omega t$$

The G' is the in-phase part of shear stress and thus is also called as storage modulus, while G'' is the out-of-phase component and referred as the loss modulus. These two shear moduli determine the behaviour of a material. For a solid-like response, G' is greater than G'', while for a liquid response the opposite takes place. A characteristic of polymers is the crossover of the moduli on the frequency domain (Figure 1.7). At low frequency, the loss modulus is higher, and a viscous behaviour is evident, while as the frequency increases, a crossover is reached where the elastic response dominates. The inverse of the frequency at the crossover is related with slower dynamics of the system, like the Maxwell's relaxation time. In the case of polymers, Rouse and reptation time are considered. [12, 14]. As, it is absent from the viscoelastic theory, rheological protocol examines large sample thicknesses (scale invariant) and does not consider the liquid-substrate wettability.

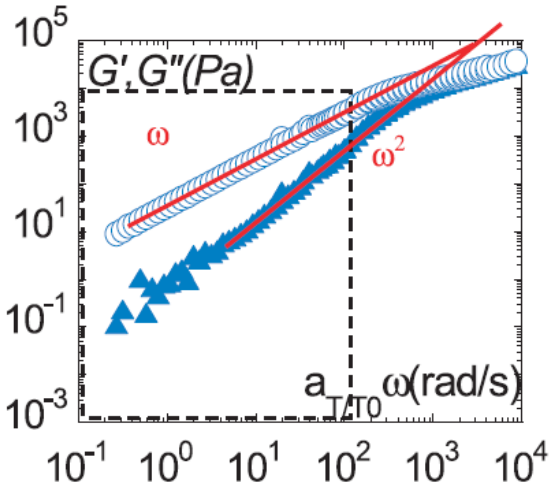

Figure 1.7: Storage and loss moduli over the frequency range measured on PBuA at room temperature (macroscopic measurements e > 1 mm) from *[24]*. The interception of the G' and G" scaling as omega square and omega is supposed to define the relaxation time of the polymer (the longest time before the system flows; i.e. G" is over G' with G" scaling as η.ω). We will see on section 1.6 that the viscoelastic response is not universal but depends on the scale at which it is measured, questioning the meaning of the viscoelastic relaxation time.

1.5.1 **Deborah and Reynolds number**

The Deborah number (De) is a dimensionless number, used in rheology to predict if the dynamic of the liquid (its molecular relaxation time) competes with the frequencies of probed dynamics [69]. It is defined as:

$$De = \frac{\tau_{rel}}{t_{appl}} = \tau_{rel}\omega$$

where, τ_{rel} is the relaxation time of the material and t_{appl} is the time of the experiment (e.g. the inverse of the frequency ω). If De < 1, then the applied excitation (frequency) is much slower than the inverse of the relaxation time of the material, meaning that, the material has enough time to incorporate the external energy. Thus, a viscous behaviour is expected. If De > 1, then a solid-like behaviour of the material is expected since, the material will not be able to relax during fast excitations.

Reynolds number (Re) predicts the state of the flow of a fluid. It is the rate if inertial to viscous forces and defined as:

$$Re = \frac{\rho u L}{\eta} = \frac{inertia\ forces}{viscous\ forces}$$

Where, ρ is the density of the material, u the flow speed, L the characteristic length (e.g. of a pipe). For small Reynolds values (below a critical one), the flow of the fluid is a laminar one, while for large Reynolds values is a turbulent flow. The value the critical Reynold number depends on the geometry of the system where the system flows.

1.6 Low-frequency shear elasticity in liquids

Based on Maxwell-Frenkel theory, liquids are not supposed to exhibit any low-frequency shear elasticity, since the excitation is smaller than the molecular relaxation time. However, experimental reports question this view by highlighting low frequency shear elastic response of polymer melts or liquids at nanoscale to sub-millimeter scale, thus showing that shear elasticity in viscoelastic/viscous fluids is a matter of scale.

1.6.1 **Confined liquids at nanoscale**

Experimental identification of solid-like responses of liquids, were first established with the use of the surface force apparatus, capable to measure electrostatic forces with great precession in the nanoscale [70]. The device was adjusted to carry dynamic measurements, such as oscillatory shears. Granick et al. were able to identify slow-down of the dynamics of few molecular layers of liquid [26, 27] and later identify a solid-like behaviour under oscillatory shear of a 2nm layer squalene confined between two solid interfaces at small deformation [71]. They measure a shear elastic response of three order magnitude smaller than the high frequency solid one (G_∞) and attribute this behaviour to the confinement of the molecules between the solid surfaces. As the stress in the liquid or the size of the layer is increased, the conventional viscous behaviour is observed, meaning that there is a point, where the excitation is strong enough to make the liquid flow.

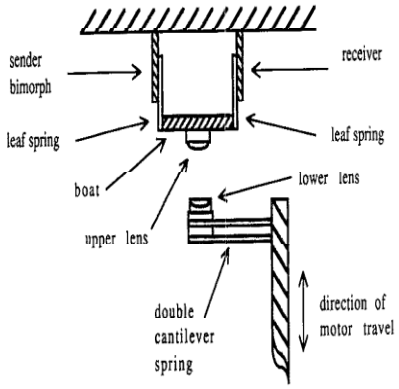

Figure 1.8: Geometry of surface force apparatus. Figure taken from *[70]*.

1.6.2 **Confined liquids at micrometre scale**

Few years earlier than the nanoscale measurements (~1985-90), Derjaguin and his group conducted "resonance measurements method" [19] with the use of a piezo-quartz [18, 19]. The liquid was placed above the piezo-quartz and while the quartz oscillates, it produces shear deformation to the studied liquid (Figure 1.9a). Before the measurements, the surface was properly cleaned, and the resonant frequency utilized was at around 73 kHz and contact measurements for various low viscosity liquid film thicknesses (1 – 5μm) of polymeric and small-molecule liquids. As seen in Figure 1.9b, shear elasticity becomes more apparent as the liquid film thickness decreases, while it decreases rapidly with the increase of the displacement. They argue that the results showcase existing shear bulk modulus in liquids even for excitation frequencies below the inverse of the Maxwell's relaxation time (around 10^{-10} – 10^{-12}s for such

liquids). Thus, they imply slower relaxation times that exist due to collective effects of the liquid molecules and they propose, "in the case of low-viscosity liquids, the nature of the viscous and elastic relaxation is essentially different from that of polymers" [19], because the elasticity of polymers is due to entanglements, thus specific to long chains. This is to our knowledge the first description of the liquid shear elasticity as intrinsic liquid property.

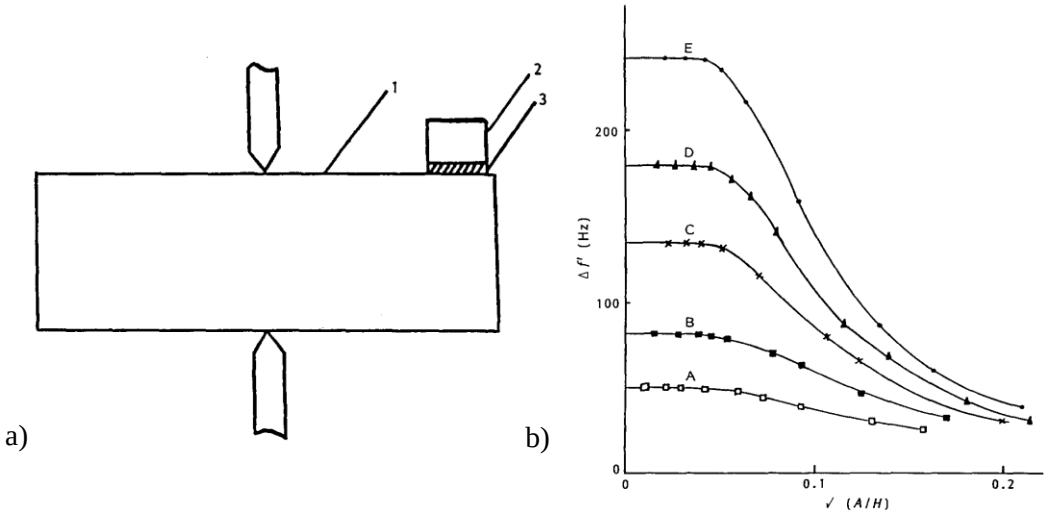

Figure 1.9: a) Experimental setup of measurement. 1) Piezo-quartz working at 73 kHz, 2) Plate, 3) Liquid layer. **b)** Evolution of piezo-quartz frequency phase shift with the shear wave of diethylene glycol film at different thicknesses (1 – 4µm). Figures taken from *[19]*.

In the same spirit as the Derjaguin's study, Martinoty and his group conducted measurement in the isotropic phase of liquid crystal polymers far from the I-N transition temperature with the use of an oscillating piezoelectric ceramic [72]. In this case, the liquid crystal film ranges from 10 to 120µm and they observed a steady plateau of shear modulus at low frequency, instead of the expected vanishing low frequency shear modulus for fluids (Figure 1.10a). They also highlighted that the shear modulus value depends on the scale of the film, with higher film size leading to smaller values and ultimately to a viscous response. Lastly, they stressed the importance of the interaction of the liquid with the substrate. When the plates were treated to provide better anchoring then the solid-like response was evident, while for the non-treated substrates, the viscous response was greater. They report similar results for linear polymer melts (polystyrene) [73].

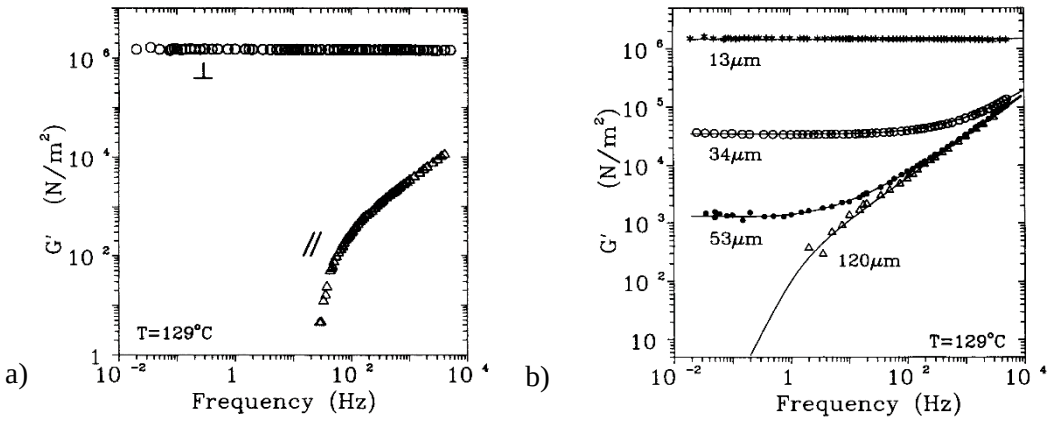

Figure 1.10: a) Shear modulus depending on the geometry of the measurement **b)** Evolution of shear modulus with film size of a liquid-crystal polysiloxane. Graphs taken from *[72]*.

1.6.3 **Accessing liquid shear elasticity liquid at sub-millimetre scale**

Noirez and her group also identified finite shear elasticity in a variety of fluids in the liquid state at larger scale, up the millimeter scale (from 20-1000μm) mainly using conventional rheometers and revisiting the protocol in order to optimize the chain stress transmission and in particular, the liquid/surface interaction forces using high energy surfaces. The type of the liquids ranges from high viscosity polymer melts at 300 - 1000μm [20, 21, 74], low molecular weight liquid crystals (8CB) at 45μm [75], liquid crystals polymer melts at 200μm [76], simple molecule glass formers like glycerol at 40μm [23] and water [22]. All measurements were conducted at temperatures, where the studied liquids were in their liquid phase away from any phase transition temperature.

A consistent observation of finite low-frequency shear elasticity was established for a variety of Van-der-Waals and hydrogen-bond liquids, challenging the conventional molecular theories (theory of viscoelasticity for example), which consider that shear elasticity is zero and scale-independent for liquids. For the interpretation of the results, they proposed that liquid molecules should interact and exhibit collective elastic correlations at small scales.

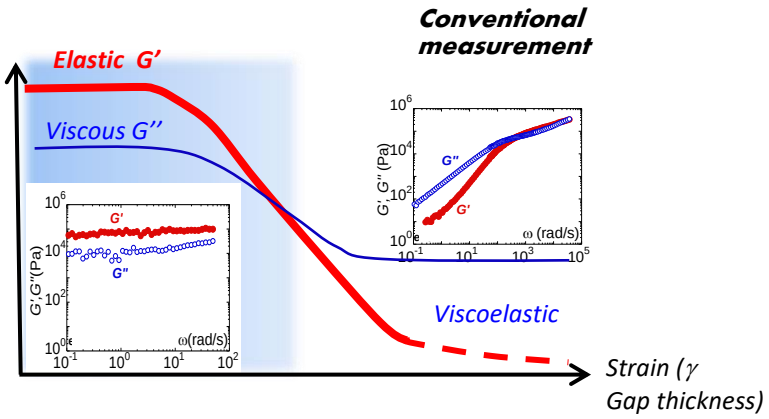

Figure 1.11: Strain dependence of shear elastic modulus G' and loss modulus G'' of sub-millimetre confined liquids. Left inset shows the moduli evolution over frequency at the elastic regime. Right inset shows the moduli evolution over frequency at the conventional viscous regime.

They showed that shear-elastic response is fragile and detectable when the amplitude of the deformation is considered. As seen in Figure 1.11, an elastic response is receivable for low strain amplitudes (blue shaded area of Figure 1.11). There, the elastic modulus is dominant and stable in the low frequency range (left inset), if the measurement is conducted under conditions as little perturbative as possible (low strain values, mesoscopic scales, strong liquid/substrate interactions). As the deformation increases, the studied liquid begins to flow gradually, leading to decrease of the elastic modulus and then to the interception of the moduli (border between blue and white shaded areas of Figure 1.11). What follows (white area of Figure 1.11) is the conventional flow regime, where elastic modulus becomes undetectable and flow properties dominate the liquid behavior at large strain amplitudes or at large gap thicknesses. The conventional viscoelastic behavior is thus the shear-thinning product (in the non-linear domain at large strain) of the shear elasticity versus frequency. The consequence of the experimental identification of shear elasticity at mesoscopic scale is that the conventional viscoelastic time, τ, is not the longest relaxation time of the material. The finite shear elasticity shows long-range correlation of liquid molecules, whose timescale is infinite.

1.7 Theoretical aspects of shear elasticity in liquids

1.7.1 Frenkel theory: the high frequency model

Even though Maxwell viscoelastic model was satisfying at describing macroscopic viscoelastic properties, this approach remains empirical and various physical problems were not resolved [25]. Y. Frenkel pointed out that the fluidic viscous approach of liquids is not satisfying and do not properly interpret their dynamic response [5]. He argued that the liquid molecules should be able to vibrate around an equilibrium position, similar to atomic vibration description. In this frame, he proposed that liquid molecule should be able to vibrate around an equilibrium position for a time τ and then the molecule would jump (diffuse) to a new equilibrium position, where it would be able to vibrate again. The equation, where Frenkel derives contains both elastic and viscous terms [77]:

$$\frac{ds}{dt} = \frac{P}{\eta} + \frac{1}{G}\frac{dP}{dt}$$

where, η is the viscosity, G is shear modulus and P shear stress. The time between the jumps is given as $\tau = \tau_0 e^{W/kT}$, where W is the activation energy needed for the jump, k the Boltzmann constant. For shear strains faster than the molecule jumps ($\omega\tau << 1$) will not produce flow but will cause a shift of the equilibrium position of the liquid molecules, similar to atom positions in a solid. For slow excitations ($\omega\tau >> 1$), the force will diffuse and give rise to viscous flow. This way, he derives at the constitutive viscoelastic equation (Eq.1.1) that leads to the Maxwell relaxation time $\tau = \eta/k$, which proposed to be the time between a jump of a liquid molecule from one equilibrium position to a new one. The high-frequency elastic response has been experimentally proved in various instances [6, 7, 8] and in agreement with numerical calculations [78].

1.7.2 Trachenko theory: the k-gap theory

Frenkel's works were considered as pioneering since it introduced a high-frequency solid-like nature of liquids about 70 – 80 years ago. Many years were needed for his theory to be verified experimentally, mostly due to Large Facilities experiments [79, 80, 81, 82, 83, 84, 10]. In the last decade, a new emphasis on Frenkel's theory derived to extension of the theory [30, 77, 85, 86, 87, 88, 89, 28]. A continuation of Frenkel's theory established what is called as k-gap [85, 89, 88]. For this theory, two approaches were established. In the first one (hydrodynamic approach), a generalized form of viscosity was written to take into account the elasticity and on the second one (solid approach), a generalized shear modulus to utilize flow. For the hydrodynamic case, from the Navier-Stokes equation, it was derived that the real part solution of the frequency of the propagating waves is written as:

$$\omega = \sqrt{c^2k^2 - \frac{1}{4\tau^2}}$$

where, c is the shear wave velocity, k is the wave vector in the reciprocal space, Fourier transformation of the real space. For the equation to have real solutions, it necessitates for $k >$

$k_g = 1/2c\tau$, thus showing the existence of the k-gap. From the above, we may extract the propagation length d_{el} of the shear wave in a liquid medium:

$$d_{el} = c\tau$$

The propagation length describes the distance of the shear wave to propagate into the liquid medium before it is disrupted due to the diffusive in nature, change of equilibrium positions of the liquid molecules after a time τ. This way "a propagating wave does not require all particles it encounters during its propagation to be solid-like" [77]. This propagation length stands for $\omega\tau >> 1$ (at high frequency regime), where per Frenkel, the elastic-like behaviour is exhibited. In the low frequency regime ($\omega\tau << 1$), the propagation length is given as $d_{el} = \frac{\lambda}{2\pi}$, where λ is the wavelength, thus proposing limited propagation of low frequency waves.

1.7.3 **Shear elasticity in the context of non-affine lattice dynamics**

In the current (Frenkel) description of liquid dynamics. liquids are not expected to exhibit any elastic behaviour in low frequency regime; thus the observed finite low-frequency shear elasticity is challenging for interpretation. Zaccone and Trachenko proposed a theory to interpret the finite shear elasticity of confined liquids, using the non-affine lattice dynamics (NALD) theory, which is primarily used for amorphous materials like glassy polymers and glasses [29, 90, 91, 92].

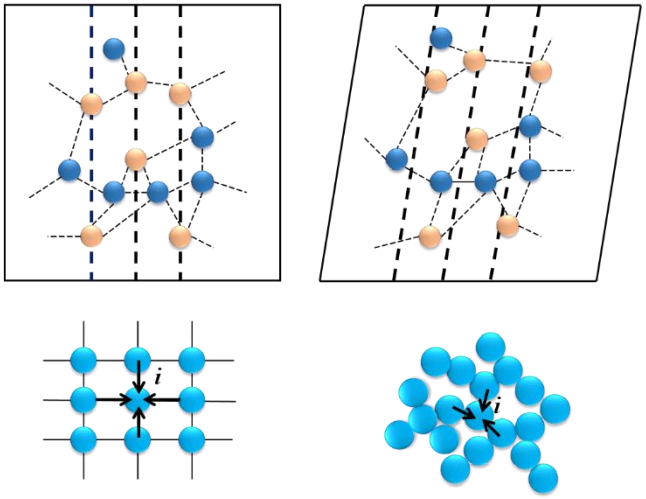

Figure 1.12: Representation of non-affine displacement in amorphous materials. Figure taken from *[90]*.

Based on NALD, the studied object (e.g. atom, molecule, polymer chain), is submitted to an affine force field, induced by a shear strain. If the average of the neighbour forces on the object is not symmetric then the result can be seen in Figure 1.12. For the mechanical deformation to relax, a non-affine deformation takes place in the material. Thus, the equation of motion of a molecule that is affected from such net force is given by [29, 91]:

$$\frac{d^3\underline{x_i}}{dt^2} + \nu\frac{d\underline{x_i}}{dt}dt + \underline{\underline{H_{ij}}}\,\underline{x_j} = \underline{\Xi}_{i,\kappa\chi}\eta_{\kappa\chi}$$

Where, $\underline{\Xi}_{i,\kappa\chi}$ the Hessian matrix of the system, $\eta_{\kappa\chi}$ the strain tensor, $\underline{\Xi}_{i,\kappa\chi}$ the force field and ν the microscopic friction coefficient due to long-range correlations of the molecules. They

calculate a shear modulus for liquid, taking into account the longitudinal and transverse modes, the k-gap theory and conclude to:

$$G' = G_\infty - \frac{\alpha}{3}k_D^3 + \frac{\beta}{3}L^{-3}$$

Where, G_∞ is the shear bulk modulus at high frequency, k_D is the Debye wavevector, where the highest vibration is achieved, L the scale of the system and α, b are numerical constants. The second term of the right side of the equation is the contribution of longitudinal waves, while the last term the contribution of transverse waves. We notice that only the transverse waves term is scale dependent and attributed this behaviour to k_g, which acts as a long-wavelength cut-off, while G_∞ is expected to be scale invariant. They conclude that the terms G_∞ and $-\frac{\alpha}{3}k_D^3$ should cancel each other, such as zero elasticity in liquids holds true in the macroscopic case ($L \to \infty$). Hence, at the microscopic scale, only transverse modes should produce a non-zero shear elasticity term:

$$G' = \beta' L^{-3}$$

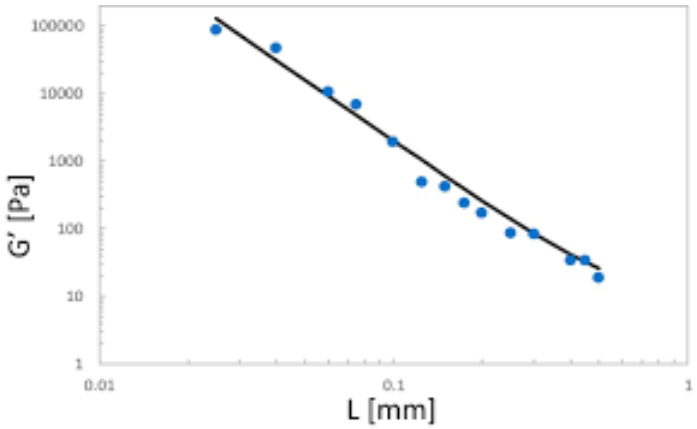

Figure 1.13: Shear modulus evolution with scale from experimental results for short-chain liquid crystalline (LC) polymer liquid $PAOCH_3$ (in the isotropic state) well above glass transition temperature T_g. Figure taken from *[29].*

Thus, they concluded to a scale dependent shear elasticity of confined liquids, which will become zero in the macroscopic limit. They plotted experimental results with the newly derived L^{-3} law and found a good agreement of theory and experiments, which measure finite bulk shear elasticity in mesoscopic liquid samples.

Baggioli et al. continued the NALD approach in the context of phonon theory of Goldstone bosons [93]. They showed that the non-affine displacement, that takes place for the material to reach mechanical equilibrium, is connecting with the resulting Goldstone phase relaxation. They argue that the k-gap theory, even if it produces correct results, it is phenomenological in nature. Then they try to interpret the results, accounting on the symmetries of the system. They propose that the Goldstone bosons have a phase relaxation rate Ω and propagate over a length l and the decay will be $\sim e^{-\Omega t}$.

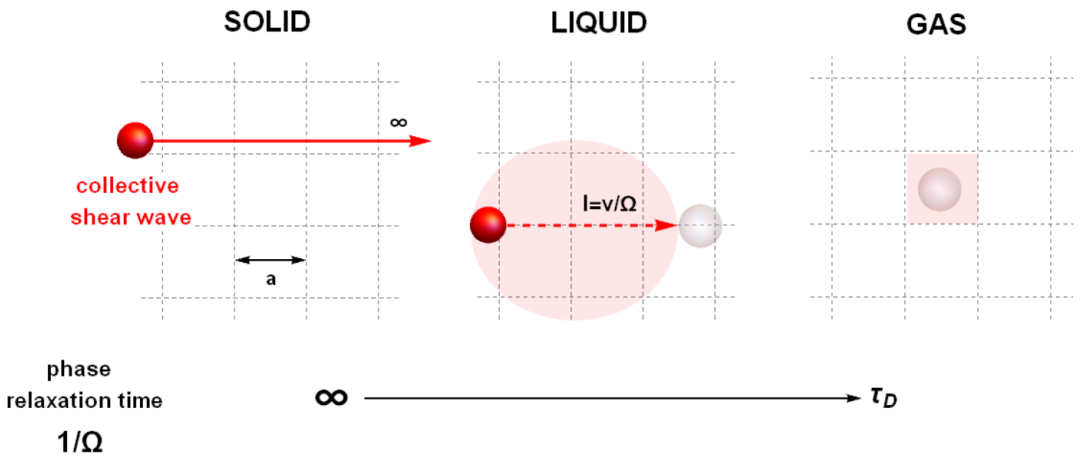

Figure 1.14: Propagation of transverse (shear) waves in every medium based on k-gap theory and Goldstone phase relaxation. Figure taken from *[93]*.

Based on k-gap theory and non-affine deformation dynamics, that shear waves can be interpreted by the Goldstone modes. A Goldstone mode exist in liquids due to non-affine deformation and it is possible to propagate in the liquid at length *l* (Figure 1.14). At higher length scales, a shear wave cannot propagate and thus the rigidity of the liquid is lost. The introduction of Goldstone modes is of great interest because this frame is consistent with the hydrodynamics of liquid in the low-frequency regime, since the phase relaxation does not impede the propagation of longitudinal waves in liquids and give rise to longer relaxation times than the Maxwell's one, which is unable to interpret any elastic characteristics of confined liquids.

Chapter 2 From shear elasticity to thermo-mechanical effects on mesoscopic liquids under oscillatory shear strain

In the previous chapter, we proposed short overview of the current state of the art and basic terms on liquid and solid dynamics. The basic description of liquids was based on the fluidic approach, which was successful for the interpretation of numerous problems in the macroscopic level, like flow. The viscous description combined with lack of periodic features ("small parameter") of liquid molecules made impossible, the complete understanding of liquids from theoretical point of view. Starting with Frenkel, a first elastic behaviour of liquids at high frequency was established and later experimentally proven. Lately, new experimental results showed that rigidity of liquids is accessible under low-frequency excitations when the liquid is confined. The size of confinement varies from nanometre to sub-millimetre scale, and its identification is strongly conditioned to the quality of the solid-liquid interactions. In parallel to these new experimental works, new theories were developed (k-gap theory, NALD) to interpret the ability of shear wave propagation in a liquid medium.

The experimental work presented in this manuscript lies within the assumption of a "static" shear elasticity in liquids. Motivated from the elastic nature of confined liquids, we subject simple polymer or molecular liquids to a dynamic shear deformation, and we study the coupling of mechanics and thermodynamics, in a familiar frame of thermoelasticity in solids. The existence of such coupling will further strengthen the existence of shear elasticity in confined liquid and the systematic study will elucidate the different mechanisms that take place within the liquid. Moreover, thermal studies of liquids in confined spaces, is of great interest in the field of microfluidics and mostly on biological research (e.g. cells/organs-on-a-chip). The blood vessel walls are strongly interacting with the physiological fluid and of various sections 8μm to 25mm), a deep understanding from physical point of view is necessary [94].

All the presented results are obtained without external heat source using strong wetting liquid/substrate conditions. We focus the impact of a dynamic mechanical field on the thermal stability of the liquid, under conditions similar as the viscoelastic measurements.

Very few dynamic measurements have carried out to examine the thermal behavior of liquids under mechanical field. However, strong thermal changes have been reported in polymer melts under dynamic shear excitation. Specifically, Baroni, Bouchet and Noirez. [95, 96] have showed thermal results of various polymer melts, like polybutylacrylate (PBuA) of Mn = 25.000 and 40.000 molecular weight and polybutadiene (Mn = 46,700) (Figure 2.1) as well as water under shear flow.

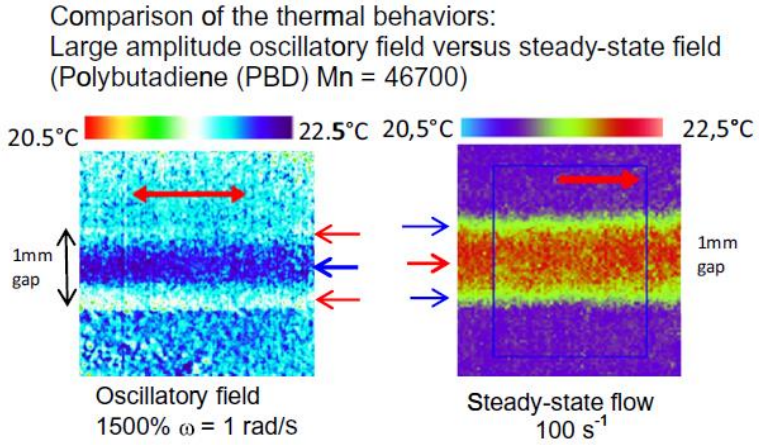

Figure 2.1: Left figure: 2D thermal snapshot of a polybutadiene (Mn = 46,700 and 1.11 polydispersity, room temperature measurements) measured a under oscillatory shear strain (γ = 1500% and ω = 0.5 rad/s, gap thickness 1 mm). The oscillatory shear produced a cold central band. **Right figure:** Under steady-state shear flow at 100 s^{-1}, the continuous shear flow induces a strong hot central band of about 0.5 °C.

They show that polymer melts of 1mm gap thickness, confined between two plates, give rise to thermal changes under oscillatory mechanical excitation of frequency ω = 1 rad/s and shear flow. Specifically, the oscillatory motion induces a central cold band of about − 0.1 °C surrounded by two higher temperature bands. The measurements were conducted in room temperature conditions and without external heat source. The conversion of mechanical to thermal energy hints an elastic nature of the effect, while the generated cold band excludes an interpretation in the frame of viscous heating. The generated thermal bands might indicate regions of different stress states similar to vorticity banding known for various soft matter systems [97, 98]. However, even though elasticity is well established for polymer melts, the interpretation of the thermal effect is difficult due to the length of their polymer chains, since for the interpretation of the seen thermal effects, both intermolecular and intramolecular interactions may be considered.

In this thesis, the challenge will be to probe low molecular liquids. We will focus our study on simple liquids (mostly glass formers because of their low evaporation rate), therefore exhibiting fast molecular dynamics (10^{-9}s). The observation of thermal effects on liquids will definitively rule out the possibility of a coupling with molecular relaxation times. We will also use a more elaborated analysis consisting in a kinetic analysis of the thermal study. We will consider the frequency and amplitude of the mechanical deformation as well as the scale of the system.

2.1 Experimental considerations

For the thermo-mechanical measurements, an elaborate setup was used to combine simultaneous thermal and mechanical measurements, as well as excellent transmission of the mechanical energy at the solid/liquid interface. We recorded both the mechanical and thermal response of the liquid gap under the external mechanical excitations (Figure 2.2). The mechanical excitation was achieved with the use of a strain-controlled ARES-II rheometer (TA-Instruments). For the mechanical response, the strain, stress, and normal stress signals were recorded with the use of Keithley multimeters. This way, the live signal that the rheometer provides was recorded for an in-detail view. The thermal response was recorded with an infrared microbolometer array (IR camera).

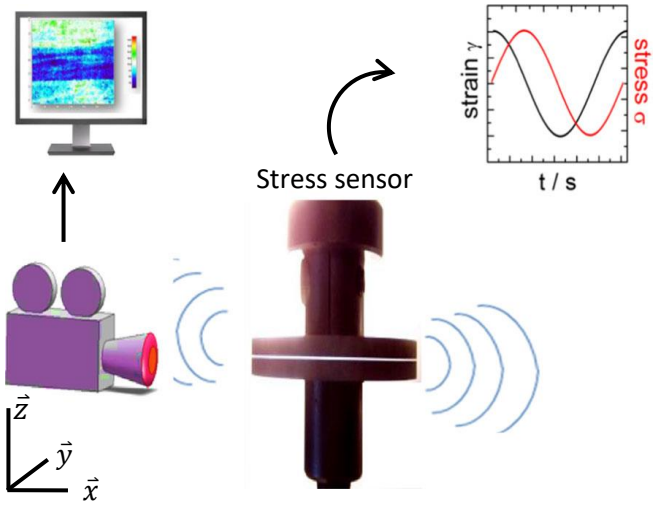

Figure 2.2: Graphical representation of the experimental setup used for the thermo-mechanical measurements *[99]*.

For the liquid to be excited mechanically, we have to confine it between solid substrates first. This exactly is the procedure in a rheometer setup. The liquid is placed in between two substrates. The substrates are mounted on special fixtures, which are placed on an ARES-II strain-controlled rheometer. The fixtures are specially designed to ensure parallel position of the substrates and connect them with the sensor (top substrate) and motor (bottom substrate) of the rheometer. The rheometer provides excellent control of the applied shear strain with high precision. The chosen applied deformation studied on the next chapter is a periodic shear strain:

$$\gamma = \gamma_0 \sin(\omega t) \tag{3.1}$$

The shear strain γ is defined as $\gamma = \delta l/e$, where δl is the displacement of the plate and e the gap thickness of the confined liquid. Thus, the important variables that we alter during the study is the strain amplitude and the frequency. The amplitude γ_0 varies from 1% (linear regime) to even 4000% (non-linear regime), when it is permitted by the limitations of the rheometer. The studied strain amplitudes could reach values much higher than the ones usually studied on the conventional rheology [100, 101]. In addition, each time we make sure that liquid is not ejected during the measurements, especially when the deformation is large. The liquid is not easily ejected on the side but remains in place due to the high energy surfaces, especially as the scale is decreased. The chosen frequency range is from 0.5 rad/s to 5 rad/s. We probe slow external excitations (ω_{exc} ~ 1 Hz), much slower than the inverse of the molecular relaxation time of the

studied liquids (ω_{rel} ~ GHz). Thus, on the classical level, we expect no coupling of the excitation with the relaxation time. Another variable that does not appear directly to the equation (3.1) is the gap thickness of the liquid system. The measurements were carried out for different gap thickness to highlight the scale dependence of the phenomenon. The gap values range mainly from 100μm to 300μm, limited to the mesoscale, but also measurements on higher values (~ 1mm) were conducted to connect the results with the macroscopic scale. As gap thickness decreases, the parallelism of the plates should be addressed with higher precision (for more information please see Appendix A). Each time when the gap was adjusted or a measurement was conducted, we permitted enough time to the liquid to reach an equilibrium state. The usual time interval between two measurements was between 15 - 30 minutes for the oscillatory measurements. This way, we ensure that the liquid has thermally relaxed and no connection between the measurements could be attributed.

The liquid studied in this manuscript, are called Newtonian fluids. Based on the relation $Re=\rho\dot{\gamma}h^2/\eta_0$ for Reynolds number in a rheometer setup [102], we calculate a number Re = 0.0025, for e = 0.240mm and ω = 5 rad/s, which is small and does not produce turbulent flow. At low Re, we can exclude pure elastic turbulence [103] since in our experimental conditions, Weissenberg number is small (Wi < 10^{-5}) and such an effect is observed in highly elastic materials. From the rheological results, we did not observe any secondary flows due to inertia since the shear stress response remain a perfect sin wave [104, 101].

2.2 Substrate consideration and treatment

As discussed on the previous chapter, the substrate plays an important role on dynamic measurements of confined liquid. The important parameter considered on a solid-liquid interface is the wetting. Wetting is determined on the contact angle between the interfaces (Figure 2.3). If the angle is below 90°, then we have partial wetting, while for 0°, total wetting. In general, the contact angle is given by the Young's equation *[105]*:

$$\gamma_{SV} = \gamma_{SL} + \gamma_{LV} cos\theta$$

With γ the surface tension, θ the contact angle and letters S,L,V stand for solid, liquid and vapor. The above equation dictates that the surface tension plays an important role on the wetting. However, in the last decades studies showed other parameters that determine the wetting of a substrate from a liquid like the surface roughness [106, 107, 108, 109, 40]. For rough surfaces, the slip is close to zero (no-slip condition) [107]. Another parameter is the free energy of the surface. High-energy surfaces are expected to be wetted by liquids [110]. Thus, for our experiments, we use high roughness and high-energy α-alumina surfaces. This substrate provides excellent total wetting of the tested liquids and ensure anchoring of the liquid molecules on the solid interface. This process stands important since a better transmission of the energy from the moving plate is secured.

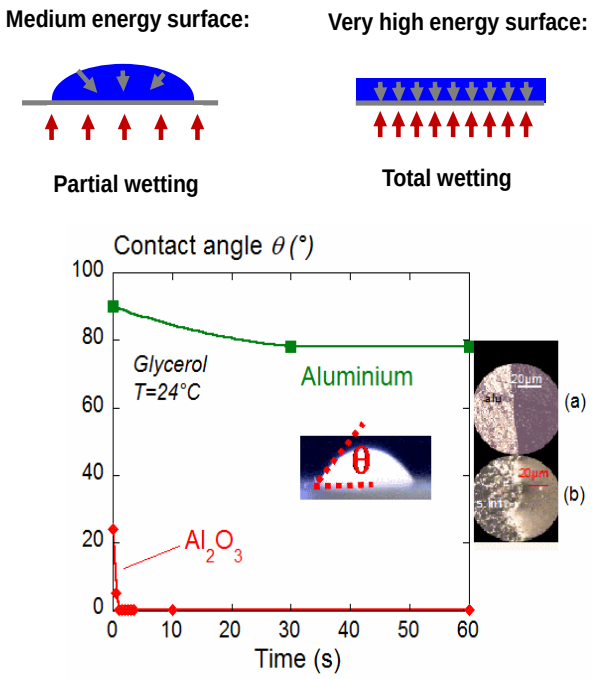

Figure 2.3: Top graph) Wetting conditions of a liquid on a solid substrate. Bottom graph) Contact angle versus time for liquid glycerol on aluminium (green points) and α-alumina substrates (red points) *[111]*.

For the measurements, a conventional ARES-II, strain-controlled rheometer was used to apply a low-frequency shear strain oscillation to the tested liquids. Great focus was given to the substrates, between which the liquid was confined. The commonly used aluminium fixtures do not provide a strong liquid-surface interaction (contact angle of about 75° - 80°). High-energy α-alumina surfaces providing a better wetting were preferred. The plates were cleaned and heated to ensure total wetting of the liquid molecules on the alumina substrate, thus providing better transmission of the energy from the plates to the liquid. In the case of poor wetting, shear elasticity is hardly observable, and the viscous behaviour was dominant (Figure 2.4). Same observations were made for high strain values, where the liquid starts to flow.

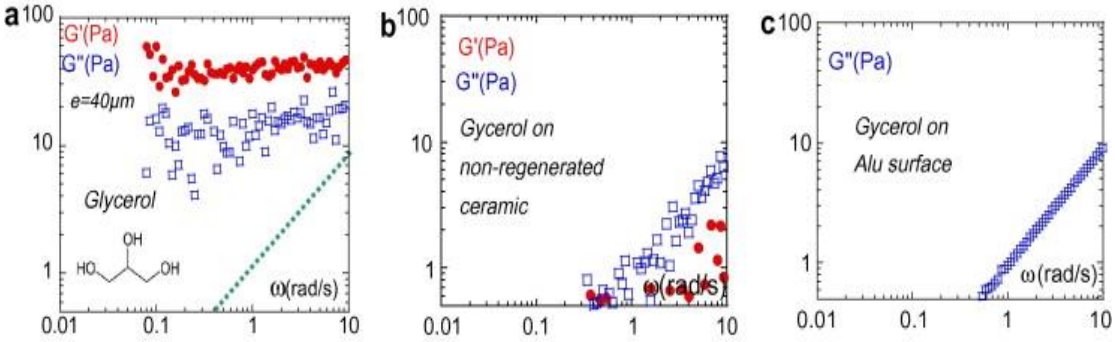

Figure 2.4: Low frequency dynamic glycerol response obtained using different substrates. Figure taken from *[23]*. G' is the shear elastic modulus and G" is the loss modulus.

The tested liquids were placed in between of two alumina (Al_2O_3) polycrystalline circular substrates of diameter d = 45mm, whose high free energy provided excellent wetting close to total wetting as seen in Figure 2.3. This characteristic of α-alumina substrate is one of the main reasons that is preferred to the standard aluminium plates. The substrates were systematically cleaned with ethanol and/or acetone inside an ultrasonic bath. Then, they were placed into an oven at 400-500°C for at least 3 hours to ensure that every hydrocarbon chemical component was removed. This process reduces the possibility of different compounds (e.g., water) to exist on the solid surface when the desired liquid is placed. The existence of such interfaces would cause additional interfacial slippage causing reduced transmission of the energy to the studied liquid [112, 113, 40]. To avoid re-pollution, the plates are mounted to the fixtures of the rheometers, as soon as are cooled down and then the studied liquid was added in less than 30 minutes.

2.3 Thermal measurements

Thermal measurements consist of a major part of the present study and thus an introduction is needed to elucidate the experimental procedure. Thermography has been widely used in the recent years, due to the evolution of better and cheaper infrared (IR) systems. For us, an utilization of such system like an IR "camera" (for simplicity) is of great importance, because it provides distant thermal measurements of a studied materials, without interacting with the material and thus allowing true study of its state.

2.3.1 **Basic concepts**

As known, solid atoms and liquid molecules have an equilibrium position (even though in liquid only this position changes over time), in which they oscillate around it in the form of thermal motion. This motion results to radiation of a material in the form of photons in the range of 700nm – 1mm. Measuring the incoming thermal photons from a body provides information about the thermal condition of a material; i.e. its temperature or its thermal evolution. The ideal case of emitted radiation is the blackbody one. It is the radiation of an idealized body, which can emit and absorb radiation regardless frequency or direction [114]. While on thermal equilibrium, it can greatly emit in certain wavelengths or frequency based on Planck's law [115, 114]:

$$M_\nu(\nu,T) = \frac{2h\nu^3}{c^2}\frac{1}{e^{\frac{h\nu}{k_BT}}-1}$$

$$M_\lambda(\lambda,T) = \frac{2\pi hc^2}{\lambda^5}\frac{1}{e^{\frac{hc}{\lambda k_BT}}-1}$$

with B_λ the wavelength dependent spectral radiance, B_ν the frequency dependent spectral radiance, ν the frequency, T the temperature, h Planck constant, c speed of light and k_B the Boltzmann constant. The previous equation results to a shape of distorted bell in the wavelength or frequency domain. The maximum of the bell is dependent on the temperature of the material as predicted from Wien's displacement law [116, 114]:

$$\frac{\nu_{max}}{T} = 5.8785 * 10^{10} HzK^{-1}$$

$$\lambda_{max} * T = 2897.8\ \mu mK$$

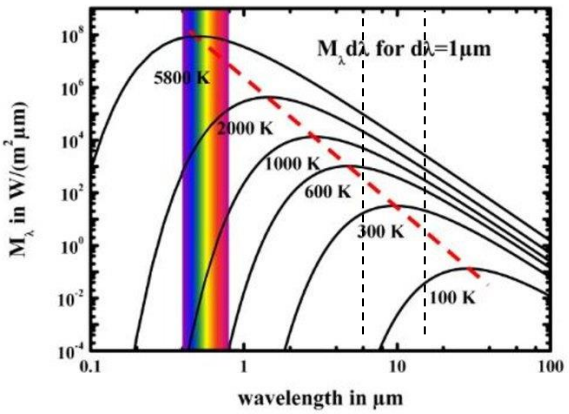

Figure 2.5: Spectral radiance based on Planck's law. Dotted red line connects the maxima as predicted from Wien's law. Figure taken from *[114]*. The area between the black dotted lines represents the range seen from the infrared sensor.

As seen in displacement law, the maximum shifts with temperature (Figure 2.5). For room temperature (300K), the maximum is located at around 8 – 10μm. That is the reason why we observe this wavelength region (long-wave infrared region) with the use of IR systems when we want to measure the thermal condition of a body. The used IR camera has a spectral range from 8 – 14μm. Glycerol and PPG exhibit absorption bands in this wavelength range and thus their thermal state can be studied (Figure 2.6). The overall emitted radiation per unit area is calculated from the Stefan – Boltzmann law as $M(T) = \sigma T^4$, where $\sigma = 5.67 * 10^{-12}\ Wm^{-2}K^{-4}$ [114]. The previous law concerns the whole wavelength range. For our case (8 – 14μm), the emitted radiation is roughly 42% of the total blackbody radiation [114].

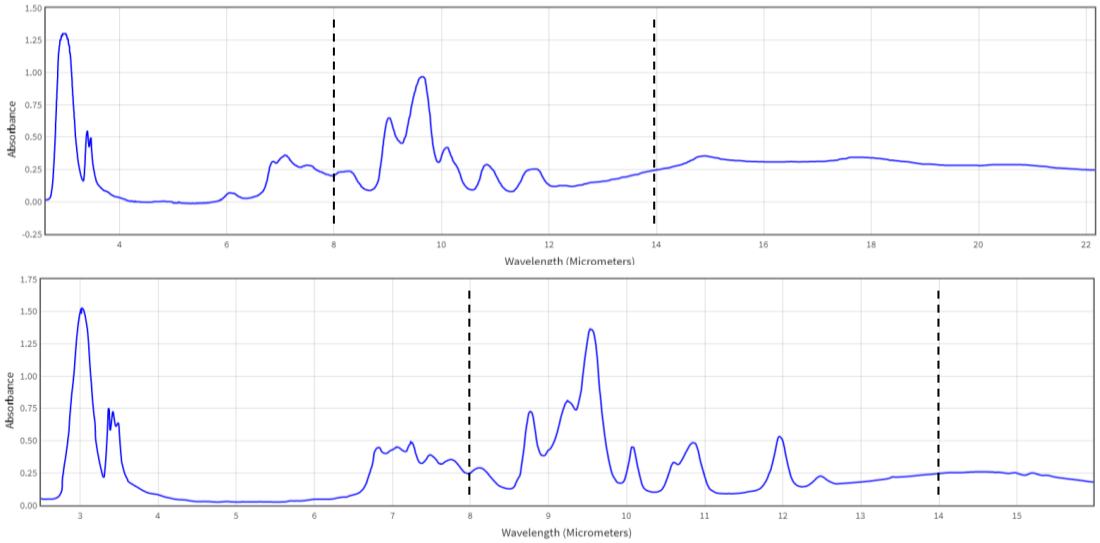

Figure 2.6: Absorbance of glycerol (top graph) and propylene glycol (bottom graph) at the IR region. Data taken from NIST database *[117, 118]*. The area between the black dotted lines represents the range seen from the infrared sensor.

Since the blackbody is an idealised one, a real material will emit less or at least will resemble a blackbody. Emissivity measures their emitted radiation in comparison with the black body. The maximum value is 1, for blackbody-like material while for values 0.7 – 0.9 the material is called as greybody. There are different parameters that determine the emissivity of a material, like the surface reflectivity, roughness, geometry and position of the IR camera. The tested

liquids exhibit emissivity value of approximately 0.9, which means that the temperatures indicated by the thermal sensor are close to absolute temperatures.

2.3.2 **Thermal experimental setup**

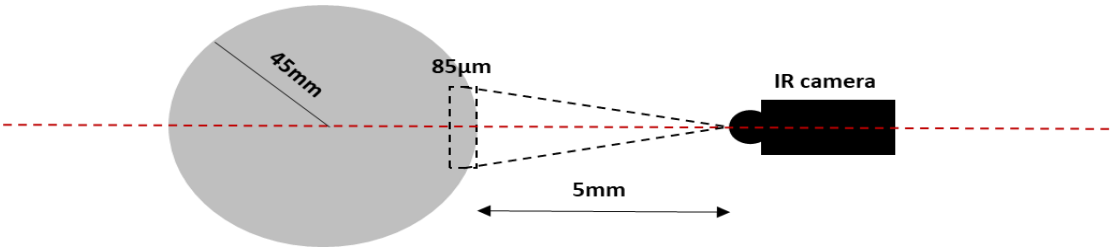

Figure 2.7: On top view of the experimental setup. Distances not on scale.

The thermal response was recorded with an infrared microbolometer array with relay lenses (IR camera). The bolometer is similar to conventional ones [114]. The used microbolometer array is of 382 x 288 pixels, having a maximum thermal sensitivity for long wave Infrared bands (LWIR), i.e., ranging between 7 to 14 µm. The size of the elementary pixel is 20 µm. Its thermal sensitivity is +/- 0.02°C in a working range of 15-25°C. The microbolometer is coupled to a home-made objective that is a combination of 12 Germanium lenses (Figure 2.8 illustrates only 8/12 lenses for a sake of clarity), called relay lenses. The focal of this objective is 7.5mm. The numerical aperture is F/1 and the spatial resolution ellipsoid is 0.1mm. The bolometric sensor is placed about 50mm on the side of the solid substrate-liquid-solid substrate system (Figure 2.2, bottom picture and Figure 2.7), thus reducing atmospheric absorbance and we consider it negligible for our measurements. The relay lenses were used to magnify the seen image and thus to access higher detail of the system on the z-direction. This setup provides a view of the liquid gap throughout the y-direction of about 5mm. On the x-direction, the field of depth depends on the liquid type. For glycerol, the penetration length is about 0.85mm. Thus, we can access the liquid bulk thermal response and we are not limited to the surface measurements as is the case for solids. The metallic fixtures, where the alumina plates are placed, are covered with a non-reflective tape to reduce any reflectivity artefacts from the high reflectivity-moving fixture. The whole system was covered to remove any reflectivity by external surfaces.

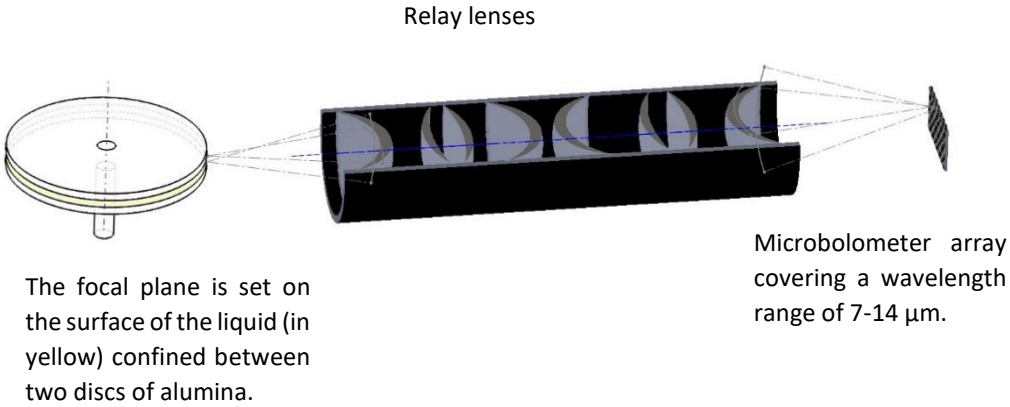

Figure 2.8: Relay lenses setup used to magnify the thermal image.

The video acquisition was done at 27 Hz. Faster dynamics would decrease the quality of the measurements since microbolometer cameras often are characterized by large response time [114].

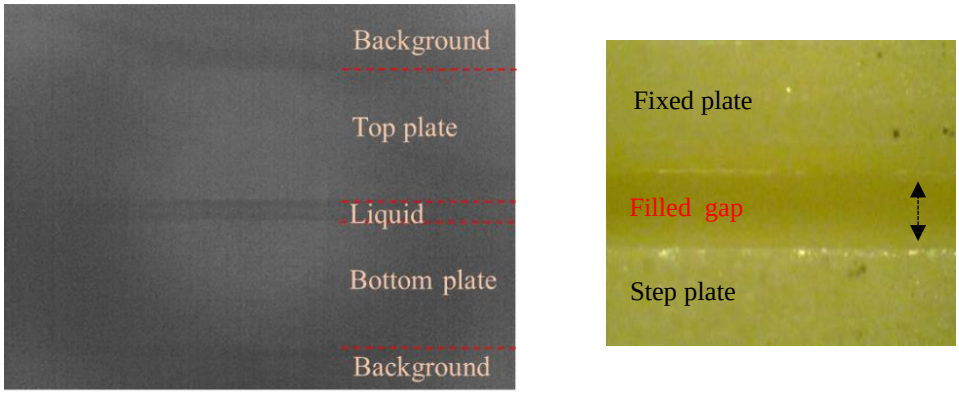

Figure 2.9: Left figure) Random frame from a raw video measurement highlighting the total acquisition of the IR sensor (240µm). Right figure) Optical frame from a conventional camera of the experimental system (100µm).

Figure 2.9 shows an example of a typical frame from the video acquisition. On the frame can be seen the alumina plates and the liquid placed in between. The alumina plates appear as brighter objects (and thus "hotter"), because their emissivity is of about $\varepsilon_{plate} \sim 0.85$, while for the liquid (glycerol, polypropylene glycol etc.), the typical value of emissivity is $\varepsilon_{liq} \sim 0.9$ close to a black body. The lower emissivity and the low thermal conductivity of the alumina substrates do not pollute the measurements since the value is not high enough to shadow the liquid emission. This would be the case if aluminium surfaces were used since the emissivity is $\varepsilon_{Al} \sim 0.1$.

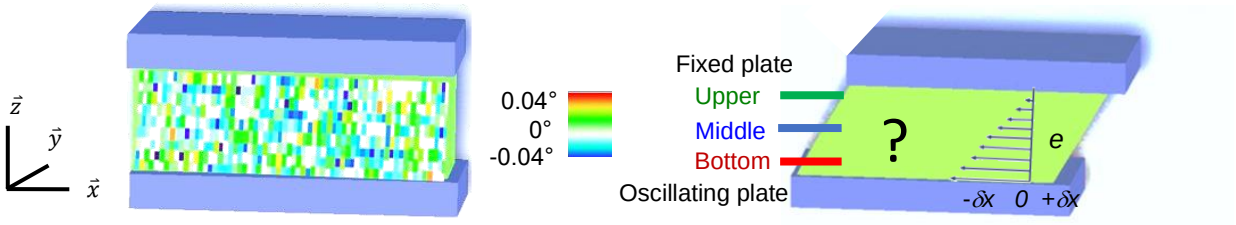

Figure 2.10: a) The liquid is confined between two high-energy plates (Alumina surfaces). At left, the real thermal image of the liquid is viewed at rest from the gap plane (xOz) (63 x 13 pixels (renormalized) thermal image of glycerol recorded at room temperature, e = 0.240mm gap). We examine the impact of a low frequency (~ Hz) mechanical shear strain on the liquid temperature is studied.

In Figure 2.10a, we show a zoomed, coloured version of a frame of the liquid from a raw video file, as well as the geometry of the shear deformation, which originates with the displacement of the bottom plate. From the succession of the frames from an acquisition with the IR camera, we generate what we call as 2D thermal mapping. The 2D thermal mapping will be the main tool to demonstrate the thermal state throughout the liquid gap. To summarize, in a 2D thermal mapping, the x - axis represents the time. Each frame is a snapshot, and the acquisition time of each frame is 0.037037s. Thus, frames placed next to each other highlight the evolution with time. The y – axis of the mapping details the evolution over the gap, while the colour scale highlights the thermal variation intensity.

To study the created thermal bands in detail, they are selected as a line usually 3 - 5 pixels wide depending on the gap thickness. The extracted value over time is the intensity I. We can derive the temperature variation ΔT by using the relation

$$\Delta T\ (K) = 1.8 * \Delta I\ \frac{y}{256} \tag{3.2}$$

where, ΔI is the intensity difference and y is a constant that varies from the camera setup settings. The typical value for these measurements is $y \sim 2.5$. The constant value 1.8 is used as a compensation of the lost emissivity due to the micro-lens equipped on the IR camera, which provides higher detail of the liquid gap (Figure 2.8) and reduced background emission. The radial geometry of the plates also contributes on the value, since its curved nature reduces emissivity seen by the camera due to focus loss (Figure 2.7).

2.4 From shear-elasticity to thermo-mechanical response: example of the liquid PPG

New advances in theoretical and experimental aspects of liquid properties showed that the liquid state is not a separate intermediate state between solid and gas phases and cannot be grouped only in the fluids category along with gas phase. In thermal equilibrium, the liquid should have macroscopically a homogeneous temperature (down to the thermal fluctuations) without external fields affecting its dynamics. It is conventionally accepted that liquids have no ability to propagate any external shear wave, meaning that the shear wave energy will be instantaneously dissipated [119]. However, the liquid nature appears more complex and exhibits solid-like properties at mesoscopic scale as different theoretical and experimental works have shown. These properties are not restricted under extreme conditions like e.g., high pressure [120, 121, 122], high frequencies close to inverse of molecular relaxation time [123, 6, 124] or temperatures close to liquid – solid transition [20]. For different liquids, from water to polymer melts, it is shown experimentally that elasticity exists in liquid systems at low frequencies for different system scales from nanoscale up sub-millimetre scale [125, 19, 18, 71]. Moreover, theoretical aspects have suggested the propagation of shear elastic waves on low frequency region [30, 85, 77]. All the above acts as a driving force to further investigate the elastic properties. In the next two chapters, we focus on the thermal response of the liquids under different types of mechanical deformation and try to characterize the seen thermal effect.

In this section, we will describe the fundamental result of our thermo-mechanical study in detail. For this purpose, we will use the results of PPG-4000 of various experimental runs at 0.100mm - 0.500mm gap thickness, ω = 0.5 - 5 rad/s and γ = 1 - 4000%. The polymer glass former polypropylene glycol-4000 (PPG-4000) ($H[OCH(CH_3)CH_2]_nOH$) (Sigma-Aldrich manufacturer), which was studied extensively in this chapter. The molecular weight is given 3500-4500 g/mol, which corresponds to about 55 repetition units. That means that it is not a complex polymer melt with huge polymer chains, but an oligomer. This is also highlighted from its properties. It is a viscous liquid at room temperature (η = 0.8 – 1.3 Pa.s) and its fast relaxation time (~ 10^{-9}s) is out of the dynamic range of conventional mechanical tools, while its glass transition temperature is at T_g = -73 °C [126, 127]. All the measurements were conducted at room temperature, where the compound is in the liquid state far away from any critical point. It has low evaporation rate, meaning that during the measurements the loss of liquid due to evaporation is negligible and not considered. The samples were prepared for the measurements by systematic freezing and defreezing from -18°C. The transition from liquid to supercooled state ensures the remove of air bubbles trapped in the liquid state. Bubbles could be a considerable problem in rheological measurements since they dissipate part of the offered energy during excitations [128, 129]. Of course, the complete removal of bubbles in nanoscale is not feasible, but their reduction in size and number is important for greater control of experimental conditions. From everyday perspective, PPG and glycerol are used in various fields like cosmetics and food conservation.

2.4.1 **Average thermal variation in the liquid gap**

First, we study what is the overall average temperature variation of the measurement during the external oscillation.

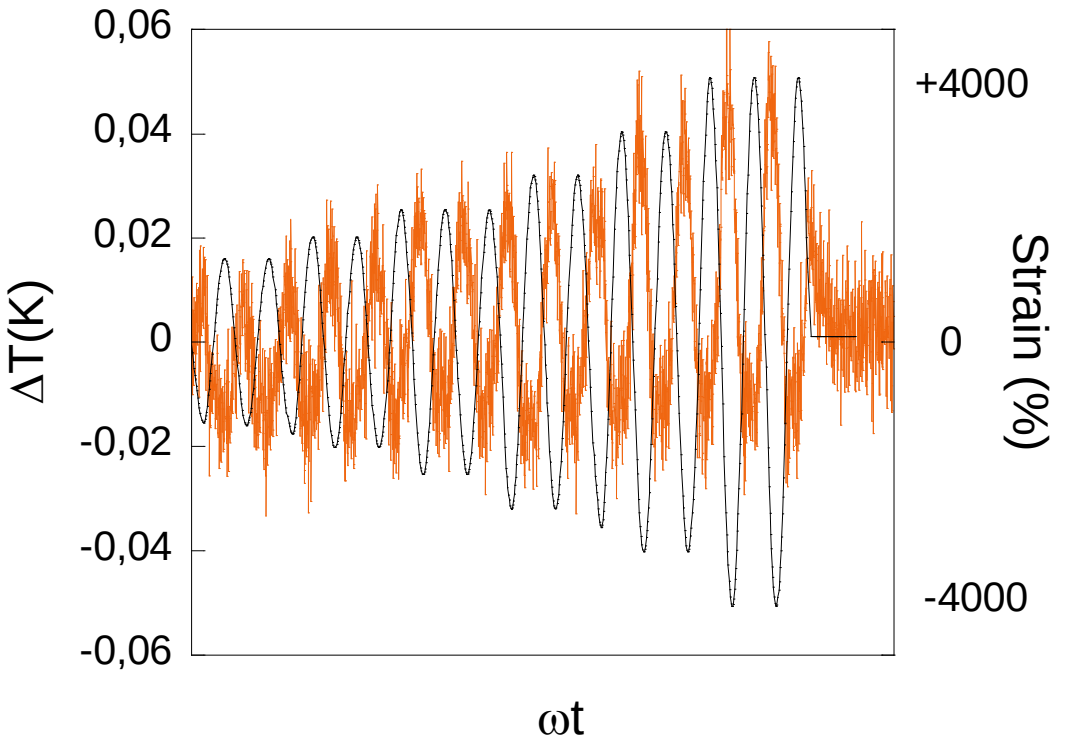

Figure 2.11: Average thermal variation of the liquid gap of PPG-4000 e = 0.240mm, ω = 1rad/s, for various strain values γ_0 = 1250 - 4000%. The zero of the thermal variation corresponds to the temperature of the total gap under equilibrium after the applied strain. Orange and black lines represent the thermal variation and shear strain respectively.

In Figure 2.11, we observe the collective response of the liquid gap during the oscillatory shear strain. In this measurement type, shear strain amplitude starts from a small value (typically around 1%) and increases progressively after repeating few oscillations of certain amplitude before it is increased. The thermal noise does not allow to identify a signal until accessing large strain amplitudes (γ_0 > 500%).

Above these strain amplitudes (γ_0 > 500%), the average temperature is not constant but evolves with the strain. The thermal variation appears almost synchronous with strain with $\delta\varphi_{average} < \pi/4$, while its amplitude increases with the strain amplitude. In figure 3.1, we observe the thermal response integrated over the total liquid (bulk response) for six strain values (γ_0 = 1250, 1500, 2000, 2500, 3150 and 4000%). The increase from one strain to another is continuous and we observe that thermal variation evolves with it. We see that the average temperature of the liquid system oscillates from hotter to colder temperatures than the equilibrium one. An important observation is that the thermal wave oscillates with the same frequency as the strain wave, implying a direct connection between those two parameters. In this chapter, we will study their connection and evolution. During the measurement, conduction between the liquid and the plates is possible even though α-alumina has a low thermal conductivity (~30W/mK), but it will be neglected, since the focus of this work is the emergent dynamic thermal effect of the

liquids. The measurements were conducted in absence of any external heat source and the only energy provided to the liquid system is the mechanical one due to shear deformation.

These results stand of great surprise from a conventional liquid dynamics point of view, where the molecular relaxation time is short (~ 10^{-9}s for the liquids used in our measurements). Thus, for the excitations applied on the measurements, demonstrated on this chapter, no response is expected to be seen since the excitation frequency ω_{exc} = 0.5 – 5 rad/s = 0.08 – 0.8 Hz, is considerably slower than the inverse of relaxation time τ_{rel} ~ 10^{-9}s, leading to a Deborah number De = $\tau_{rel}*\omega_{exc}$ << 1.

Due to their relatively low viscosity (η ~ 0.9 – 1.4 Pa.s), the liquid exhibits indeed a Newtonian behaviour throughout the measurements as seen from their stress-strain relation (δφ = 90º, section 2.9), which produces an almost perfect circular Lissajous curve [130, 131]. Another indicator is the sin-wave character of the shear stress [132, 133, 134]. The Newtonian behaviour can be also derived theoretically from the Reynolds number. For the parallel plate geometry, the number is given as [135]:

$$Re = \frac{\rho \dot{\gamma} e^3}{\eta_0 R}$$

where, ρ is the density, $\dot{\gamma}$ is the shear rate, e the gap thickness, η_0 the viscosity and R the radius of the alumina plates. For PPG, e = 240μm, shear strain from 0 to 4000% at ω = 1rad/s and R = 22.5mm, we calculate that Re = 2*10^{-5}. This value is much smaller than the critical Reynolds value, where turbulence occurs, and secondary flows should be considered. From rheological point of view, PPG and glycerol exhibit purely viscous behaviour even when the applied shear excitation is so large that reaches the limits of the rheometer.

As the standard description of the tested liquids is a viscous one, we next turn on viscous dissipation to interpret the results. For the observation window of the measurement, we do not detect any heating of the total liquid gap due to viscous dissipation. To deduce if viscous heating might play a role, we will rely on theoretical predictions. Viscous dissipation plays important role when the studied material has high viscosity, and the excitation is large [136]. Viscous heating is reported and discussed for high viscosity polymer melts [137]. For PPG, no systematic study came to our attention. Thus, viscous heating is expected to be negligible for our experimental results, but due to the extreme deformations applied, we study theoretically the expected viscous heating. PPG-4000 is an oligomer with viscosity comparable to glycerol (~ η_0 = 1 Pas for PPG, η_0 = 1.412 Pas for glycerol). A qualitative approximation of the significance of viscous heating might be done with the use of Nahme's number developed for highly viscous fluids (molten polymers) [138]:

$$Na = \eta_0 \beta h^2 \dot{\gamma}^2 / \kappa < 1$$

where η_0 is viscosity, h gap thickness, κ thermal conductivity, $\dot{\gamma}$ is shear rate and β=-*(1/ η_0)(dη/dT)* shows the dependence of viscosity with temperature. For the case of our studied liquid, the dependence is exponential-like. In our experimental conditions, we get *Na* ~ 6*10^{-6} meaning that the viscous heating is negligible [139]. Based on Nahme's number, we derived that viscous heating is not significant for our experimental conditions and not systematic temperature rise is observed in our measurement. A report from A. J. Giacomin *et al*. [140], on viscous heating at large amplitude oscillatory shear predicts the temperature variation of liquid due to viscous heating. This theoretical study on large amplitude oscillatory shear flow in between adiabatic walls, demonstrates that viscous heating is possible under shear, and it is considerable for polymer melts that exhibit high viscosity. However, this work focusses on

highly viscous polymer melts, as it is expected for viscous dissipation to be significant. The viscous heating consists of two terms, a time-average increase term and an oscillating one. For our experimental conditions, based on their work, we calculate for PPG at $\omega = 0.5 - 5$ rad/s and $\gamma = 4000\%$, the average temperature increase is negligible. However, they predict the existence of an oscillating temperature term, which in our case translates to 0.0023 K during the mechanical oscillation. The result is one order smaller than the experimentally observed one, but the theoretical model does not consider the interaction between the liquid with the substrate, and it is based on the classical Maxwell approach of the liquid. Thus, the viscous origin of the liquid is unable to describe the origin of the thermal response, which shares the same fundamental frequency with the applied shear. Finally, it is very important to point out that the thermal signal contains both hot and cold waves. The identification of a cold part is the proof that non-dissipative effects take place that are mechanically induced. Correlatively, the hot wave should be thus also treated as a non-dissipative effect, both being local non-equilibrium thermodynamic states. Therefore, the present observation of a thermal response challenges the conventional description in terms of viscous behaviour and fast relaxation time.

2.4.2 **Generated thermal bands under shear strain periodical deformation**

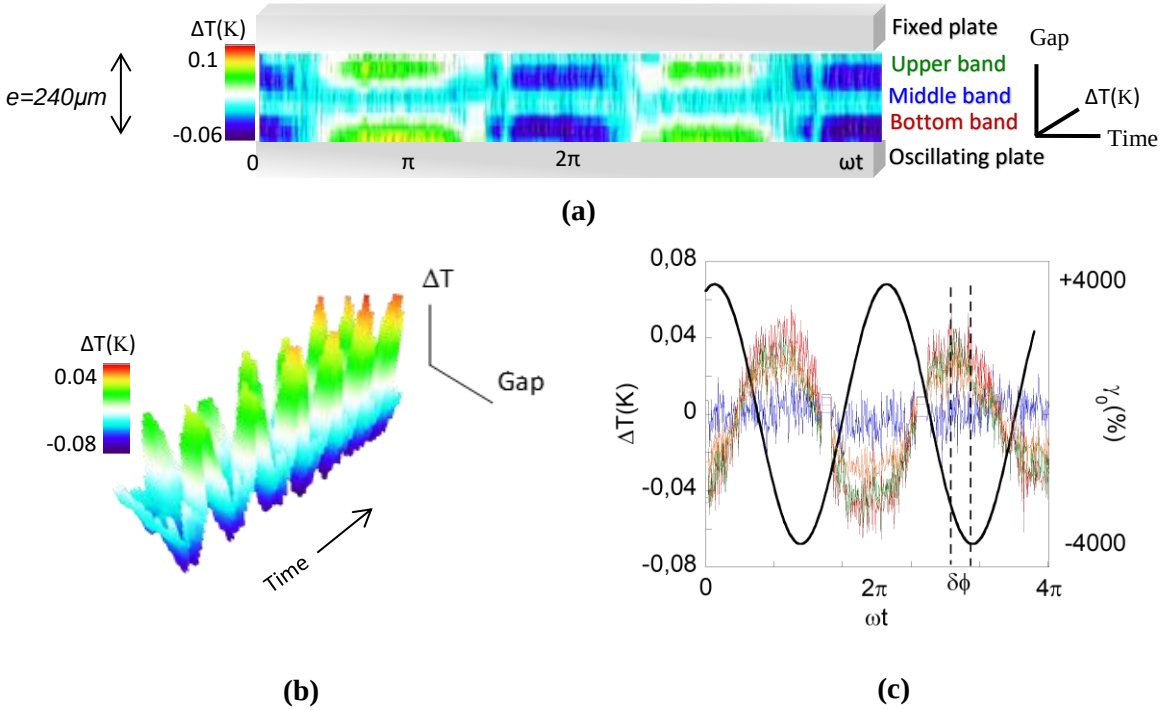

Figure 2.12: a) Micro-thermal mapping (gap view) of a liquid under low frequency oscillatory shear strain (room temperature measurements carried out on polypropylene glycol (PPG-4000) at 0.240mm gap thickness, ω=0.5 rad/s and γ = 4000% versus time (~679 frames), alumina substrate). Black line is an eye guide for the applied strain. **b)** 3D view of the thermal behaviour of Fig 1a. **c)** Temperature variation versus time Red, blue, green and orange data points represent the temperature variation localized at the bottom, middle, upper bands and total volume respectively and the continuous black line is an eye guide for the applied shear strain. Δϕ is the phase shift between the thermal and strain wave.

In the previous section, we studied the average temperature change of the bulk liquid gap. However, the liquid is not thermally homogeneous as seen in Figure 2.12, but is split in different thermal regions. Figure 2.12 contains the information extracted from the data treatment. In Figure 2.12a, we see the main result of the treatment, the 2D thermal mapping. The thermal mapping highlights the time evolution of the effect throughout the gap. The first observation is that the temperature of the liquid is not homogeneous along the gap, but bands of different temperatures coexist as the phenomenon occurs. These bands dynamically change along with the periodic strain. We notice that three thermal bands are created relative to the z – axis (y-axis of thermal mapping), which shows the evolution along the gap. Another presentation of the thermal effect can be seen in Figure 2.12b. In this one, a higher emphasis on the thermal variation is given. We categorize the thermal bands as follows:

- "Bottom band" for the thermal band closer to the moving (oscillating) alumina plate (Figure 2.12a)
- "Middle band" for the band located in the middle of the gap
- "Upper band" for the band closer to the fixed top alumina plate

We observe that the bands change of temperature depending on the applied strain. Their evolution is periodic following the frequency of the applied strain. The thermal evolution of the bands can be seen in detail at Figure 2.12c. The figure was created by choosing three (3) pixels wide bands, which were located from the 2D mapping. This way, the edges of each thermal band were excluded since the border of the bands from each other is not clear. Figure 2.12c highlights a thermal variation ΔT, where zero was chosen as the temperature at equilibrium for each band after the experiment. This way, we deduce when the temperature evolves hotter or colder than the equilibrium. We observe that the bottom and upper band oscillate simultaneously, and their temperature variation is almost at the same amplitude (Figure 2.12c). The thermal variation ΔT from the maximum to minimum value in one period is 0.087K for the bottom band and 0.07K for the upper band. This variation is symmetric with respect the zero thermal variation, meaning that the bands oscillate around zero and achieve colder temperatures even if we apply work on the system. While the bottom and upper band oscillate with time, the middle band is mostly constant with a thermal variation within the experimental error bar. However, for some intermediate strain values the middle band appears to oscillate weakly, in an opposite manner from the other bands (Figure 2.13). When the bottom and upper bands get hotter, the middle gets colder and vice versa, showing different thermodynamic states in the liquid.

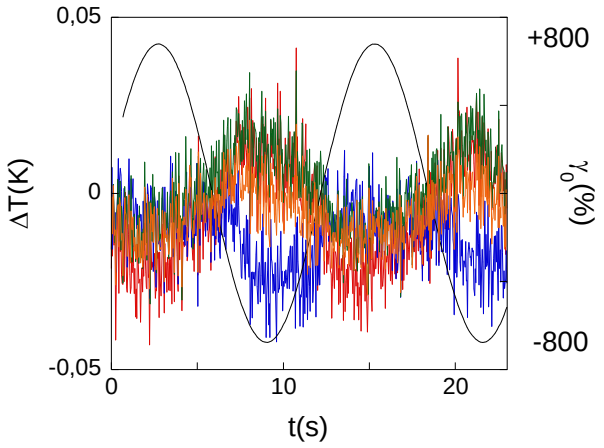

Figure 2.13: Temperature variation versus time for PPG, e = 240μm, ω = 1rad/s, γ_0 = 800%: Red, blue, green and orange data points represent the temperature variation localized at the bottom, middle, upper bands and total volume respectively and the continuous black line is an eye guide for the applied shear strain.

An interfacial effect is expected to exist at some nanometres length, while the thermal bands are 50μm wide and around 15-30μm far from the interface. With the present experimental setup, a detailed study on the interface is not possible, due to limitations of the IR camera. In our experimental geometry, we approximate that the volume of the system is constant on the z-direction (xy plane), thus the thermal variation of the bands indicates different non-equilibrium states of the liquid corresponding to slightly different densities and/or volume changes - on the free from walls - directions. In other words, the thermal bands implies that the liquid is locally compressible. Following the thermal response, the liquid in parts is compressed and then stretched as the shear strain oscillates. The compressed and stretched states of the liquid alter each time close to strain absolute maximums. Thus, the liquid remains in a compressed or stretched state as long as the shear stress is strong enough to provide the liquid the required energy to maintain/increase this non-equilibrium state. Close to maximum strain, the thermal

wave relaxes accordingly. With the new applied shear rate in the opposite direction switches to the other non-stable state in order to integrate or restore the provided shear energy.

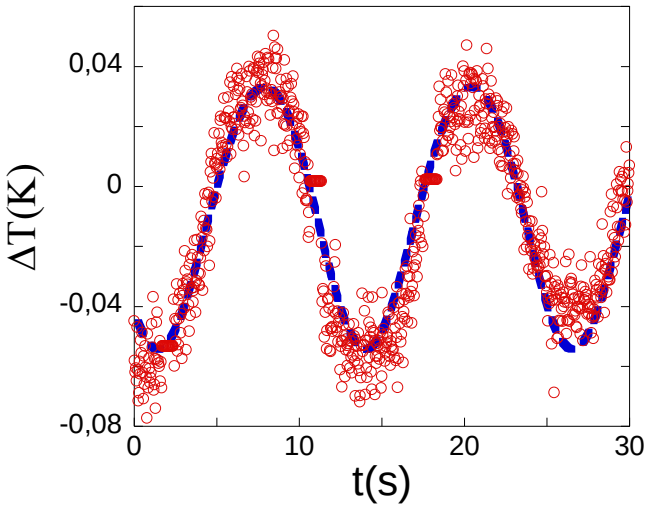

Figure 2.14: Data points (blue circles) corresponds to the thermal variation ΔT within PPG-4000 bottom band at 0.240mm, ω = 0.5 rad/s and γ_0 = 4000%. The blue dotted line corresponds to a sin fit $f(t) = A_0 + A_1 sin(\omega t + \delta\varphi)$.

The above mechanism becomes clearer, if we compare the thermal waves with the periodic shear strain and investigate the associated phase shift. The shape of each thermal band in the time domain is similar with the applied shear strain deformation. The thermal waves (each band) can be modeled by a simple sin wave (in the linear region) as $\Delta T = \Delta T_0 \sin(\omega t + \delta\varphi)$. In analogy with the viscoelastic analysis (Chapter 1), we determine the phase shift which will give information about the loss and of the stored energy during the process .In Figure 2.14 can be seen an example of the sin fit of the bottom band (which was displayed in fig, 3.3c). We calculate that the bands have the same frequency as the applied strain, but with a phase shift difference. Specifically, the phase shift is $\delta\varphi_{bottom} \sim 39° \pm 3°$ and $\delta\varphi_{upper} \sim 43 \pm 2°$, for the bottom and upper bands respectively. We see that the phase shifts of each band are close, meaning that the bands are dependent to each other. The phase shift is not random but related with the mechanical excitation. Thus, an analogy is possible with a spring ($\Delta T/\gamma$ is the equivalent spring constant. We observe that the maximum increase or decrease of temperature is at maximum displacements (zero velocity) and ends at zero displacement (maximum velocity). This is repeated each time, meaning that the temperature variation of each band is related with the rate of energy given to the system. As the amount of energy is decreased, the bands are not capable to further increase their temperature and after a critical point, they decrease their temperature leading to the resulting phase shift.

To elucidate the origin of the thermal effect, an interpretation is possible if we consider the elastic nature of the liquid, since the viscous one fails to explain as seen in the previous section. As theoretical reports displayed [29, 90], shear elasticity becomes relevant as the scale of the system is reduced as $G' \sim e^{-3}$. Thus, the elastic characteristics of the liquid, which are negligible at the macroscale, are noticeable even in mesoscale. As example rests the measured shear elasticity at sub-millimetre dimensions for low frequency weak oscillations, which vanishes as the strain increases. Of great interest are studies that show a continuity of the elastic behaviour of the liquid state from the high frequency regime (MHz, GHz) to the low frequency one (Hz) [85, 77]. Particularly it proves that shear waves should be able to propagate in the liquid medium even at low frequency with propagation length $d_{el} = c\tau_M$, where c is the speed of sound

of the medium and τ_M is Maxwell's relaxation time. For PPG and glycerol, we calculate the propagation length d_{el} ~ 3 – 4μm, meaning that the liquid is not completely blind to the shear energy, but could store it. In our study, the only source of energy for the liquid during the measurements is the work produced when the plate oscillates. Therefore, the only source of energy to the system is a shear one. Thus, the ability of the tested liquid to respond thermally to the shear excitation acts as an indirect proof of shear wave propagation in a liquid medium. Since, the propagation length is smaller (around 4μm) than the thermal bands (~ 50 – 80μm) or the total gap thickness (100 – 500μm), it is expected for the effect to be scale dependent.

2.4.3 **Strain dependence of thermo-mechanical effect**

In the previous sections, we displayed an example to introduce the observed thermal effect. The generation of bands is systematic for different shear strain values induced to the liquid system.

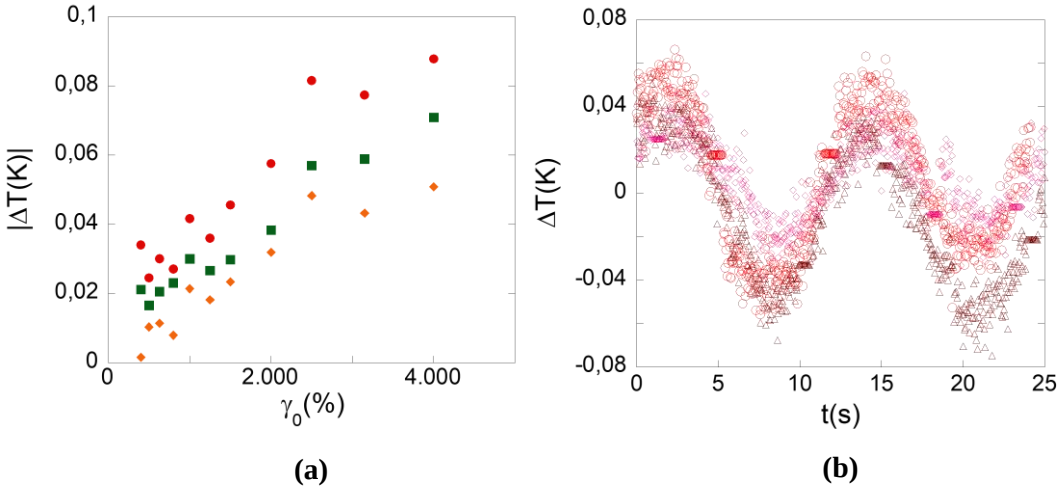

Figure 2.15: a) Strain dependence of the maximum of the temperature variation amplitude (from maximum to minimum temperature) $|\Delta T(K)|$. Sample: PPG-4000 at gap thickness 0.240mm, ω=0.5 rad/s, as extracted from the sin harmonic fit for bottom band: (●), middle band: (■), upper band: (◆) and total gap: (▲) respectively - measurements below 400% are below the accuracy. **b)** Graph illustrates the thermal waves at same gap thickness for strain values 1500% (rose points), 2500% (dark red points) and 4000% (light red points) of the bottom band (0.240mm gap, ω=0.5rad/s).

In Figure 2.15a, we show the evolution of the thermal variation (amplitude value from maximum to minimum temperature) of each thermal band for different shear strain values. The middle band's thermal variation is much lower for most of the strain values in these experimental conditions and thus not depicted in the graph. For intermediate stain values, we measure a small periodic variation for the middle band opposite in nature in respect with the other two bands. We observe that both the bottom and upper bands and the average of the total liquid exhibit a linear relation with strain with a slight deviation of linearity at higher values reaching a constant value, where the thermal variation remains constant with strain. From the seen linearity, we can define a dimensionless thermo-(strain)elastic constant $\Theta_{shear}(\Delta T,\gamma)=(\Delta T/T)/\gamma$. This constant shows the resulted thermal variation of each band under a certain shear strain (stretching) and under a certain temperature value. For our case, all our measurements were conducted at room temperature (~ 300K). These values are about $\Theta_{strain} = (6.66 \pm 0.5)*10^{-6}$ for the hot band (red points) and about $\Theta_{strain} = (5.83 \pm 0.5)*10^{-6}$ for the upper

band (green points). Due to limitations of sensor resolution, we are not able to directly observe any thermal variation for strain values $\gamma < 200\%$, while for $200\% < \gamma < 800\%$ the thermal response is noisy and close to the IR camera error bar. However, utilizing the linear relationship (Figure 2.15), we deduce that the thermal mechanism should occur for smaller shear strain values, as we suspect that the origin of the effect is an elastic one. The elastic origin of the effect allows an analogy with solids. Then, an equivalent of the dimensional constant can be derived for metals: $\Theta_{elongational} = (\Delta T/T)/E \cong 0.45$ where E is the elongational strain in the case of steel-sheets submitted to cycle strain fatigue [141]. The constant Θ is about four decades higher for the metal indicating that for the same temperature variation, smaller deformation is needed in a solid than in a liquid. The phenomenon encountered in solids is called thermoelastic stress analysis (TSA). There, upon applying a periodic strain (load), periodic thermal changes exhibit in "opposite" phase with the applied strain [142, 62]. The temperature variation ΔT in solid thermoelastic processes is given as:

$$\Delta T = -T_0 \frac{\alpha}{\rho c_p} \Delta\sigma \tag{3.3}$$

where α the linear expansion coefficient, ρ the density of the material, T_0 the reference temperature and c_p the specific heat at constant pressure [62]. In the equation (3.3), we see the linear relation of the thermal variation with stress and not with strain as we demonstrate in our case. The resulting temperature variation is of the order of 0.001°C, and the resulting stress is of the order of MPa. However, the equivalent strain applied to the solids is much weaker than the strain applied in our measurements. The strain values that we apply could even cause to overcome the yield stress of a solid material, while for our liquid system, such a violent displacement is possible.

Figure 2.15b shows the thermal evolution of bottom band for different strain values. The thermal evolution over time seems to be constant and equivalent to a sin wave for an excitation of $\omega = 0.5$rad/s. We see the resulting thermal response of the bottom band superposed for different strain values, meaning that the sin waveform holds true as the deformation is increased, showing the linearity of the phenomenon. Thus, we may propose that the temperature oscillates symmetrically around its equilibrium, meaning that for a thermal variation of 0.07K, the hot and cold parts amplitude have the same value of 0.035K. We observe the periodic nature of the effect and its strong connection with the period of the strain deformation, highlighting the thermo-mechanical coupling of the studied effect. As the strain value is decreased, the sin wave shape of the thermal response becomes noisier, with R-values of the sin fit smaller than 0.7.

Strain (%)	$\delta\varphi_{bottom}$ (degrees)	$\delta\varphi_{middle}$ (degrees)	$\delta\varphi_{upper}$ (degrees)	$\delta\varphi_{average}$ (degrees)
400	3		12	14
500	4		5	22
630	5	23	3	8
800	7	1	12	13
1000	16	14	19	23
1250	32		35	33
1500	27		27	27
2000	36		39	40
2500	38		42	42
3150	41		46	42
4000	39		43	41

Table 2.1: Phase shift values of the thermal bands and total liquid volume in respect with the applied strain for PPG, e = 0.240mm, ω = 0.5rad/s.

In the Table 2.1, we observe the values of the phase shift of bands and the total liquid system ($\delta\varphi_{average}$) over strain. We see that the phase shift evolves as the strain increased. For strain values, where we begin to distinguish thermal oscillations (γ_0 = 400 – 800%), we calculate a phase shift $\delta\varphi \leq 10^o$ for all bands and total liquid volume. As the strain amplitude increases, so does the phase shift until it reaches a plateau of 40º – 45º for 2500 – 4000% strain values. This value highlights a direct relation between the shear-strain mechanical excitation with the resulting thermal response and it is characteristic of a solid-like response. For elastic materials like solids or polymers and liquid in the MHz and GHz region, such a behaviour is known as an elastic behaviour, while for viscous materials the phase shift is $\pi/4 < \delta\varphi < \pi/2$ between stress and strain. The observed thermal effect seems not to produce phase shift between thermal waves and strain that deviate at maximum from $\delta\varphi \sim \pi/4$, implying that the seen effect is primarily elastic in nature.

Specifically, at lower strain values, the instant thermal response simulates an elastic response, while for higher strain, we observe a viscoelastic behaviour. The saturation of the thermal effect is not only observed by the phase shift plateau, but also from the constant thermal variation values for large strain values as seen in Figure 2.15a, implying that the excess shear energy is not stored after a point and partly dissipates in a higher rate.

2.4.4 **Frequency dependence of the thermo-mechanical effect**

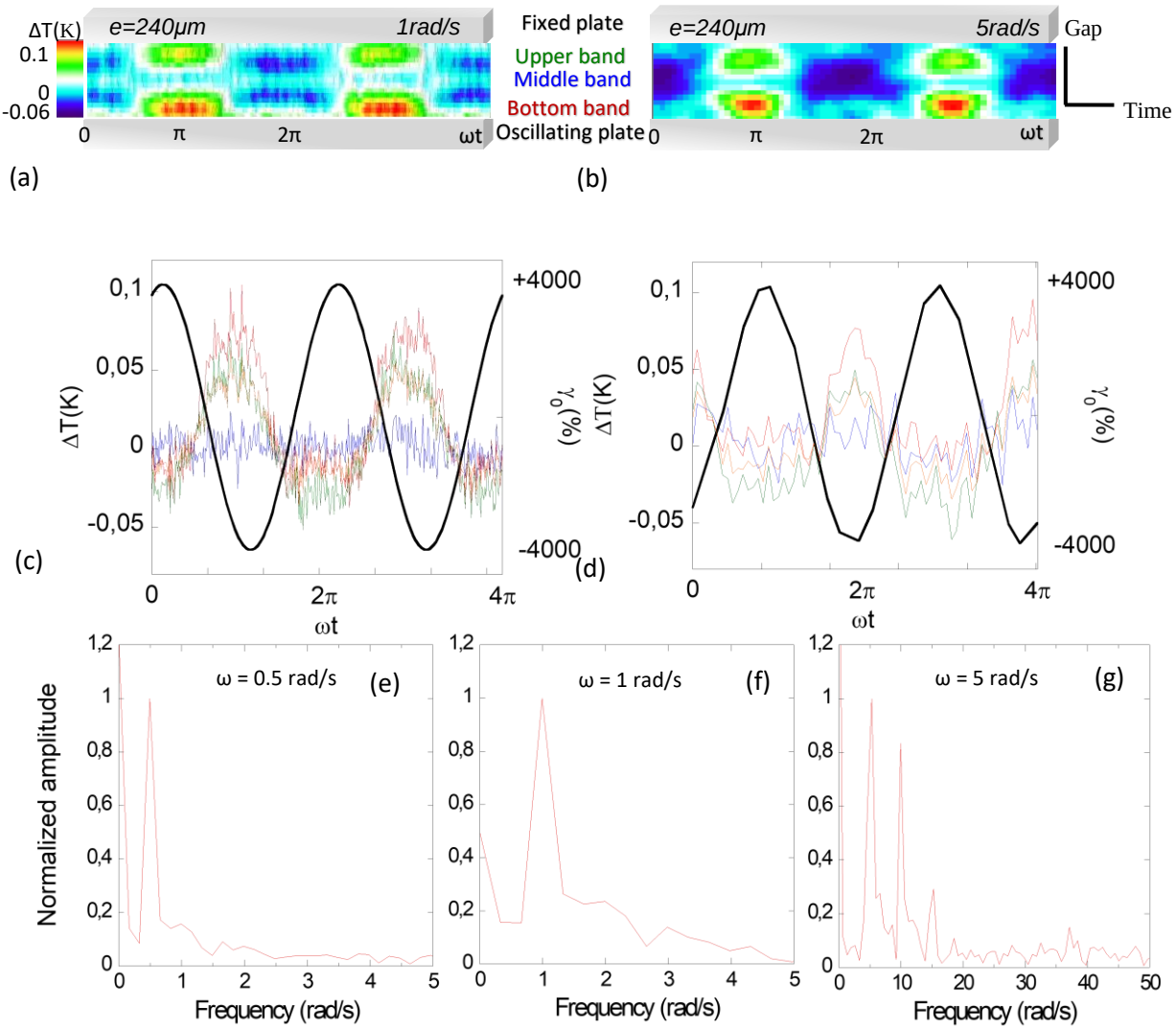

Figure 2.16: PPG-4000 confined in a 240µm gap (gap view), alumina substrate at room temperature measurements. **a)** Real-time mapping of the temperature γ = 4000% (gathering about ~640 frames): at ω = 1 rad/s **b)** same at ω = 5 rad/s. **c)** Thermal waves recorded for the bottom (●), middle (■), upper (■) bands and total liquid volume (♦) respectively at γ = 4000% and ω = 1 rad/s. The black continuous line illustrates the applied shear strain. **d)** Same for ω = 5 rad/s. Fourier Transform signal of the waves depicted of **e)** Figure 2.12c, **f)** Figure 2.16c, **g)** Figure 2.16d.

Next, we study the thermal effect for different frequencies. On Figure 2.16, we display the response for frequencies of 1 rad/s and 5 rad/s. Figure 2.16a & b show the thermal state of the whole gap during two oscillations for the same strain value (γ_0 = 4000%). We observe that the 2D mappings are qualitatively similar with the one of 0.5rad/s (Figure 2.12a), as a continuous alternation between cold and hot states is observed at top and bottom bands. However, the middle "bulk" band does not remain constant as reported in the 0.5rad/s case for 4000% strain but alternates its temperature as the frequency is increased. This behaviour becomes apparent for ω = 5rad/s, where the middle band oscillates weakly (ΔT_{max} = 0.02K) in phase with the other bands. Even if the middle band response is weak and far from a sin wave, it shows that as the shear rate increases with frequency, the phenomenon propagates to the bulk area.

The 2D mapping show that the effect maintains the same characteristics in total, but in detail the thermal response differs with frequency. Particularly, the time evolution of the temperature deviates from the sin-wave form as the frequency increases. The comparison is evident if we compare Figure 2.12c (ω = 0.5 rad/s), Figure 2.16c (ω = 1 rad/s) and Figure 2.16d (ω = 5 rad/s). However, this change is not random, but the signal is composed from higher harmonics. As seen in Figure 2.16e, the Fourier decomposition of the thermal signal at ω = 0.5 rad/s, shows the existence of the first harmonic and a small contribution from the second one. For ω = 1 rad/s, the contribution from the second harmonic becomes more significant, while a small contribution from the third one is noticed. For ω = 5 rad/s, the contribution from the first and second harmonic are comparable, while the third one is contributing considerably. The effect is not linear with frequency, implying that the liquid is not able to integrate the provided shear energy rate as the higher frequency increases, as the oscillating excitation reaches time scale close to the thermal relaxation time. Then, non-linear effects take place that leads to the generation of harmonics and to smaller thermal variations as seen for ω = 5 rad/s.

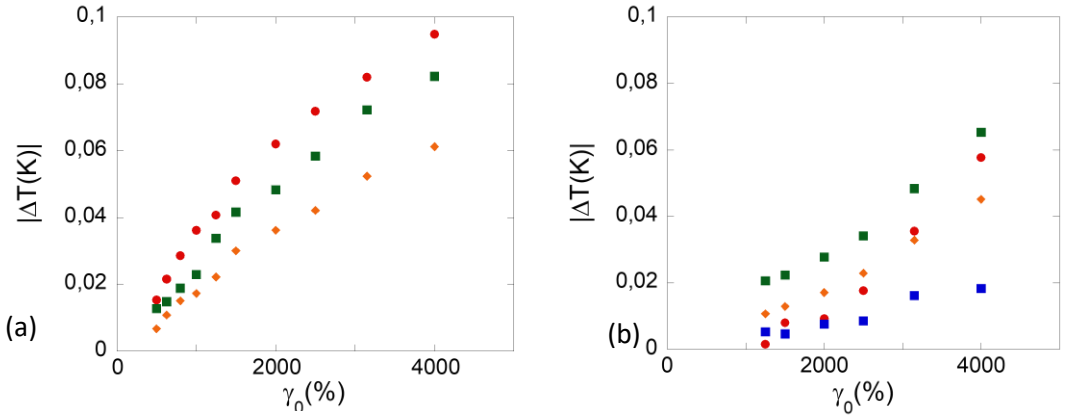

Figure 2.17: a) Strain dependence of the maximum of the temperature variation amplitude (from maximum to minimum temperature) $|\Delta T_0(K)|$ versus shear strain as extracted from the sin harmonic fit for the bottom (●), the middle (■), upper (■) bands and total liquid volume (♦) respectively at ω = 1 rad/s, **b)** same at ω = 5 rad/s.

From solid point of view, generation of second harmonic wave from a principal shear wave is possible, when the fundamental shear wave is considered polarized and the solid is anisotropic [143, 144], which stands for the case of the liquid where no periodicity is located. Particularly, the second harmonic amplitude scales linearly with the square of the first harmonic. A rise of second order shear waves could eventually contribute to double frequency thermal waves. From fluidic point of view, the seen thermal harmonics maybe associated with oscillatory temperature variation due to viscous heating [140], even though the theoretical calculation is one order smaller than the observed variation.

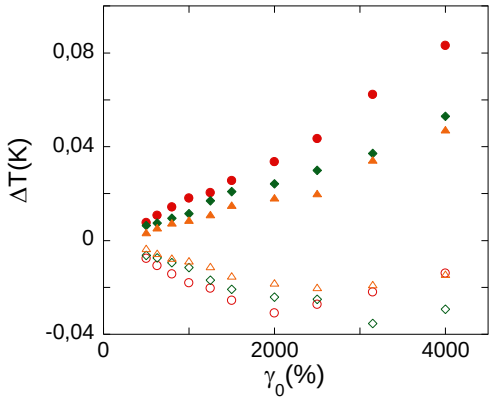

Figure 2.18: Strain dependence of the hot part (above thermal equilibrium, filled points) and cold part (below thermal equilibrium, non-filled points) of the temperature variation ΔT(K) as extracted from the sin harmonic fit for the bottom (●), upper (■) bands and total liquid volume (♦) respectively at ω = 1 rad/s.

In Figure 2.17, the strain evolution of the thermal response is highlighted for two frequencies. For ω = 1rad/s, the thermal evolution is similar with the one of 0.5rad/s (Figure 2.15a). The thermal variation is increasing with strain in two linear regions (different slopes). The region swap takes place at 1500 – 2000%, while the thermal variation values are comparable for these two frequencies. A noisy but detectable thermal variation is possible for 400% <γ_0 <1000%, while for γ_0 < 400% no thermal variation is detected within the error bar. All of the above hold for bottom, upper band and the total volume, with the bottom band, which is close to the oscillating plate to exhibit the higher thermal values for every shear strain. For the middle band, the response is too weak close to the error bar and thus a satisfying systematic conclusion is not evident for these experimental conditions. In Figure 2.18, we separated the amplitudes of the hot and cold parts for the thermal variation, and we see their evolution with strain. In the first linear regime, the hot and cold parts are equal since the thermal response is a sin wave, but in the next regime, this does not hold. The hot part appears to increase faster, while the cold part is decreasing in amplitude. Such a behaviour further strengthens the possibility of viscous heating contribution in the thermal signal. As the viscous heating component has double frequency, it will increase the hot and cold parts of the signal. In Figure 2.17b, the thermal variation for 5rad/s is highlighted. Here, a measurable thermal variation is possible for γ_0 > 1000%. In this case, the bottom band gives a weaker response than the upper band, implying a great complexity in the thermal signal. Both bottom, upper band and total volume have a quadratic-like increase with strain and no linear region is present as in lower frequency values. In overall, the thermal response is weaker in respect with the lower frequencies, meaning that due to the fast excitation, the liquid cannot effectively integrate and store the provide energy. Finally, a thermal variation is measured for the middle band, which increase appear as linear, but it is weak in nature, further confirming that as the frequency increases, higher portion of the liquid is affected thermally.

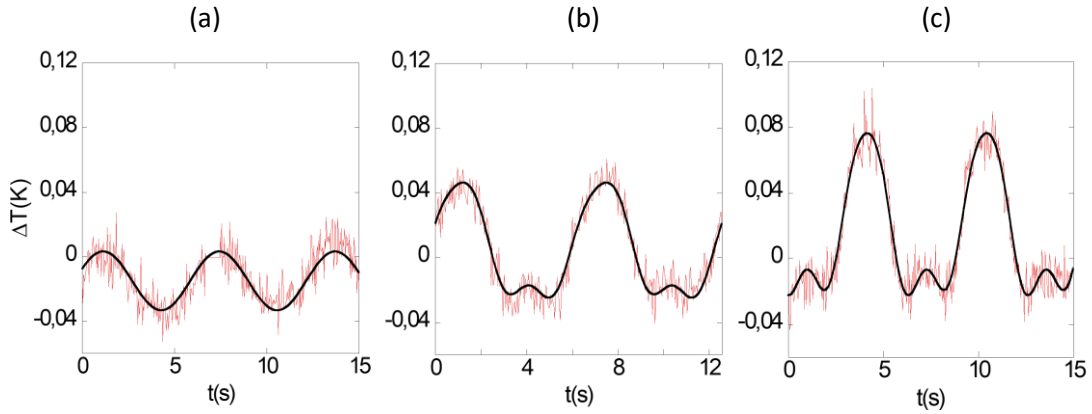

Figure 2.19: Thermal waves of bottom band of PPG, e = 240μm, ω = 1rad/s oscillatory motion for **a)** γ_0 = 1000%, **b)** γ_0 = 2500%, **c)** γ_0 = 4000%.

As seen in Figure 2.19, the shape of the thermal bands is not constant as the strain is increased for the case of 1rad/s. Instead, they progress from seemingly periodic sin waves to periodic waves, where the negative ("cold") part of the oscillation is no more seen, leading to the generation of the harmonics. Thus, we notice that the non-linear effect responsible of the generation of the harmonics is not connected only with the applied frequency, but also with the applied shear strain. Combining these two parameters, we conclude that the shear strain rate is the main factor that defines the form of the thermal response when the scale of the system remains constant. The shear strain rate is the rate between the deformation that we wish to apply (strain) over the time needed for the deformation to be applied. In our measurements shear rate is not constant since we do not apply shear flow. It is oscillating from zero at the maximum strain values to a maximum value at zero strain. As we increase strain, the desired deformation is increased, while with increased frequency, the time needed to reach the desired strain, decreases.

Strain (%)	$\delta\varphi_{bottom}$ (degrees)	$\delta\varphi_{bulk}$ (degrees)	$\delta\varphi_{upper}$ (degrees)
400	13		-
630	19	26	20
800	25	26	27
1000	22	16	26
1250	25	27	23
1500	30	31	34
2000	30	31	34
2500	31	34	37
3150	34	35	37
4000	36	38	40

Table 2.2: Phase shift values of the thermal bands and total liquid volume in respect with the applied strain for PPG, e = 0.240mm, ω = 1rad/s.

The phase shift between thermal signal and strain follows similar behaviour for ω = 1rad/s. As the strain increases so does the phase shift. However, in this case the phase shift starts with higher values at low strain and reaches lower values for high strain values (Figure 2.20). As seen in Figure 2.20, Table 2.1 and Table 2.2, there is a change of the slope of the phase shift with strain at around 1500%, leading to almost stable phase shift. Similar evolution is seen on the thermal variation versus strain graphs at around same strain value (Figure 2.15a & Figure

2.17a). This could mean that the departure from an elastic-like response ($\delta\varphi \sim 0$) to a non-linear viscoelastic-like response ($\delta\varphi \sim \pi/4$), leads to deviation from the linear evolution of thermal variation with strain by increasing dissipation. The above results elucidate that the origin of the phenomenon is elastic in nature, while non-linear effects possible viscous and/or elastic in nature impede the evolution of the effect. For $\omega = 5$rad/s, the phase shift of the thermal signal does not change with strain. However, for this case a detectable signal is possible only for $\gamma_0 >$ 1000%, which seems to be in agreement with the behaviour of the phase shift for lower frequencies at high strain values. The phase shift is $\delta\varphi \sim 1^o \pm 15^o$. The error bar is large at fast frequency rate but the phase shift remains always below $\pi/4$.

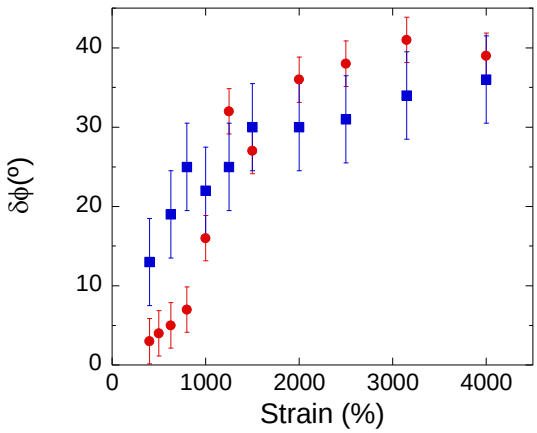

Figure 2.20: Phase shift between thermal signal of bottom band and applied shear strain for PPG e = 0.240mm, ω = 0.5rad/s (●) and ω = 1rad/s (■).

The thermal behaviour has shown that the region mostly affected from the shear-induced temperature variation is the bottom band, which lies closer to the source of the shear energy. However, the top band, which is next to the fixed alumina plate is also affected, but in a weaker manner as the $\Delta T(K) = f(\gamma_0)$ graphs show (e.g., Figure 2.17). Moreover, the two bands oscillate almost in-phase, with occasions where the bottom band is in advance of about 4°. This discrepancy between the phases of the bands is close to the error bar but seems systematic for large thickness (e = 240μm). The in-phase respond of the bands show that the thermal variation takes place almost instantly in every region of the liquid, but if we account the measured phase shift, the delay is slower than the speed of sound in the medium. For a delay between the peaks of the bands of ~ 0.055s, d = 106m. This is expected since the shear wave propagation does not take place in the entirety of the liquid but only on the first few μm. However, since the propagation of shear takes place for a few μm, we would expect that any response should be local. Thus, another mechanism related to the storage of the shear energy and minimization of the new total free energy takes place, whose process seems slower in relation to wave propagation. The existence of such collective response of the liquid volume suggests that liquid's molecules are long-range correlated [145]. For these kinds of correlations to be possible, slower relaxation processes are a necessity to exist. Such processes have been indirectly identified with the measured finite low-frequency shear elasticity and continue to exist even when the viscous rheological behaviour becomes dominant. Moreover, newly proposed theory of collective shear waves based on phase relaxation due to non-affine deformations give rise to relaxation times that could be much larger than the Maxwell molecular relaxation time [93].

2.4.5 **Frequency dependence of average thermal variation**

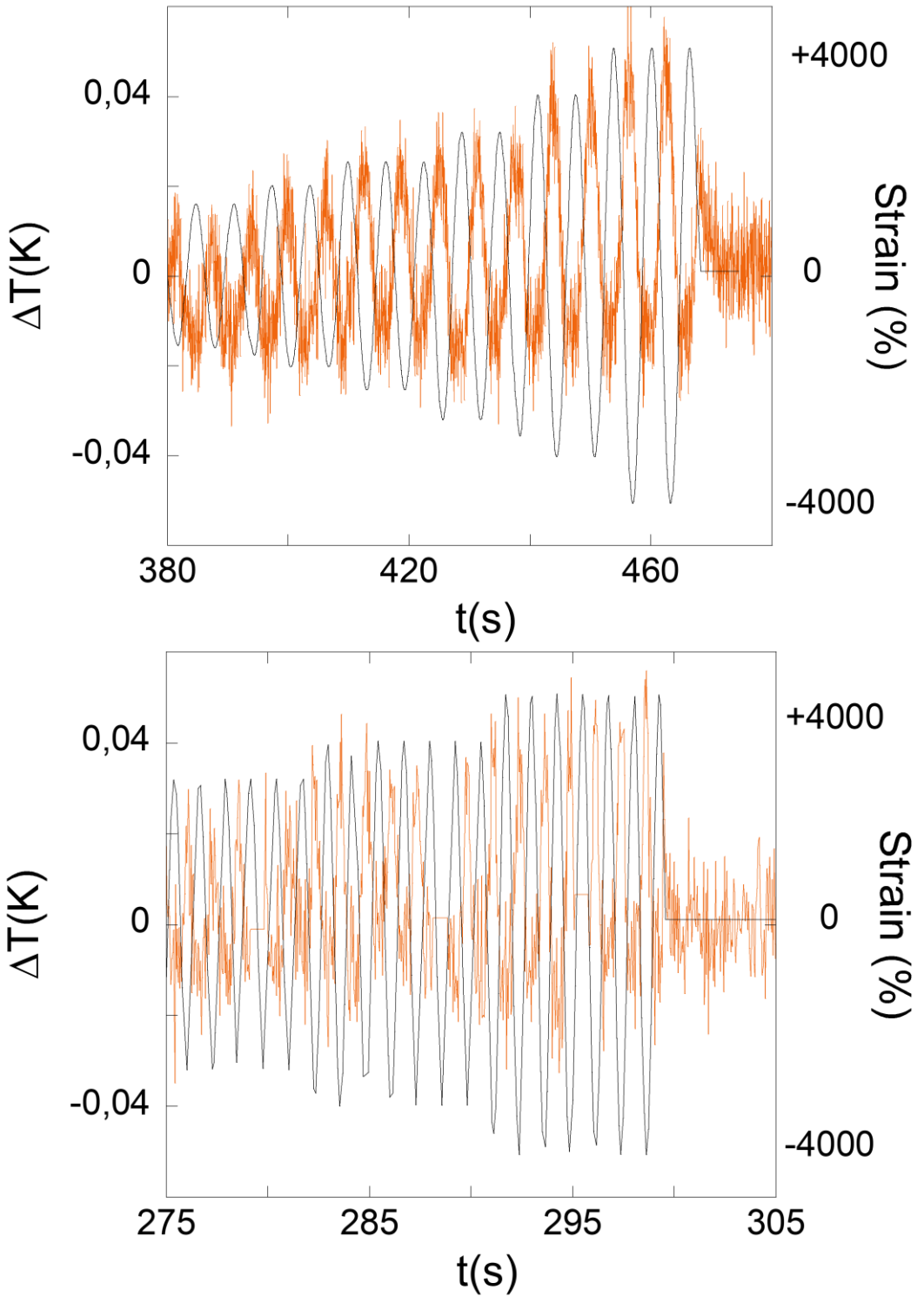

Figure 2.21: a) Average thermal variation of the liquid gap of PPG at e = 0.240mm, ω = 1rad/s, versus strain from γ_0 = 1250 to 4000%. **b)** Average thermal variation of the liquid gap of PPG e = 0.240mm, ω = 5rad/s, for various strain values γ_0 = 2500 - 4000%. The zero of the thermal variation corresponds to the temperature of the total gap under equilibrium after the applied strain. The black continuous line corresponds to the applied strain.

In Figure 2.21, the average thermal response of the whole liquid in the gap is shown for two studied frequencies ($\omega = 0.5$ & 5 rad/s). For the thermal oscillation, we observe that the negative part of the sin wave is three times smaller of the positive one for both frequencies. However, the periodicity of the thermal variation persists and its phase shift from the applied strain is $\delta\varphi < \pi/4$. Through the time scale of the measurements, there is no systematic increase of the average temperature apart from its oscillating form. Thus, as expected experimentally there is no observed systematic temperature rise (time average). The constant generation of stable thermal waves of the overall liquid system shows that it remains in non-equilibrium states as long as the shear strain is changing, and thus different energy rate is provided. This observation is in agreement with thermal diffusion time of the liquid in this scale, which is of about 0.82s based on $\tau_{th.rel.} \sim e^2/D$ ($D_{PPG} = 0.07$ mm^2/s). Thus, for the overall thermal variation to return to equilibrium state due to thermal diffusion of the acquired thermal energy, we would need slower mechanic excitation ($\omega < 0.01$ rad/s) but in such a case the amplitude of the thermal signal would be also weaker.

2.4.6 **Highlighting strain and gap dependences of thermo-mechanical effect**

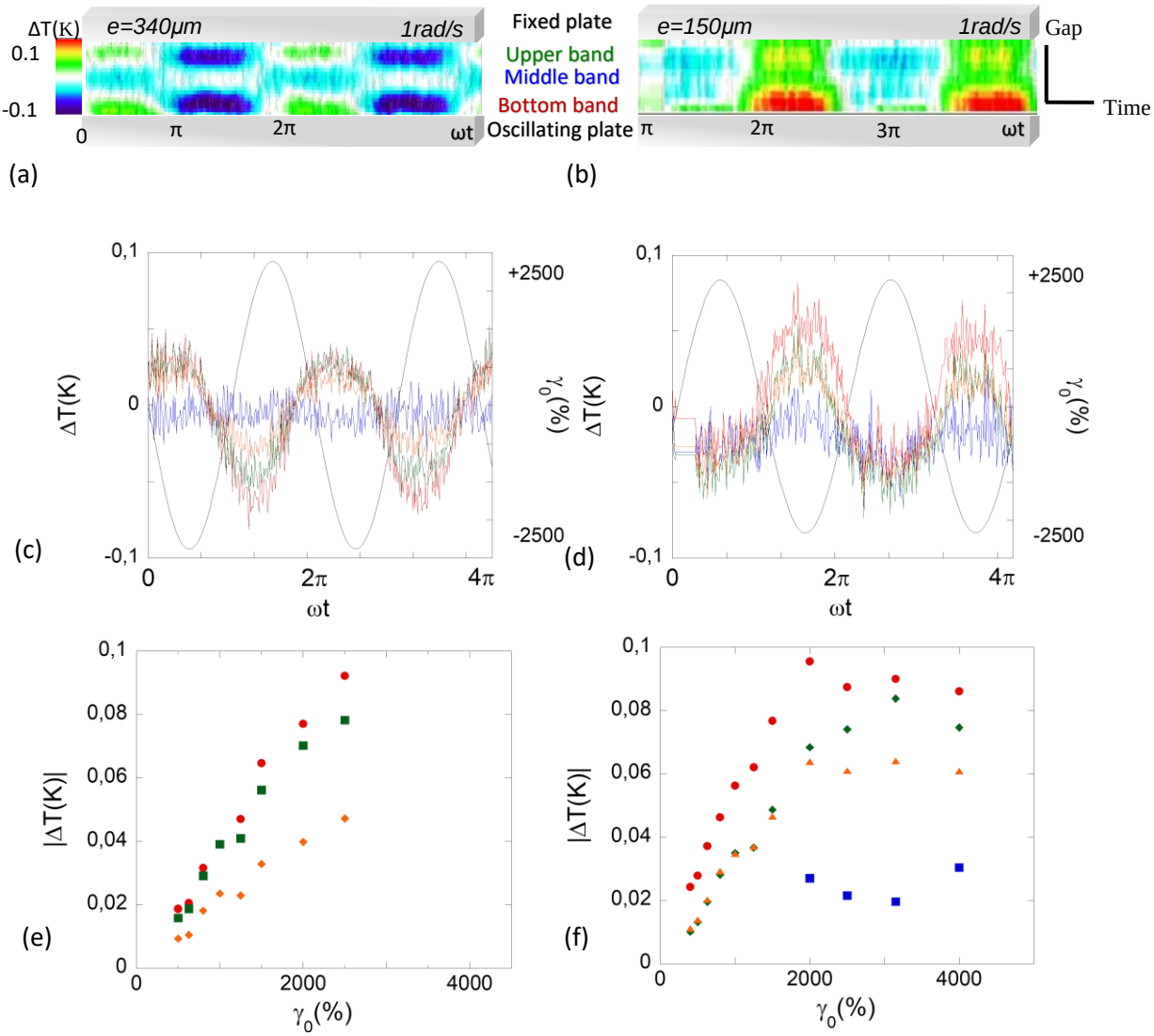

Figure 2.22: PPG-4000 confined (gap view), alumina substrate at room temperature measurements. **a)** Real-time mapping of the temperature γ = 2500% and ω = 1 rad/s (gathering about ~640 frames): at *e = 340µm* **b)** same at *e = 150µm*. **c)** Thermal waves recorded for the bottom (●), middle (■), upper (■) bands and total liquid volume (♦) respectively at γ = 2500%, ω = 1 rad/s and *e = 340µm*. The black continuous line illustrates the applied shear strain. **d)** Same for *e = 150µm*. **e)** Strain dependence of the maximum of the temperature variation amplitude (from maximum to minimum temperature) $|\Delta T(K)|$ versus shear strain as extracted from the sin harmonic fit for the bottom (●), the middle (■), upper (■) bands and total liquid volume (♦) respectively at *e = 340µm*, **f)** same at *e = 150µm.*

In Figure 2.22, we observe the thermal response of PPG for different gap thicknesses, e = 340µm (Figure 2.22a, c & e) and e = 150µm (Figure 2.22b, d & f). The 2D mapping for e = 340µm (Figure 2.22a) shares common behaviour with the one of e = 240µm (Figure 2.16a). A key difference is seen for the middle band, where for e = 340µm it appears to be larger in width. Nevertheless, its temperature does not change in a noticeable amount, if we consider that the band is stable in the y – axis position, as we do when measure each thermal band. If we consider that, the bands position may change then we notice a more considerable thermal variation (light blue to light green/white colours). This thermal variation is opposite in nature of the other two

bands (bottom and upper bands). When the middle band is cooling, then the other bands are heating and vice versa. The thermal waves of bottom, upper bands and total volume maintain a sin wave shape even for the highest strain possible for this gap thickness. For e = 150μm (Figure 2.22b), the thermal mapping appears similar to Figure 2.16b, for e = 240μm, ω = 5rad/s. Thus, even for less violent excitations as the gap thickness is decreased, the relatively stable bulk band is diminished and establishes a weak behaviour but similar with the upper and bottom bands. The only difference comes to the thermal wave shape, which resembles a sin wave (Figure 2.22d), even if the cold part of the oscillation is weaker than the hot part.

The strain dependence of PPG for e = 340μm (Figure 2.22e) is similar to the one of e = 240μm (Figure 2.17a). We notice a linear region for γ_0 = 500 – 2000% and a decrease of the slope after. Unfortunately, the restrictions of the rheometer do not allow us to increase further the strain. For e = 150μm (Figure 2.22f), we notice the same linear region for γ_0 = 500 – 2000%, but the expected second linear region has a zero-value slope instead of a smaller one, meaning that after a threshold, non-linear effect halt the temperature variation. The above stand for the bottom and upper bands as well as for the total volume. However, for e = 150μm, we also measure a weak but stable thermal response for the middle band for $\gamma_0 \geq$ 2000% yet again.

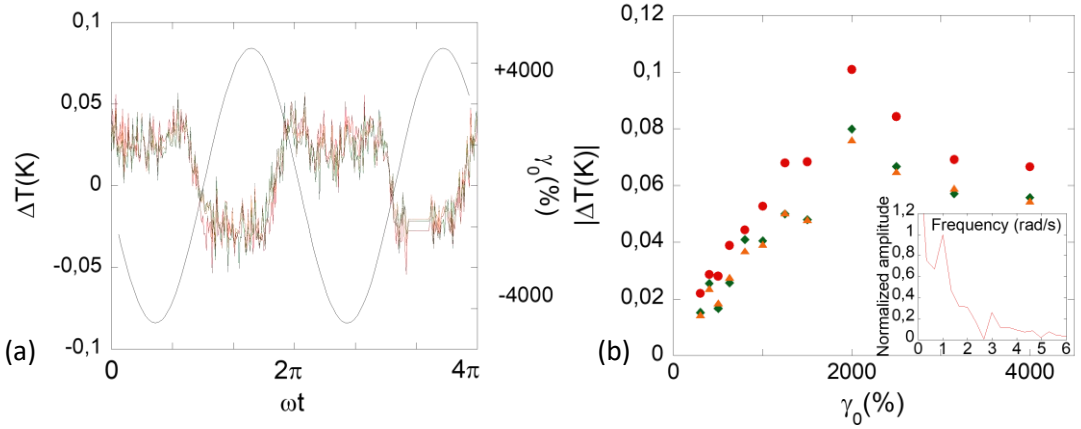

Figure 2.23: a) Thermal waves recorded for the bottom (●), upper (■) bands and total liquid volume (♦) respectively at *γ* = 4000%, *ω* = 1 rad/s and *e = 100μm*. The black continuous line illustrates the applied shear strain. **b)** Strain dependence of the maximum of the temperature variation amplitude ΔT(K) (from maximum to minimum temperature) versus shear strain as extracted from the sin harmonic fit for the bottom (●), upper (■) bands and total liquid volume (♦) respectively at *e = 100μm.* Inlet: FFT analysis of the thermal response of the bottom band for γ_0 = 2500%.

As the gap thickness of the system is reduced, its thermal response alters. In Figure 2.23a, we can observe by eye the existence of harmonics. However, in this case we observe a double pick of the maximum temperature, while the cold part is left mostly unaffected. Moreover, the two maxima correspond to zero strain value, where the velocity of the liquid is larger, hinting a viscous heating contribution. Nevertheless, as seen in Figure 2.23b inlet, the thermal variation varies from a sin-form and second and third harmonics are identified in the signal. Thus, it is possible to obtain harmonics in the thermal signal not only be increasing the frequency of the excitation but also by decreasing the scale of the system. This behaviour implies that as the scale decreases the liquid cannot integrate the energy from slower excitation, meaning that its thermal relaxation time is increasing. This result is contrary to that thermal relaxation $\tau_{th.rel.} \sim e^2/D$, where D is thermal diffusion, reduces with decreasing the scale of the system and implies that existence of longer thermal relaxation times.

In Figure 2.23b, the strain dependence for e = 100μm is shown. The linear relation of thermal variation and strain is observed for this gap thickness too and a new region is observed at $\gamma_0 >$ 2000%, where the thermal variation appears to decrease with strain. We conclude that the generated non-linear effects that lead to higher harmonics signal, are capable to even reduce the generated thermal variation under certain circumstances, like reducing scale, increasing deformation or/and increasing frequency. We should note that the maximum thermal variation $|\Delta T|_{max} \sim 0.1K$ is seen for every gap thickness value, thus no strong relation between gap thickness and the maximum value of temperature oscillation can be concluded. The fact that $|\Delta T|_{max}$ is constant with scale shows the limits of the liquid in terms of shear energy integration before exhibiting any non-linear effects. However, this thermal maximum is reached at different strain values for different system scale, meaning that sample volume plays a decisive role.

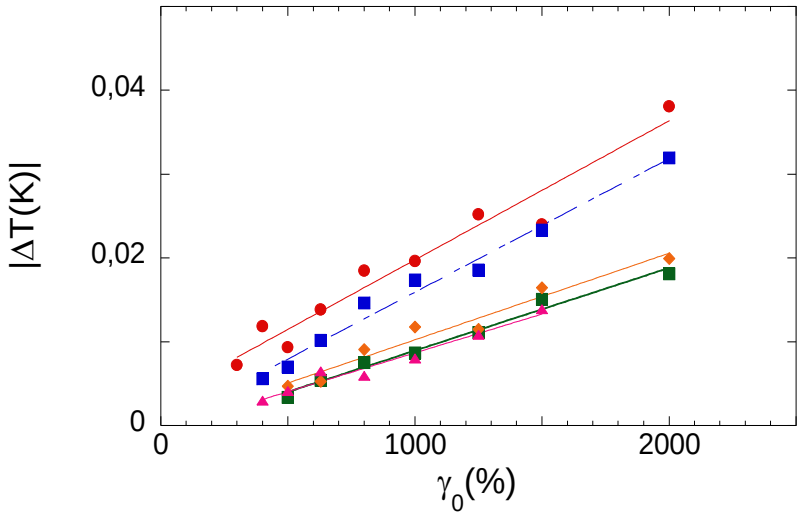

Figure 2.24: Linear region of strain dependence of absolute value of thermal variation of the whole volume (half of maximum to minimum temperature) for a periodic strain excitation of ω = 1 rad/s. Red, blue green, orange and pink points correspond to gap thickness of 100μm, 150μm, 240μm,340μm and 500μm respectively. The straight lines correspond to the respective linear fits.

As mentioned, the thermal response is linear at $\gamma_0 \leq$ 2000% for the gap thicknesses studied in this chapter.

The behaviour is consistent, but the rate of average thermal variation increase is dependent on the gap as seen in Figure 2.24. From this linear region, we calculate the thermo-(strain)elastic constant $\Theta_{shear}(\Delta T/T,\gamma)=(\Delta T/T)/\gamma$ and receive the table below:

e (μm)	$\Theta_{shear}(\Delta T/T,\gamma)$ (x 10^{-6})
100	5.5 ± 0.5
150	5.3 ± 0.3
240	3.3 ± 0.2
340	3.4 ± 0.3
500	3.1 ± 0.3

Table 2.3: Thermo-(strain)elastic constant $\Theta_{shear}(\Delta T,\gamma)$ as measured for different gap thicknesses for PPG at ω = 1rad/s.

We notice that Θ_{shear} is evolving with gap thickness. As the gap thickness decreases the Θ_{shear} increases. This is also observed from the fact that for the same shear strain value, the thermal variation increases with decreasing the gap thickness as seen in Figure 2.24. This behaviour appears to be in agreement with the notion to characterize the seen thermal effect as a thermo-elastic one.

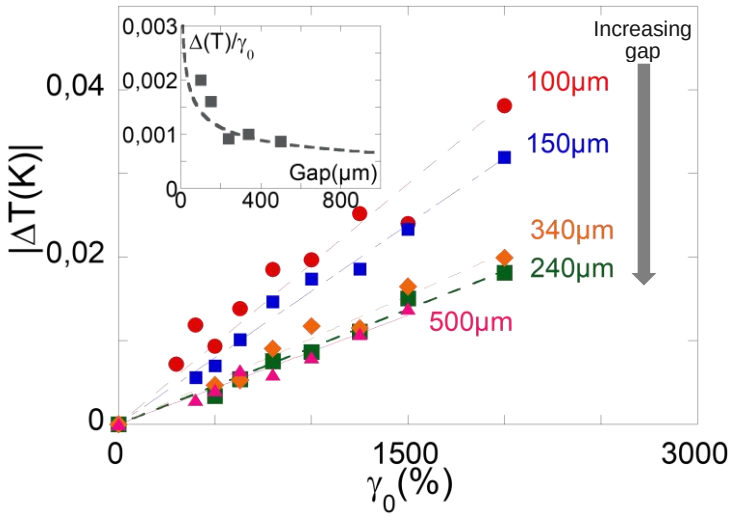

Figure 2.25: Influence of the gap size: Strain dependence of the amplitude of the thermal wave at ω = 1 rad/s at different gap thicknesses (values determined from the bulk thermal variation in the harmonic regime). Red, blue green, orange and pink points correspond to gap thickness of 100μm, 150μm, 240μm, 340μm and 500μm respectively. The straight lines correspond to the respective linear fits assuming a thermoelastic behavior ($\Delta T_{->\gamma=0} = 0$). The insert shows the evolution of the temperature variation normalized by the strain (slope value) versus gap (μm). The dotted line is a L^{-3} fit of $\Delta T_{->\gamma=0}/\gamma_0$ pointing out the analogy with the predicted evolution of the shear modulus *[29]*).

As reported recently, not only the low-frequency shear modulus G' is measurable for simple liquids (e.g. water, glycerol) [23, 22], but also the shear modulus follows a scaling law $G' \sim e^{-3}$ [29, 90], meaning that for standard liquids, its elastic nature is more evident as the scale of the system is decreased, which is in agreement with the presented results. If we consider zero thermal change at zero strain, then we receive the points seen at Figure 2.25 inset and we see an e^{-3} evolution for the $\Delta T/\gamma_0(e)$ slope. Another parameter to be considered for the tendency of increased slope is the volume of the system. As the volume is decreased, smaller and smaller quantity of liquid will incorporate the same given shear energy (same strain), giving a higher thermal response. This parameter would be considered for gap thicknesses, where the bulk middle band is not present ($e \leq 150\mu m$). The vanishing of the thermal effect at large scale is in agreement with the common observation of absence of noticeable thermal macroscopic effects.

2.5 Large gap thickness thermal response

In the previous section, we observed that the thermal response is related to the scale of the system for PPG. With higher thickness, we get weaker thermal response. Here, we will show that the scale dependence seems to be generic also observable for the case of glycerol.

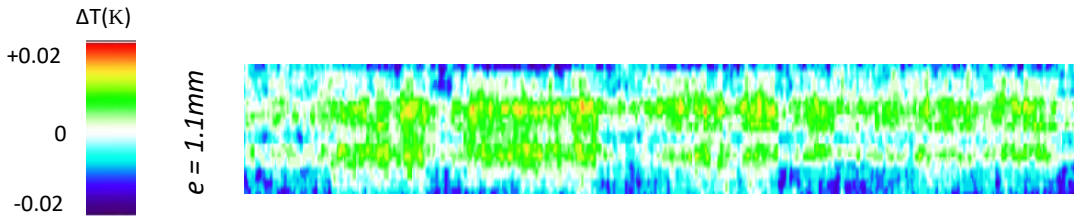

Figure 2.26: Thermal 2D mapping of glycerol for **a)** e = 1.1mm, ω = 1rad/s, γ_0 = 500 - 800%.

In this section, we study the thermal effect at higher scale. In Figure 2.26, are displayed the thermal evolution of glycerol at e = 1.1mm. We notice that the temperature does not change during the periodic strain oscillation except from the area close to the oscillating bottom plate. However, the thermal oscillation is weak and observable only at the highest strain value (800%), making difficult to conclude if a systematic thermal oscillation is possible at such gap thickness (Figure 2.26). As the thermal effect is not observed for high gap thickness, it is deducted that the effect is scale dependent since its response becomes greater for smaller excitation as the scale of the system is reduced. Of great interest would be if we implement higher strain values to large gap thickness systems, which is not feasible with the present instrumentation.

2.5.1 **Stability of thermal signal**

Next, we study the stability of the thermal effect. We set an example as seen on Figure 2.27 of PPG-4000 at almost 1mm thickness and frequency of 1 rad/s. We notice that the gap thickness is large and thus the thermal response is weak relatively to lower gap. Specifically, the minimum to maximum amplitude is about 0.015K for the bottom band closer to the moving plate, further confirming the gap dependence of the thermal effect. For the other two bands (middle and top), we observe that the thermal variation is even more limited to 0.01K.

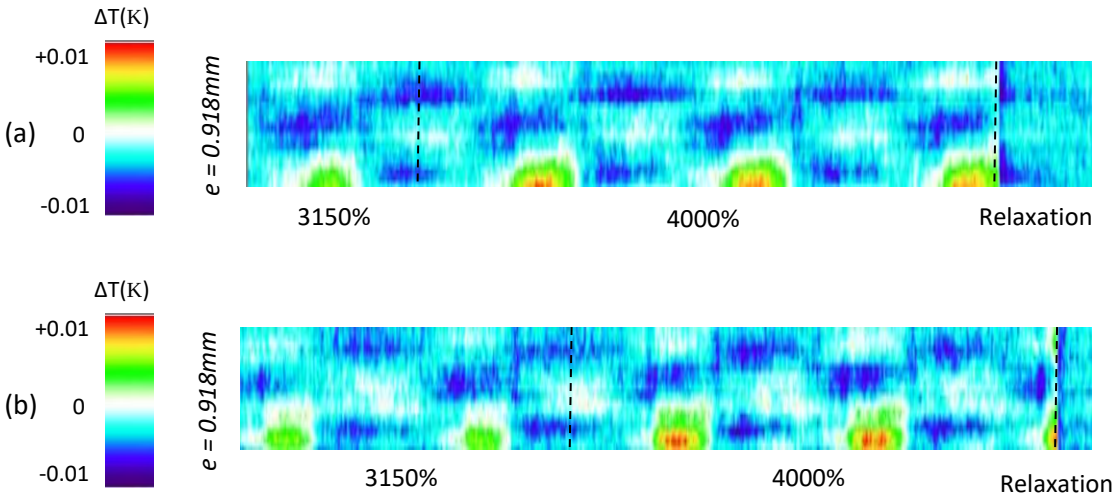

Figure 2.27: Thermal response of PPG-4000 at e = 918µm, ω = 1rad/s at 3150% and 4000% strain values. **a)** Measurement before continuous shear rate. **b)** The same measurement after the liquid was subjected at a shear rate of $15s^{-1}$ for 180s.

Later, we subjected the liquid under continuous shear rate of $15s^{-1}$ for 180s and then we conducted the same oscillatory measurement (Figure 2.27b). We observe that the thermal response of the whole gap does not change and remains nearly similar after the pre-shear. This result could be in agreement with the fact that the liquid responds thermally for different gap thicknesses even though at each gap thickness the oscillatory shear strain is large enough to make the liquid flow (e.g., solid-liquid slippage, liquid-liquid interfacial slippage due to generated shear bands). This stability of the thermal measurements seems to challenge the apparent viscous response measured by rheology at large strain amplitudes; shear elasticity measurements where the generated slippage due to high shear will be sufficient to destroy the transmission of stress from the moving plate to the liquid and thus elastic modulus would be devaluated or even immeasurable. Thermal measurements can consistently show an elastic response, without perfect conditions being present.

2.6 Time evolution of the thermo-elastic effect

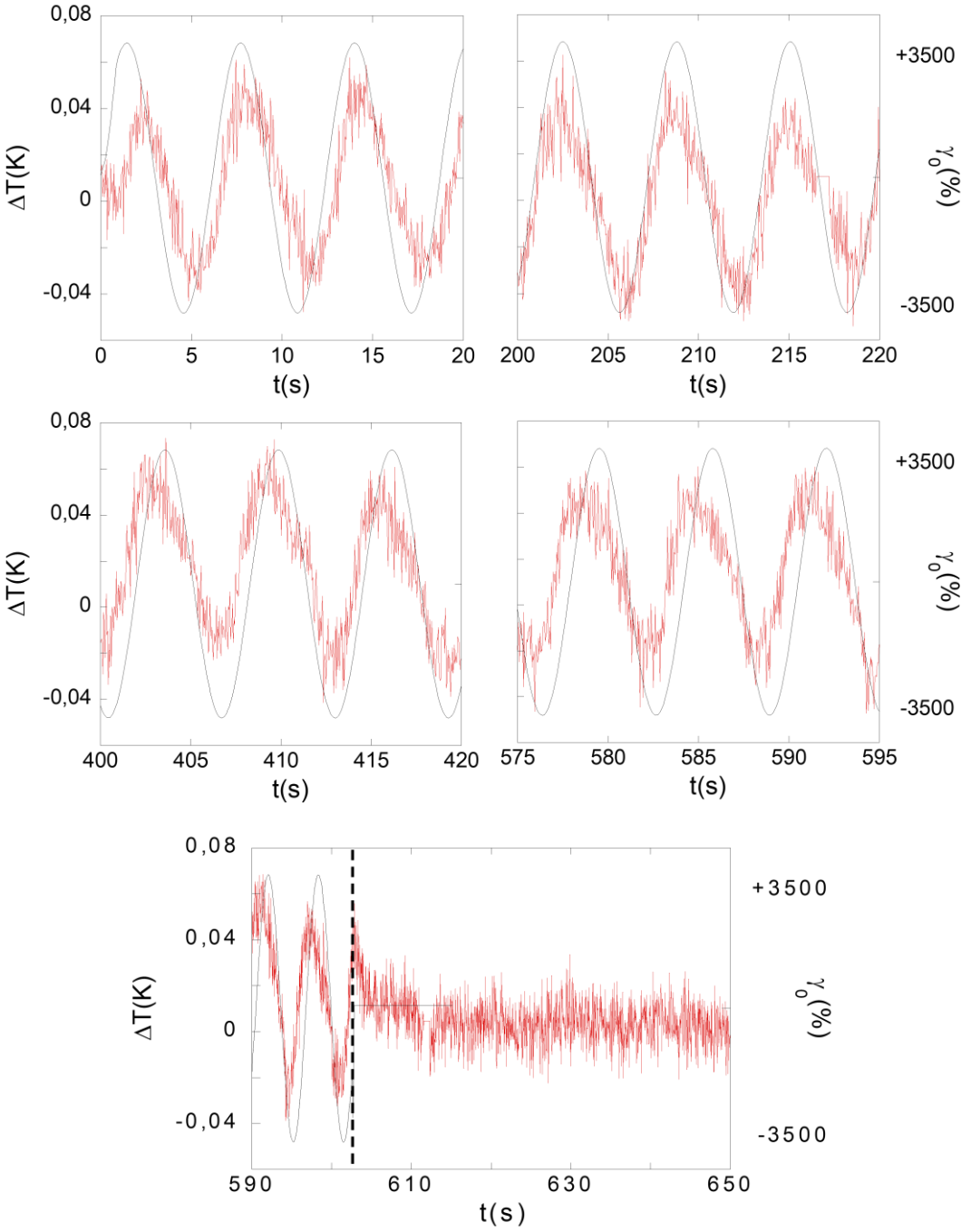

Figure 2.28: Time evolution of thermal response of bottom band close to oscillating plate in relation with applied shear strain. Glycerol, e = 240µm, ω = 1rad/s, γ_0 = 3500% for 600s. Alumina plates diameter d = 40mm.

Another question rises if we wonder about the time evolution of the thermo-mechanical effect studied in this chapter. In Figure 2.28, we see an example of a time experiment where we applied an oscillation shear strain γ_0 = 3500%, ω = 1rad/s to a glycerol sample of e = 240µm enclosed between two alumina plates of diameter d = 40mm. Unlike the strain sweep experiments where the strain was increasing every two to three oscillations, here we start

instantly with a very large shear strain value and apply this value for a long time. We notice that the bottom band first is heated and for the first oscillations the phase between the thermal response and the strain is different from the one reported in this chapter. Instead of the thermal response to be in advance of the strain is in arrears ($\delta\varphi \sim 50^{o}$). However, this behaviour does not appear to be constant. As we notice from the time progression in Figure 2.28, the phase shift is not constant but changes with time. Specifically, the phase shift is decreased gradually to zero value and then increases again but on the opposite side where the thermal response is in advance of strain, restoring the general picture that we observed during the various strain sweep measurements. Within the error bar of the measurement, we deduce that the thermal variation does not change even 10 minutes after the start of the oscillations, with the maximum thermal variation (from maximum to minimum values) being around 0.06 – 0.07K. However, we should keep in mind that the studied thermal band could displace slightly within the gap, while for this demonstration it was considered as spatially fixed over time. The constant nature of the thermal variation is also observed at the total volume response (Figure 2.29) and remarks the stability of the thermal effect. We notice that the waveform of the thermal response is not exactly a sin one but an asymmetric sin wave. The slope of the temperature increase region is bigger than the slope of the cooling counterpart. This mechanism is more noticeable at the response of the total volume of the same experiment (Figure 2.29). This implies that the thermal response is a non-linear one. However, the stability of the thermal response is maintained, showing that non-linear effects emerge when the offered shear energy is over the limit that the liquid can accept. The limit is constant when the parameters do not change, like in this time measurement, but changes with scale. On the last graph of Figure 2.28, we record the end of the measurement. We observe that the rheometer stops the measurement at a random strain value since we are unable to impose the value ourselves. However, at this certain value, the band temperature is out of equilibrium. As soon as the strain is stopped (vertical black dotted line), the temperature appears to relax in an exponential manner to its equilibrium value. This result shows the existence of relaxation time of the thermal effect. A more in detail study will follow in the next chapter.

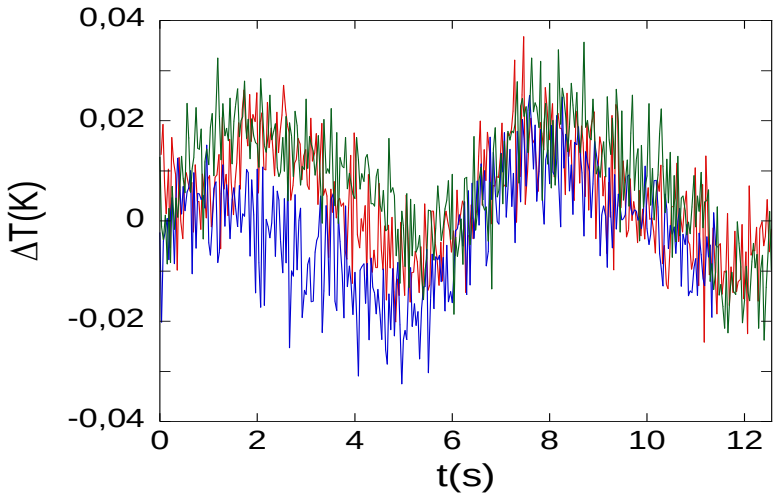

Figure 2.29: Evolution of thermal response of the total volume of glycerol at e = 240μm, ω = 1rad/s and γ_0 = 3500%. Red, blue and green line correspond to thermal oscillations at t = 0s, t = 300s and t = 580s from the start of the shear strain.

An interesting result was observed for a measurement of same experimental conditions but shorter in duration (Figure 2.30). Here is noticed that the thermal response of the bottom band

is not a sin wave but a complex harmonic one. A significant change in respect with the Figure 2.28 is the behaviour of the temperature at the start of the excitation. We first notice an increase of the temperature at the strain onset observed at the same strain for the two examples. However, in the second case, a strong cooling is achieved before the heating while in Figure 2.28, only a hint of a cooling is observed. This could mean that the established thermal response could be dictated by the initial response of the system. In Figure 2.30, there is no observed phase shift, while the temperature variation is constant during the measurement with value at approximately 0.04 - 0.05 K. Figure 2.30 shows a slightly different mechanism of the thermal response from the one described initially and strongly resembles the response at lower thicknesses (Figure 2.23). The thermal response does not follow in this case the direction of the moving plate by increasing or decreasing continuously from minimum (negative) strain to maximum (positive) strain or vice versa, as reported in the majority of the reported responses. Thus, instead of one maximum and one minimum of the temperature along one period, two maxima and two minima are reported. The maximum values are achieved a little before zero strain, while the minimum temperature little before we arrive at peak strain value (as an absolute value). Thus, when the shear strain is increased (from zero to maximum value), the liquid decreases its temperature (stretching phase), while on the opposite direction it increases its temperature (compressed phase). The tendency to this behaviour is the main reason of the created harmonics. However, the behaviour is not observed if frequency or/and system scale requirements are not met because it is not favoured from energy point of view. To change the state of the liquid from a compressed to stretched state or vice versa, while the liquid has established maximum velocity at zero strain should be more costly from a change of thermodynamic state when the liquid is immovable temporally at maximum strain.

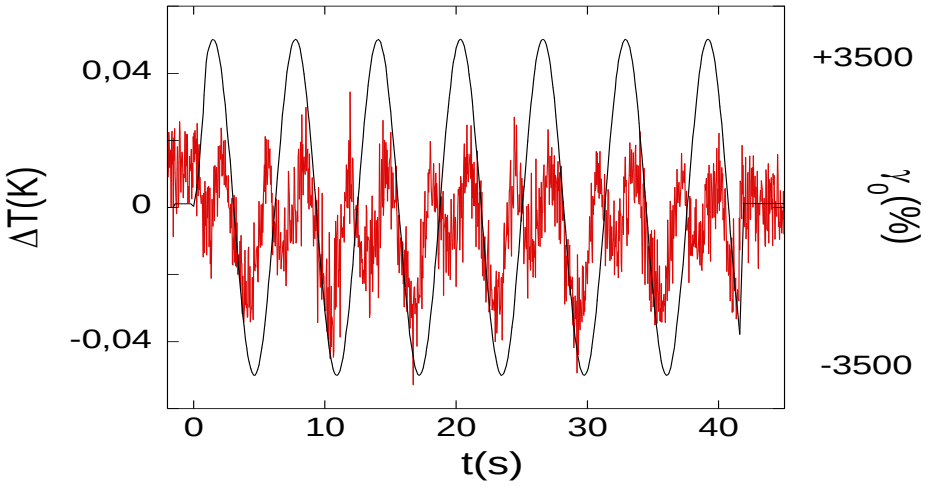

Figure 2.30: Time evolution of thermal response of bottom band close to oscillating plate in relation with applied shear strain. Glycerol, e = 240μm, ω = 1rad/s, γ_0 = 3500% for 35s. Alumina plates diameter d = 40mm.

2.7 Thermal response of glycerol and strain dependence:

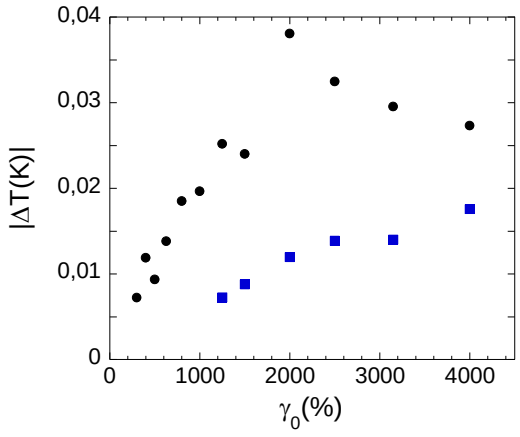

Figure 2.31: Strain dependence of the maximum of the temperature variation amplitude ΔT(K) versus shear strain as extracted from the sin harmonic fit for the total liquid volume of PPG (●) and glycerol (■), at *e = 100µm* and ω = 1rad/s.

The glycerol ($C_3H_8O_3$) is a well-known liquid due its extremely wide range of uses and its biocompatibility. It is a glass former which exhibits at room temperature of viscosity (η= 1.41 Pa.s) and glass transition temperature at T_g = -93 °C. The molecular relaxation time (~ 10^{-9}s) is far away from the dynamic range of mechanical tools, being accessible by Brillouin scattering at 7 GHz *[146, 147]*. In Figure 2.31, we observe the thermal response of the total volume for glycerol and PPG. It appears that the thermal response of glycerol is weaker than the one of PPG and it is more difficult to detect it as the strain value decreases. Then why the thermal amplitude appears different if glycerol and PPG have similar viscosity values (1.4Pas to 0.98Pas respectively) and are both glass formers? What we could hypothesize, is that the interaction of glycerol molecules is different since PPG is an oligomer with polymer chains consisting of 68 repetitive units. This extra cohesion granted to PPG could possibly be responsible for this discrepancy of their thermal variation amplitude difference.

2.8 Thermal response of water

In this section, some measurements were conducted on liquid water. However, water plays a dominant role in everyday life, especially to biology, where all body liquids have water as their main ingredient. Thus, its study is of great interest. Water (H_2O) is a hydrogen bond polar molecule. At room temperature, its viscosity value is $0.89*10^{-4}$ Pa [148]. The relaxation time of water is of 10THz [149].

Water stands also as a great challenge to the thermal measurements due to its evaporation. Since, water has a high evaporation rate and the volume of liquid used small, the measurements should be conducted rapidly.

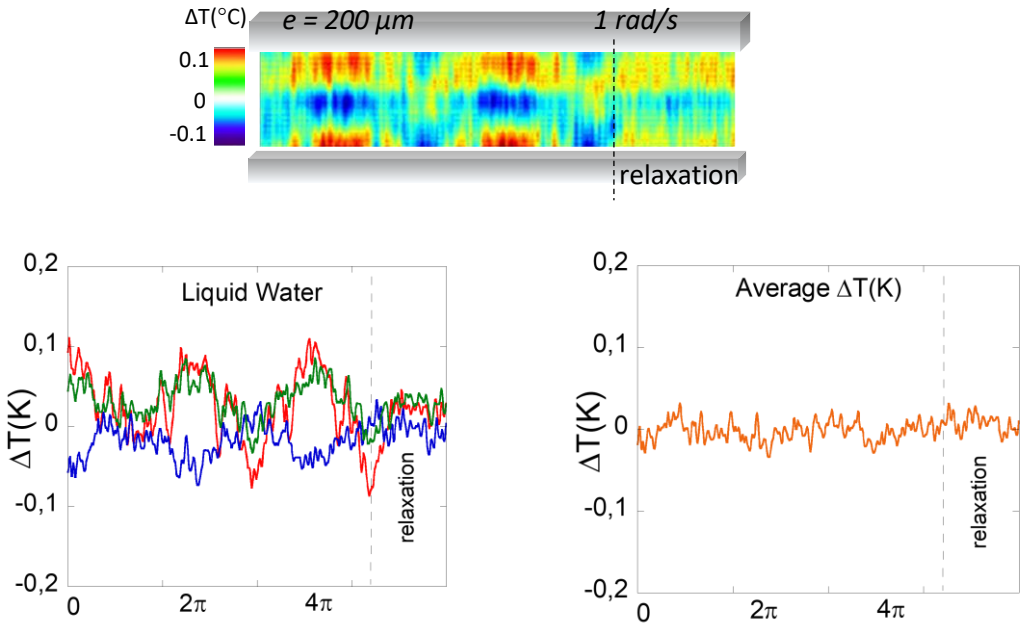

Figure 2.32: Thermal waves exhibited by a liquid water layer confined between wetting surfaces (gap: 200 µm, 1 rad/s, 4000%). Green, red and blue lines represent upper, bottom and middle waves respectively. The yellow line shows the average thermal variation in the layer (alumina substrate, room temperature measurements).

In Figure 2.32, we observe the thermal response of water at thickness of 200µm and frequency of 1 rad/s. From the 2D thermal mapping (Figure 2.32a), we notice that the response to an oscillatory motion stands similar in respect with PPG-4000 and glycerol. We observe that the established thermal bands are two and are of the opposite nature in accordance with [150]. Top and bottom band oscillate in a synchronous matter, but they have opposite temperature response. This can be seen from the Figure 2.32b. Here, we observe that top and bottom bands oscillate with minimum to maximum variation of around 0.01K with the maxima and minima of the bands being synchronous. For smaller strain values, a thermal response is not detected within the experimental error bar. Lastly, the average temperature change in the water seems not to oscillate over time (Figure 2.32c), which is in agreement with the observation since the thermal bands compensate each other. Such a result means that in average, water does not change its average temperature, with this not being the case locally, where thermal bands can be generated when the conditions are appropriate. It also shows that the liquid can generate different thermal behaviors with different band locations, but all keeping in time and/or in space, the average sample temperature unaffected (in the linear range of strain amplitude).

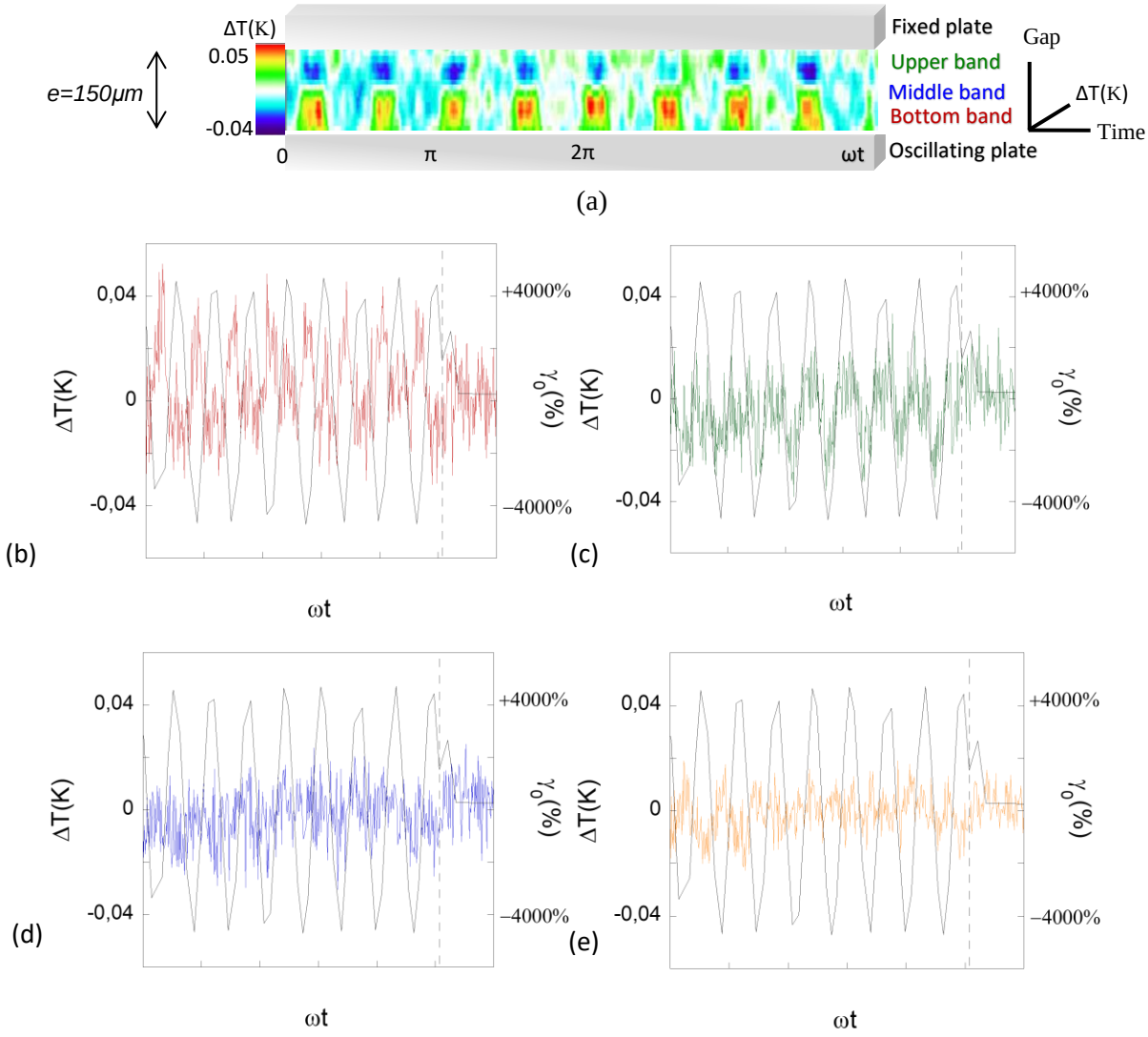

Figure 2.33: Thermal response of water of e = 150μm, ω = 10 rad/s at 4000% oscillatory strain value. **a)** 2D thermal mapping for γ_0 = 4000%. Dashed vertical line shows the moment where the strain stops. **b)** Bottom band. **c)** Top band. **d)** Middle band. **e)** Average bulk response.

Next, we study the thermal response of water for 10 rad/s (Figure 2.33) for e = 150μm. This high frequency value is of interest since it corresponds to average heartbeat rate, and we know that blood plasma contains about 90% of water. We observe a slightly different thermal response, where two thermal bands are generated (Figure 2.33a). However, in this case the thermal bands are well defined spatially and not fluctuate at different height over time. The temperature amplitude of the bands and average bulk scales from 0.015K – 0.035K for strain values from 2000% - 4000%. The thermal bands exhibit harmonics as in the case of PPG-4000, 5 rad/s, meaning that frequency plays like strain an important role in the thermal response. We notice that the thermal variation is of the same amplitude as the 1 rad/s, further showing that there is a maximum temperature variation, which is not strongly dependent on the frequency of the excitation. The phase shift of the thermal bands is about zero, like PPG-4000 5rad/s, meaning in-phase elastic behaviour, which deviates from the case for slower dynamics (e.g., 1 rad/s). The average thermal variation of the bulk does not exhibit any oscillatory change. These thermal changes observable for high frequency (10 rad/s), are of interest to study since the experimental conditions are close to blood plasma circulation that contains 90% of water of blood vessels of various diameter from μm to cm. It reveals that even if the water has low viscosity, is still capable to express elastic collective behaviour. Of course, a more detailed and

elaborate set of experiments is needed to reach definitive conclusions. However, with the present experimental setup, an extensive and accurate study of liquid water under slow (relatively to the molecular dynamics) mechanical excitation is limited without evaporation rate control. For this reason, a more elaborate system should be used, and a possible candidate is a standard microfluidic channel. The microfluidic channel is closed, preventing evaporation and various channels with different widths and heights can be created. A consideration is that the top view of the chip should be transparent (fully or partially) to infrared radiation, for the acquisition of the thermal response.

2.9 Mechanical response

2.9.1 **Shear stress and thermal waves**

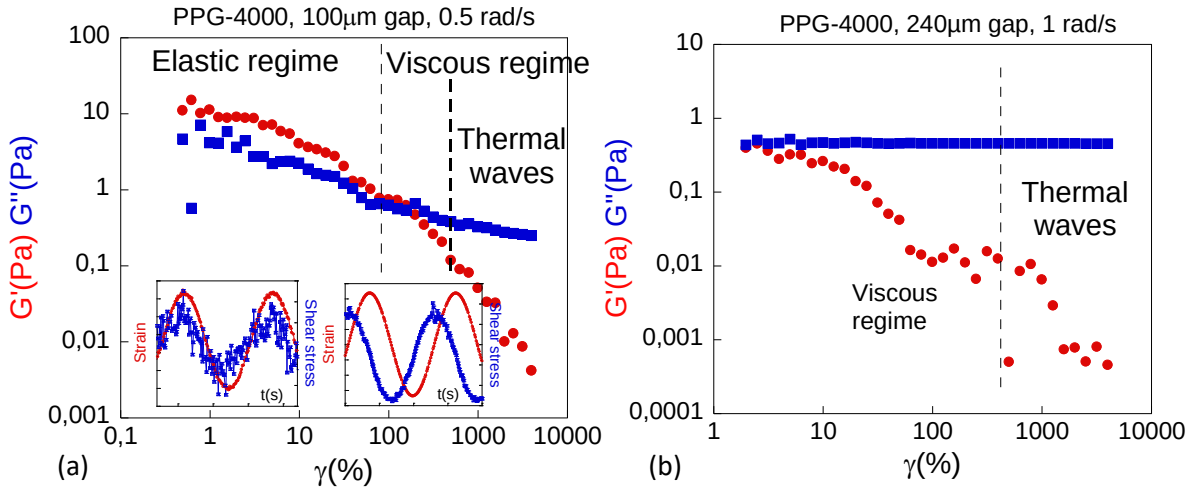

Figure 2.34: Storage and loss moduli of PPG-4000, e = 100µm, ω = 0.5rad/s, wetting substrate conditions (alumina). **a)** Shear strain dependence of the moduli. Left insert: Shear strain and stress evolution with time for shear strain amplitude in the elastic regime. Right insert: Shear strain and stress evolution with time for shear strain amplitude in the viscous regime. **b)** Strain dependence of storage and loss moduli of PPG-4000, e = 240µm, ω = 1rad/s.

Figure 2.34 displays the strain-stress viscoelastic spectrum of PPG4000 at 1 rad/s and confined geometry (using the wetting protocol with alumina substrate). A shear elastic plateau is identified at low strain amplitude, visible at 100µm and almost at 240µm [23]. As seen in Figure 2.34a, a shear elastic response is detected from small strain values up to 100% applying a low-frequency excitation much smaller than then inverse of the basic relaxation time as defined from Maxwell theory (~ 10^{-9}s). The elastic modulus is relatively constant in this area and greater than the viscous modulus (elastic regime); i.e., the stress response is nearly in-phase with the strain wave (left insert of Figure 2.34a). As the strain value grows, the liquid loses its ability to resist flow, as seen from the rapid decrease of the measured elasticity (viscous regime – right insert of Figure 2.34a).

The regime at which the thermal waves are detected is at large strain amplitudes. It corresponds to a regime, where the shear elasticity is not accessible since the measurement indicates that the flow behaviour is dominant. Our main thermal observations are carried out in the so-called viscous regime of high shear strain (>250%), in a region where the flow (viscous) behaviour dominates (Figure 2.34a, thermal waves regime). How to conciliate the apparent viscous response and the identification of a thermal response? Even if shear elasticity is not dominant in the conditions of the thermal effect observation, being able to measure a finite shear elasticity value at low strain is important. It means that the shear elasticity at low-frequency regime and gap values below 200µm is not zero but finite. In other words, the viscous regime at large strain amplitudes might be the "strain-thinning" of the initial elastic response. Does it mean that the initial elasticity is strain-melted or that the viscoelastic measurement is not adapted to identify shear elasticity at large strain?

Since the thermal waves exhibit characteristics of an elastic-like mechanism (section 2.4.2), it might be possible that the elastic nature of the liquid is revealed via its thermodynamic state.

We are not in a position to provide an experimental answer about the thermal response at strain amplitude lower than < 250%. However, we cannot conclude that no response exists in this region, because of the linear dependence of the thermal signal with respect to the strain amplitude, also verified at different gap thicknesses (Figure 2.25), the thermo-mechanical is proven to be linear. Thus, a thermal response may be present, but not detected due to the thermal noise limitation of the IR setup. As seen, there is a general tendency suggesting that the thermal response tends simply linearly to zero strain.

2.9.2 **Shear and normal stress variations during thermo-elastic effect:**

As mentioned in the previous section, the thermal waves are observed for in the high shear strain regime (from 350% to even 9500%) amplitudes. This range corresponds typically for large amplitude oscillatory shear measurements to values that reach the rheometer's limits at the certain gap thickness. At these strain values, the shear stress indicates the viscous response as seen from its mechanical response (Figure 2.34 and Figure 2.35a)

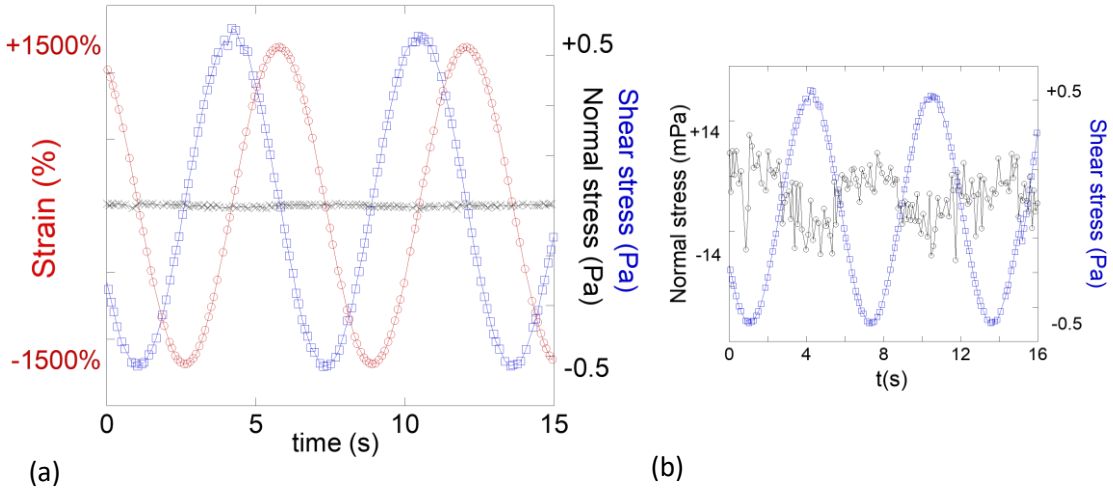

Figure 2.35: a) Strain, normal stress and shear stress variations for PPG 0.340mm at ω = 1rad/s and γ = 1500%, where thermal waves relate to sin waves (only fundamental harmonic). The shear stress is π/2 phase shifted with respect to the strain signal. **b)** Details of the normal stress (mPa) and shear stress (Pa) signal for PPG 0.340mm at ω = 1rad/s and γ = 1500%.

In Figure 2.35, the mechanical response of PPG is highlighted at relatively high strain (γ = 1500%), but within the linear region of thermal variation (see Figure 2.25). In Figure 2.35a, we compare the shear stress and the normal stress variations recorded during the thermal measurements detailed in 2.4.6. The stress response is a sin wave in advance with the strain wave, sharing the same frequency and a relative phase shift at around 90º. This is a typical viscous behavior, meaning that the stress behaviour is the standard one of a Newtonian liquid under low-frequency oscillatory shear. However, we have observed that in this flowing regime, the mechanical energy partially converted in thermal bands. This means that the conventional rheology is unable to detect internal stress changes revealed by the temperature differences, the bands should possess different stress states form each other.

The normal stress variation is below the rheometer accuracy. However, they seem oscillate periodically. Its relative phase shift to strain is approximately 90º, meaning that it is on phase (but opposite amplitudes) with the shear stress. The maximum variation of the normal stress is less than 2% (~15mPa) in comparison with the variation of shear stress, meaning that the normal stress response is weak and negligible. The examination of the normal stress is nevertheless interesting. First, it confirms that the origin of the thermal waves is not due to any parallelism defect and thus the shear stress is at the origin of the thermal effects.

Second, variations of normal stress are known within the context of vorticity banding seen in soft matter materials [97, 98]. In this case, bands of different stress states exhibit under shear rate giving rise to a normal stress. We could view our system in a familiar manner since the thermal bands are areas of different stress states. In these measurements, we are able to measure

the normal and shear stress over the whole volume and not for each band individually. Moreover, the measured normal stress is below the sensor limitation. How to understand the absence of significant normal variation in our case? Actually, we have also observed that these different thermal states balance each other to minimize the total free energy. As a result, the nearly instantaneous compensation of the stresses (visible by the superposition of hot and cold bands in the thickness) diminishes strongly the global bulk stress, minimizing the normal stress. We show in the next chapter that it is no more the case in the conditions of a step strain experiment.

In Figure 2.36a, we show the evolution of the normal force with strain as second thermal harmonics develop (Figure 2.36c). We observe generated harmonics as well for normal force with peaks at shear stress minimums and maximums (zero strain points), thus maintaining its relation to shear stress as in Figure 2.35. When, third thermal harmonics develop (Figure 2.36b, d), the normal force seems to be in phase with the thermal waves and deviates its response from the shear stress, which maintains its conventional $\pi/2$ shifted sin-wave form. At higher scale (0.240mm), part of the energy is dissipated on the bulk, allowing a smoother transition of temperature by maintaining an almost thermal sin-wave form, while at smaller scale dissipation on the liquid volume becomes restricted. When third thermal harmonics exhibit, the normal stress variation becomes non-linear, similar to the rise of normal stress of solids under shear, known as Poynting effect. Reports on the normal stress variation under shear strain is observed mainly on solids *[151, 152, 153]*, while new reports highlight negative normal stress in biopolymer gels *[154]* that could eventually lead to rearrangement processes of the chain due to failure *[155]*. The present results hint that thermal variation, shear stress and normal stress may be connected as balance mechanisms. All the parameters are quantities that elucidate the efforts of the liquid to minimize its total free energy during the integration of the given shear energy by creating unstable non-equilibrium thermodynamic states prioritizing the regions near the interfaces. However, we should point out that shear and normal stress are measured over the whole liquid volume, and it is not possible to measure the stress of an individual thermal band, thus making the connection between stresses and thermal waves difficult. Moreover, great attention should be given on the normal stress since it is below the sensor limitation.

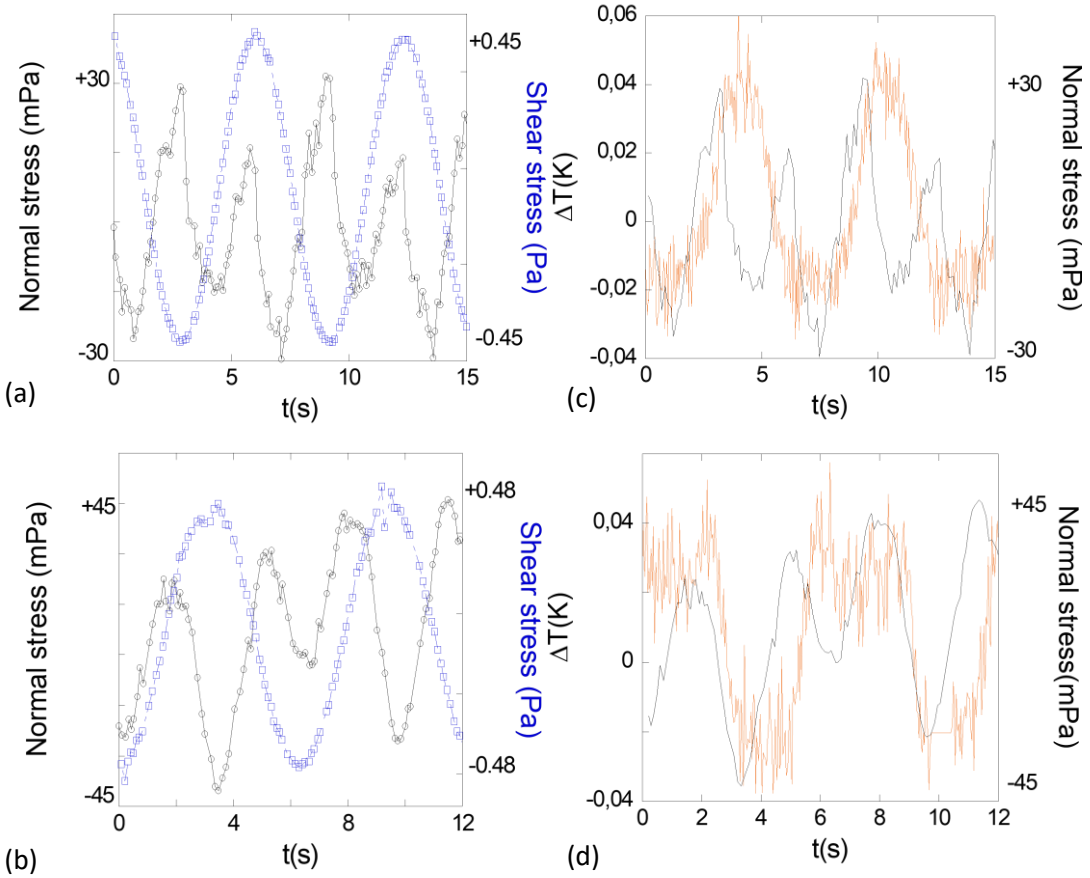

Figure 2.36: a) Normal and shear stress signal for PPG 0.240mm at ω = 1rad/s and γ = 2500%, where the thermal wave develops second harmonic. **b)** Same for 0.100mm, where the thermal wave develops second and third harmonics. **c)** Thermal waves recorded for the total liquid volume (♦) at γ = 4000%, ω = 1 rad/s and $e = 240\mu m$. The black continuous line illustrates the measured normal stress. **d)** Same for $e = 100\mu m$.

A great challenge for the described thermal effect is the understanding of the stress in the different thermodynamic regions in the liquid. We are unable to measure the stress state of these regions since the measured shear stress is over the whole volume. Moreover, at high shear strain values slippage interfaces are generated between the liquid and substrates or even within the liquid, further reducing the measured stress. Deviation of the shear stress from the viscous conventional response was not reported (Figure 2.35). However, we observed weak changes on the normal stress (Figure 2.35), which may be coupled with the shear strain as discussed in previous paragraphs. A connection between normal stress and thermal variation is observed from the thermoelastic theory. The simple equation of stress in a thermoelastic isotropic solid is given as [49]:

$$\sigma_{ij} = \frac{\nu E}{(1+\nu)(1-2\nu)}\varepsilon_{kk}\delta_{ij} + \frac{E}{1+\nu}\varepsilon_{ij} - \frac{\alpha E}{(1-2\nu)}\Delta T\delta_{ij}$$

where, ε_{ij} is the strain tensor, σ_{ij} the stress tensor, ε_{kk} the dilatational components, E the bulk modulus, ν the Poisson ratio, α thermal expansion coefficient. This equation proposes that the volumetric strain ε_{kk} is the connection between thermodynamics and mechanics and relates temperature change with the normal stresses. To clarify, the above equation is not expected to stand true for the case of liquids in this form since other parameters should be taken also into account for the scale dependence of the thermal property, in mesoscopic liquids but stands as a

starting point to understand the mechanism of the seen thermal effect. Even if the measurements are below the device resolution, an interesting comparison might be attempted since in some cases, normal stress and temperature variations show similar harmonic evolution, since both normal stress and temperature seem to show harmonic behaviour (Figure 2.36). As shown in [44], at high shear amplitude, normal stresses are possible to generate with double the frequency of the excitation. These normal stresses could be connected with the oscillating part of temperature rise due to viscous dissipation [140], which also share the same frequency as the normal stresses. Thus, we may assume that the generated even harmonics (in our case, we identified only the 2^{nd} harmonic contribution) of the thermal signal could relate to dissipation processes, while the odd harmonics with elastic processes (like Poynting effect). As mentioned, the measured normal stress is over the whole volume and below the limitation of the sensor, but nevertheless its evolution with the scale and its apparent connection with the evolution of harmonics of the thermal bands may hint that the described thermal effect is viscoelastic in nature.

Chapter 3 Thermo-mechanic response under step shear strain and thermal relaxation mechanisms

In the previous chapter, we studied the thermo-mechanical response of fluids under oscillatory shear. When the motion stops, the moving plate goes back to its equilibrium position. As the equilibrium position is reached, the temperature of the thermal bands tends to its equilibrium temperature position. As described in Figure 3.1, the temperature (here bottom band) relaxes rapidly to the equilibrium temperature when the motion stops. However, we notice that its relaxation differs with gap thickness. For large gap thickness (Figure 3.1b), the relaxation seems nearly instantaneous, while for small gap thickness (Figure 3.1a), longer time is needed to reach the equilibrium temperature. Thus, questions arise on the nature of this thermal relaxation time, as well as its relationship with the sample size. We focus its study on a new type of measurement in the present chapter.

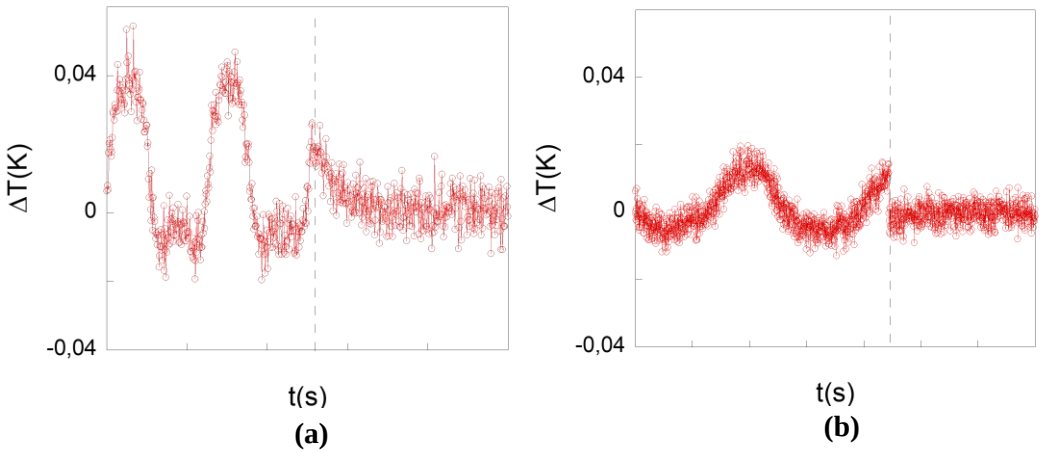

Figure 3.1: Influence of the sample size on the thermal relaxation time (bottom band) of PPG-4000 right at the stop of the oscillatory excitation for **a)** e = 240µm, **b)** e = 918µm gap thickness. Black dotted line shows the time where the strain is removed.

In the chapter, we try to investigate mechanisms of the thermo-mechanical effect in mesoscopic liquids introduced/evidenced in the previous chapter. For this study, we test the thermal stability of the liquid to a shear step strain. The interest is to examine the thermal response to this sudden deformation since the relaxation scales the different relaxation times that have been excited.

Chapter 3: Thermo-mechanic response under step shear strain and thermal relaxation mechanisms

We use liquid glycerol at room temperature. Glycerol exhibits almost similar properties as PPG-4000, a similar viscosity, a weak evaporation rate, a molecular polarity, and a glass transition temperature, but it is a molecular liquid (and not an oligomer). The use of glycerol is justified due to its popularity on various field applications and its "simplicity" as a molecule in relation to oligomer (PPG-4000) and polymer melts acts as a step to establish the seen thermal effect as a generic effect of the liquid matter. Here, we will investigate how the liquid glycerol is responding to a (shear) step strain step. The initial thermal response and its timescale will be investigated, as well as the relaxation mechanism that follows.

3.1 Experimental details

The experimental setup is similar with the one utilized in the previous chapter. The two main changes are:

a) The focused liquid is mainly glycerol.
b) The type of the excitation is in shear geometry but approaches a shock wave.

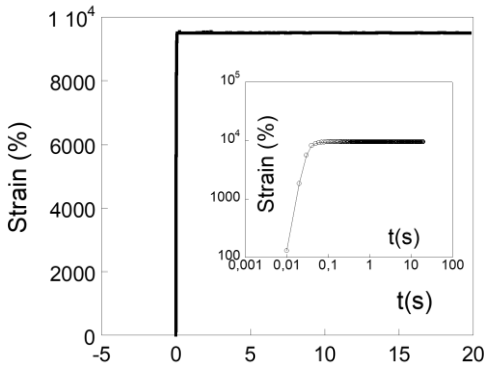

Figure 3.2: Applied (shear) step strain function (real data) as given from the rheometer. Inset: the same graph in logarithmic scale.

We take advantage of the stress relaxation mode offered from the rheometer software, which is used in studies that investigate the relaxation of stress in viscoelastic materials (polymers, polymer melts, gels, emulsions) when shear strain is kept constant for long time (even hours) [156, 157]. We focus again on the thermal response to elucidate the thermodynamic response of the liquid. However, in these measurements, we do not provide continuously oscillatory shear energy to the liquid, but only for a very brief time in a form of shock wave. The applied deformation (step strain) is a (nearly) Heaviside function of time $H(t)$, where $H(t) = \begin{cases} 0, & t_{ap} < 0 \\ \gamma, & t_{ap} > 0 \end{cases}$ (Figure 3.2). Each step shear strain measurement can be divided into several time steps:

a) The whole system (liquid and plates) is in equilibrium with its environment after remaining at rest for substantial amount of time (> 10 min). Thermal equilibrium with the environment is an important condition because it eliminates any other conduction and relaxation phenomena not related with the present measurements. Sample equilibrium is expected to be reached in less than 10 minutes in the case of a small molecule (glycerol) away from its glass transition (T_g = 190 K).
b) The shear strain is applied to the system, so that the desired shear strain γ_0 is achieved from zero strain, in very short time assimilated to a Heaviside function. From the limitations of inertia, the rheometer achieves an "instant" displacement in τ_{shear} ~ 0.03s. Thus, we can calculate the average shear strain rate $\dot{\gamma} = \gamma_0/\tau_{shear}$. This rate is an approximation and not representative at the very start or end of the shear. During τ_{shear}, shear strain energy is provided to the liquid and is the only source of energy during the whole experiment. As the rheometer is a strain-controlled one, the desired strain is achieved in great precision without instabilities that can be generated from stress-controlled rheometers [158].

c) After the desired shear strain is achieved, the moving bottom plate stops and maintain this position (a time of 20s is chosen for most of the present measurements). The system is under strain along this time, but no energy is offered to the liquid throughout this relaxation period.
d) To stop the measurement, the moving plate returns to its initial position at t_{rem}. This movement is achieved with a slower backward motion.
e) The system maintains the initial equilibrium (from strain perspective) position for several seconds.

The shear strain measurements were conducted simultaneously with the thermal measurements for different scales and at different shear strain amplitudes to study the connection of the thermal response with scale. We once again take advantage of the ability of liquids to dissipate (at least partly) shear stress and withstand much higher strain values in comparison to solids. The shear value ranges from 20% to 9500%, depending on the gap thickness and approaching the limitations of the rheometer.

3.2 Liquid glycerol under step shear strain

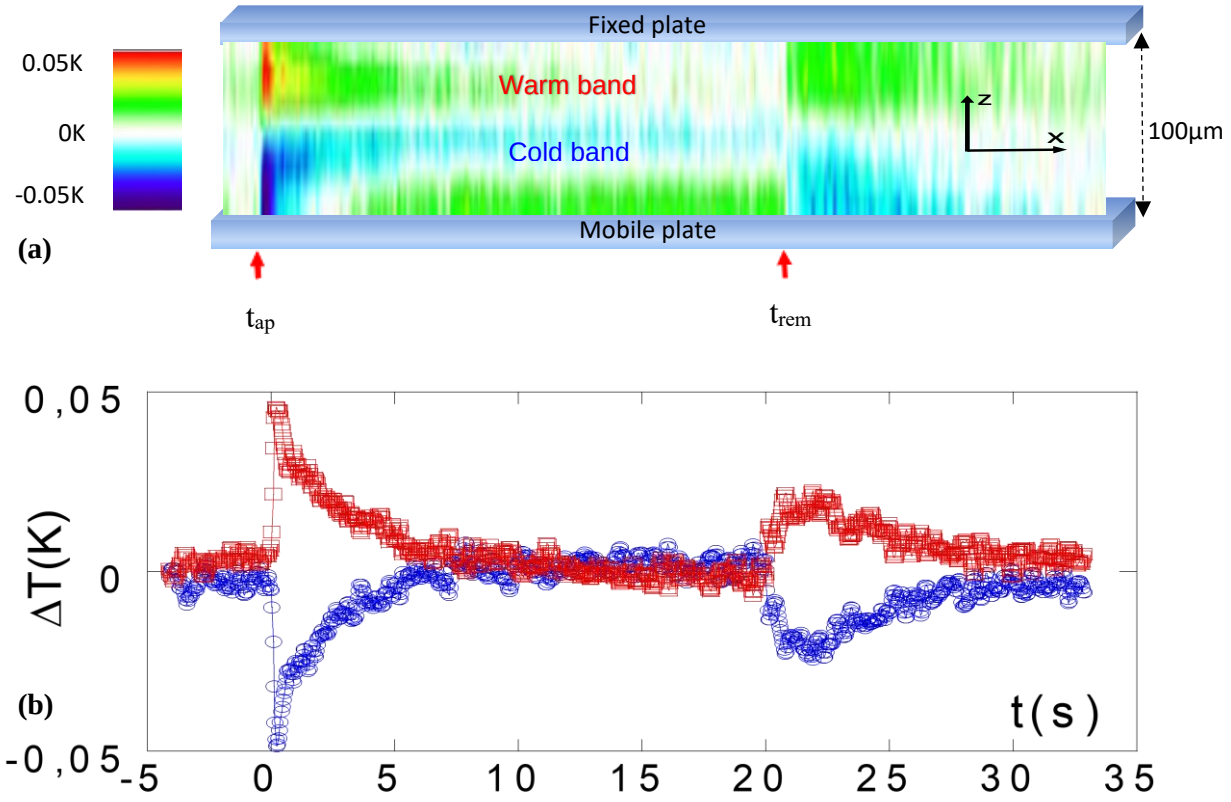

Figure 3.3: a) Real-time thermal mapping showing that the liquid glycerol emits a transient thermal signal by applying a step strain mechanical stimulus (shear step strain of γ=9500% applied at t_{ap}, followed by a backward motion to the equilibrium at t_{rem} (t_{rem} - t_{ap}=20s) during 0.18s, room temperature measurements). Forward and backward steps were achieved in 0.03s and 0.08s respectively by moving the bottom plate. X-axis is the time; z-axis is along the gap thickness (100µm). The colour index indicates the temperature variation with respect to the equilibrium temperature (at $t < t_{ap}$). **b)** Graphical representation of Fig.1a. Top (hot) band:□, bottom (cold) band: ○.

In Figure 3.3, we show a typical example of the thermal response of liquid glycerol at e = 100µm to a step shear strain of γ_0 = 9500%, maintained for 20s. In Figure 3.3a, the 2D thermal mapping is displayed, which highlights the evolution of the effect over time in the whole liquid volume. We observe:

a) Before we apply the strain at t_{ap}, the liquid is in thermal equilibrium with the environment.
b) Right after the step shear strain, where shear energy was provided, we observe that the liquid responds thermally. Specifically, it splits in two thermal regions of opposite temperature variation. In the bottom region, closer to the moving substrate, a strong cooling is observed, while in the top region a symmetrical heating is seen. As seen in Figure 3.3a & b, the two bands have equal thermal variation amplitude in absolute value ($|\Delta T| = 0.04 \pm 0.01$K). We measure that the maximum temperature from the equilibrium value is achieved in 0.19 ± 0.04s. The time where maximum temperature establishes is six times greater than τ_{shear} (~ 0.03s), meaning that the time to integrate the energy is higher than the time where the energy is established.

c) From t= t_{ap} to t_{rem}, the strain is maintained constant, the thermal evolution shows a symmetrical relaxation pattern for both thermal regions. Noticeable is that the thermal relaxation process is not instantaneous as it should be expected throughout the liquid. Specifically, in Figure 3.3b, we focus on the thermal bands, in the bulk of the liquid, and notice a slower relaxation compared to the liquid close to the walls. Possible explanations for this behaviour are different dynamic conditions due to the anchoring to the high energy surfaces or possible conduction with the solid walls in the interface.
d) At t = t_{rem}, both bands seem to have reach the initial equilibrium temperature. The strain is released, and the bottom plate returns to its equilibrium position (backward motion). Thermally, the two regions respond thermally again, but the temperature variation is about 1/3 of the initial response. The displacement of the plate back to equilibrium does not correspond to a Heaviside function (τ_{shear} ~ 0.08s), meaning a slower backward motion and thus producing smaller thermal variation. The thermal response reports a first maximum at 0.15s and a higher second overshoot is seen 0.75s after the shear.
e) Afterwards, the thermal bands again relax over time.

3.2.1 **Initial thermal response**

In this chapter, we study in detail the initial thermal response and not the one produced by the backward motion to equilibrium position (t_{rem}). There are different reasons for this decision. The rheometer is designed for a forward step strain test controlling the strain, while we cannot impose the step strain for the backward motion (which does not follow a Heaviside-like function).

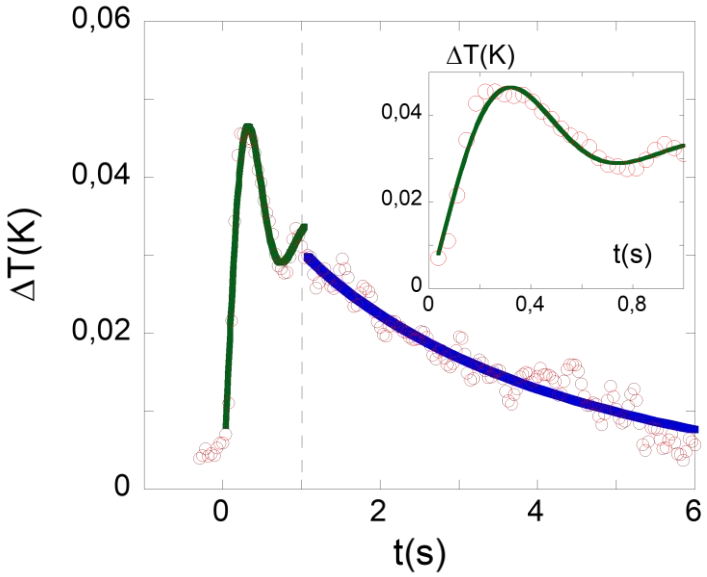

Figure 3.4: Modelling of the thermal response of the hot (top) band of glycerol at 0.100mm, 9500%. Green and blue lines represent the fits with Eqs. (1) and (3) respectively Inset: Detail and fit of the early times (left of the dotted line) of the thermal overshoot (green line).

In Figure 3.4, the initial thermal response of the hot band right after the step shear strain is reported. The response of the cold band is not studied, but we may proceed without loss of generality since the bands are symmetric in nature. We observe that the initial response is divided in two parts. First, it is observed an overshoot, where we receive the maximum temperature variation (in this example $\Delta T \sim 0.04K$) and the time two achieve this variation is 0.19s. Then follows a decrease of the temperature and before the first second a second smaller in scale is observed. The first second of the initial thermal response (left of the dotted line) can be described by a second order transfer function:

$$H_{nf}(s) = H_0\left(\frac{\omega_0^2}{s^2 + 2\zeta\omega_0 s + \omega_0^2}\right)$$

where ω_0 is the natural frequency, ζ is the damping ratio, s the Laplace variable and H_0 the system gain. The mathematical solution is written as [159]:

$$\Delta T_{fit}(t) = A[1 - \frac{e^{-\zeta\omega_n t}}{\sqrt{1-\zeta^2}}\cos\left(\omega_n\sqrt{1-\zeta^2}t - \varphi\right)] \quad (1)$$

where, A is a constant, φ is a phase shift and ΔT_{fit} is the temperature variation based on the second order step response. Known equivalent systems that exhibit similar response are: an electronic RLC circuit [159], hydro-mechanical [160] or spring-mass-damper systems [161]. The equation (1) is fitted on the thermal response as seen at inset of Figure 3.4. As we can observe, the fitting is acceptable, but we are not able to retrieve the value of natural frequency

ω_n with great accuracy because the fitting stops abruptly at 1s. From the fitting of Eq. (1), we deduce: $\zeta = 0.35 \pm 0.03$, while $\omega_n = 8 \pm 0.3$ rad/s. The scale of the order of the natural frequency ω_n is of Hz; i.e. it describes a collective thermal effect. However, for a better approximation of natural frequency, we can utilize the peak time t_p, which is the time needed for the system to reach its first peak. As mentioned before this time for our case is 0.19s. The peak time can be written as:

$$t_p = \frac{\pi}{\omega_n \sqrt{1-\zeta^2}}$$

For the damping value calculated before, we get ω_n = 17.65Hz or ω_n =110.9rad/s.

The characteristic overshoot is noticeable at 0.2s (inset of Figure 3.4), as expected for the underdamped case ($\zeta < 1$) [159]. The steady state value (asymptotic value at long timescale) is derived from the overshoot value, with the equation [162]:

$$\frac{Overshoot\ value - Steady\ state\ value}{Steady\ state\ value} = \exp\left(-\frac{\zeta\pi}{\sqrt{1-\zeta^2}}\right) \quad (2)$$

The Eq. (2) foresees an asymptotic value of $\Delta T_{t\to\infty}$ = 0.03°C, which stands as the gain of the system from the step excitation. Figure 3.4 shows that after the first second, the thermal band does not maintain $\Delta T_{t\to\infty}$, but relaxes over time and returns to equilibrium. The long-time thermal relaxation to equilibrium (both cold and hot bands relax symmetrically) can be modelled by a stretched exponential decay (Figure 3.4 right of the dotted line)

$$\Delta T = \Delta T_{max}\left(e^{-\frac{t}{\tau}}\right)^{\beta} \quad (3)$$

In next section, we will discuss on how we estimate exponent β. For the current example (100μm, 9500%), we estimated a thermal relaxation time $\tau_{thermal}$ ~ 3s. We can estimate the thermal diffusion time $\tau_{diff} \sim H^2/D$, where H the band thickness and D the thermal diffusivity. For glycerol, D = 0.098mm^2/s, we get $\tau_{diff} \sim 0.1s$. We observe a significant discrepancy between the two times, with the thermal relaxation time being larger by two scales and ruling out a diffusive process. Thus, there is a need to interpret the slower thermal relaxation.

In collaboration with A. Zaccone, we deploy knowledge from glass former systems. It is known that stretched exponential relaxation arises when there is a distribution of relaxation times in the system (e.g. from dynamical heterogeneity which is ubiquitous in glassy systems),

$$\exp(-t/\tau)^{\beta} \approx \int_0^{\infty} \rho(\tau)\exp(-t/\tau)\,d\tau \quad (4)$$

where $\rho(\tau)$ is a suitable distribution of relaxation times, which must satisfy few mathematical requirements [163]. Since τ in our system is related to the normal mode ω_n of the liquid system, the distribution $\rho(\tau)$ must be given by the distribution of vibrational normal modes in the liquid, $\rho(\omega_n)$, also known in condensed matter physics as the vibrational density of states (VDOS). Hence, upon using the VDOS of a glassy liquid in Eq. (4) we obtain [45, 164, 165]

$$\Delta T(t) \sim \exp(-t/\tau)^{\beta} \approx \int_0^{\infty} \rho(\omega_n)\exp(-\zeta\omega_n t)\,d\omega_n \quad (5)$$

with $\tau = (\zeta\omega_n)^{-1}$. The validity of Eq. (6) for the case of glycerol in the supercooled liquid state was numerically verified in Ref. [45]. It was shown that the boson peak (excess of vibrational modes over the Debye level ~ ω_n^2) in the VDOS represents a crucial requirement for Eq. (5) to produce a stretched-exponential relaxation in the measured dielectric response of glycerol. Therefore, the experimentally observed stretched-exponential profile in the current system may suggest the existence of low-energy transverse phonon modes of the kind that constitute the boson peak excess of low-energy modes in glasses [45]. In turn, this directly hints to the existence of long-range shear elastic waves in the sub-millimeter confined fluids.

3.2.2 **Behaviour of the liquid gap**

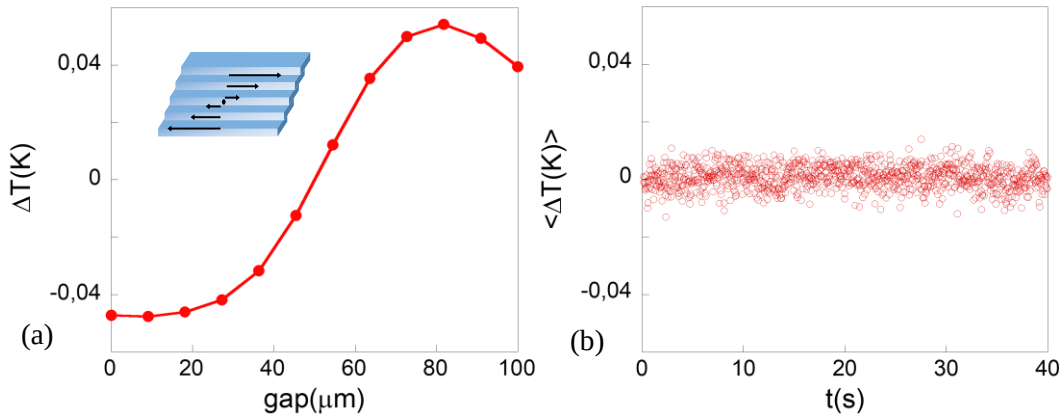

Figure 3.5: a) Temperature variation profile across the gap (z-axis) at t = t_{ap}+Δt, averaged over three successive frames (t_{tot}=0.11s) just after t_{ap} (Figure 3.3). The insert schemes the strain gradient viewed from the middle of the gap. **b)** Average temperature variation integrated over the whole gap versus time during the experiment (data of Figure 3.3a).

Next, we study the evolution of the temperature in the gap right after the shear step strain (Figure 3.5a). The maximum heating and cooling are seen in the regions closest to the substrates, while around the middle, there is no thermal variation and acts as an intermediate zone (reversal point) between the hot and cold thermal bands. From Figure 3.5b, we get that the temperature of the whole volume does not alter during the measurement, even during the initial strong response and the relaxation process. Combined with the nature of the excitation, which provides work to the liquid and not heat, we can justify that the phenomenon is adiabatic within the experimental error bar. Taking into account, that the thermal bands return to equilibrium state after a certain period of time, we may hypothesize an isentropic-like process. Thus, we can justify the use of Anderson-Grüneisen parameter to describe the state of the bands. The parameter is [166]:

$$\gamma = -\frac{d\ln T}{d\ln V}$$

For glycerol, it is γ = 0.75. Thus, we may assume that the cold band is associated with regions where the liquid is locally expanded, whereas the hot band is associated with regions where the liquid is locally compressed. An approximation on the pressure change is possible by utilizing the thermal pressure:

$$\gamma_V = \left(\frac{\partial P}{\partial T}\right)_V = \alpha K_T$$

where, α is the volumetric expansion coefficient and K_T is the isothermal bulk modulus. For glycerol, we calculate that for 0.05K temperature change, it requires a pressure change of 0.11MPa. However, it should be noticed that the calculations were made with conventional values and under the assumption that the volume remains constant.

Another approach on the existence of the bands is possible by utilizing the normal modes that exist in the system. The bands are macroscopically large since they contain a huge number of molecules, hence it makes sense to define long-wavelength phonon modes that live in these regions. In the hot/compressed regions the volume V of the region gets reduced, whereas in the cold/expanded regions the volume V is enlarged. Then, we may write the microscopic definition of the Grüneisen parameter:

$$\gamma = -\frac{d \ln \omega_n}{d \ln V}$$

Since the Grüneisen parameter γ is positive for liquids [167], this relation gives (upon integration) that the phonon frequency ω_n increases as the volume V decreases, whereas ω_n decreases as the volume V increases. Since the vibrational frequency is related to temperature, via $T = h\omega_n/k_B$, it is clear that T increases in the regions where V decreases ("compressed" regions), whereas T decreases in the regions where V increases ("expanded" regions), thus leading to a hot and a cold band for the compressed and the expanded regions, respectively.

3.3 Thermal relaxation time

From step strain measurements of various strain values and different gap thicknesses, we fitted their exponential relaxation with Eq. (3), resulting to an exponent estimated at $\beta \approx 0.8$ - 0.85. Then, the thermal relaxation time $\tau_{thermal}$ was measured and the results are displayed in Figure 3.6.

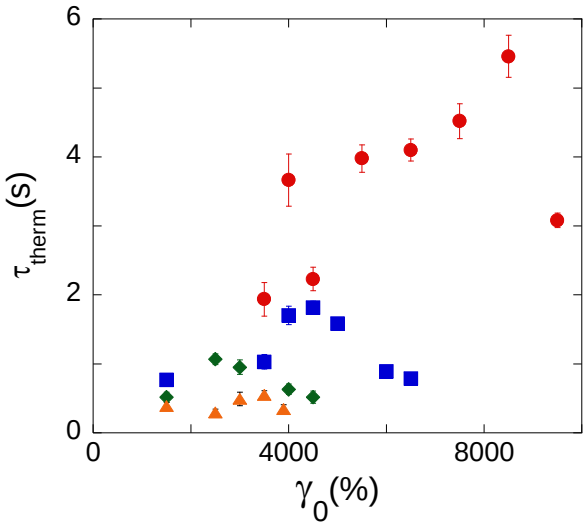

Figure 3.6: Relaxation time τ_{therm}(s) of the top (hot) thermal band versus shear strain amplitude (after the step strain ramp (0.03s)) deduced from $\Delta T(t) = \exp(-t/\tau)^{\beta}$. Red, blue, green and yellow points correspond to 100µm, 150µm, 200µm and 250µm gap thickness respectively.

From the graph, no clear dependence of $\tau_{thermal}$ with strain amplitude is apparent, since the data appear dispersed. However, a progressive increase of the relaxation time is observed as the gap decreases, implying a dependence of $\tau_{thermal}$ on the scale. Specifically, was measured that: the thermal relaxation time is $\tau_{thermal} \approx 0.3$ - 0.5s, for $e = 240$µm. The time evolves with thickness, and we measure a thermal relaxation time $\tau_{thermal} \approx 0.5$ - 1.8s for 150µm < e < 200µm, while the time is $\tau_{thermal} \approx 2$ - 5.5s for the smallest thickness measured here, e = 100µm). From the stretched exponential relaxation, we are able to relate the thermal relaxation time with the normal modes:

$$\Delta T(t) \sim \exp(-\zeta \omega_n t)^{\beta} = \exp(-t/\tau)^{\beta}$$

Then we define the characteristic relaxation time $\tau_{thermal} = (\zeta \omega_n)^{-1}$. According to this definition, the increase of τ upon decreasing the thickness e could be explained with the decrease of damping ζ upon decreasing e. Since we relate the damping as a viscous characteristic, the decrease of ζ is indirectly related to the increase of rigidity. This observation is in agreement with experimental and theoretical works that show an increase of shear elasticity as the scale decreases [29, 18, 22, 23], even as $G' \sim e^{-3}$ [90].

3.4 Strain dependence of thermal overshoot

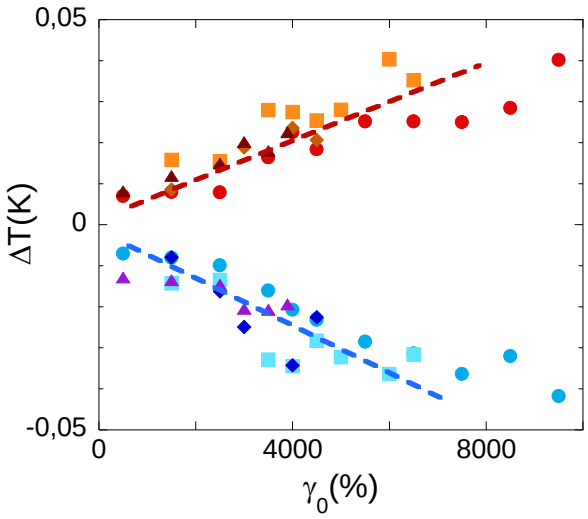

Figure 3.7: Amplitude of the thermal overshoot variation versus strain at different gap thicknesses. Warm band: 100µm: (●), 150µm: (■), 200µm: (◆) and 250µm: (▲). Cold band: 100µm: (●), 150µm: (■), 200µm: (◆), 250µm: (▲). Room temperature measurements.

Figure 3.7 shows the influence of the strain amplitude on the temperature variation of the generated bands. The highlighted thermal variation is the maximum value exhibited for each measurement. The amplitude of the temperature variation increases nearly linearly with increasing strain for all gap thicknesses. We can thus define a thermo-(shear)elastic constant as the ratio of the temperature variation to the strain value.

Gap(µm)	Θ_{shear} $(\Delta T/T,\gamma_0)$(x10^{-8}) hot band	Θ_{shear} $(\Delta T/T,\gamma_0)$(x10^{-8}) cold band
100	1.1 ± 0.1	1.3 ± 0.1
150	1.5 ± 0.3	1.4 ± 0.4
200	1.5 ± 0.4	2.2 ± 1
250	1.3 ± 0.2	0.8 ± 0.2

Table 3.1: Evolution of thermo(strain)-elastic constant Θ_{shear} $(\Delta T,\gamma_0)$ for different scale of the system based on the maximum temperature variation displayed on each measurement.

As seen from Figure 3.7 and Table 3.1, the thermo(strain)-elastic constant Θ_{shear} $(\Delta T/T,\gamma_0)$ = $(\Delta T/T)/\gamma$ is lower from the oscillatory measurements (Table 2.3), where the constant was calculated for the variation of the bands closer to the plates. The maximum temperature variation (both for cold and hot bands) is observed closer to the bulk (centre of the gap) and not close to the walls. Within the band, the maximum variation is located in its centre, showing that abrupt thermal gradients are not generated. Moreover, the dependence of thermal variation over strain is constant over different scale for the tested gap (within 100 - 250µm) indicating a stability of the thermoelastic constant. The evolution is symmetrical for the two thermally opposite regions over strain, leading to an approximately same magnitude for each strain value. This behaviour stands as an indication that the adiabatic nature of this effect stands true and local thermodynamic changes.

3.5 Viscous friction heating

Literature reports effects of viscous friction heating that might occur due to the heat generated by friction and produces a local increase in temperature near the walls. This effect is mainly expected in high molecular weight fluids (e.g., polymer melt). As shown in Figure 3.5b, no local increase of the temperature is observed close to the surfaces, and no global heating of the liquid is present all along the step strain process, even during the strong thermal response at the start of the experiment. The temperature is constant over time.

This result is in agreement with reports on high shear rates on glycerol [168]. It can be also verified numerically using the Nahme number, which gives an estimation of the importance of viscous heating in a system. As mentioned in the previous chapter, Nahme number is defined as [139, 169]:

$$Na = \frac{\eta_0 \beta e^2 \dot{\gamma}^2}{\kappa}$$

where, η_0 the viscosity, β=-($1/\eta_0$)($d\eta/dT$), e gap thickness, κ thermal conductivity and $\dot{\gamma}$ shear rate. From the equation, it is clear the relation of viscous heating with the applied shear rate during the strain ramp of the excitation. For the highest shear rate (~ 3167s^{-1}) applied during this short time (0.03s), Nahme number is much lower than 1 (Na=0.041 γ = 9500%), meaning that viscous heating is negligible in our experimental conditions.

.

3.6 Peak time

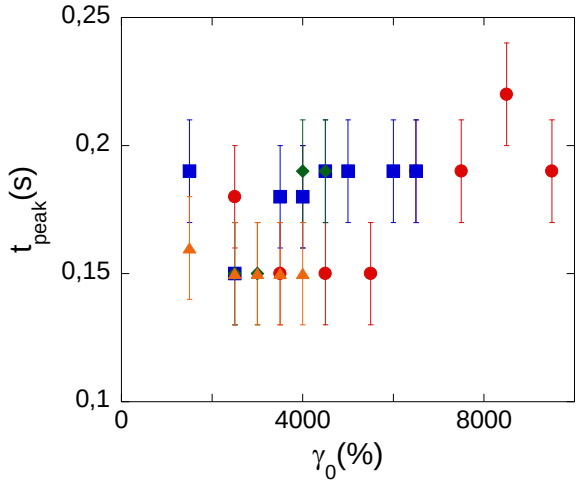

Figure 3.8: Time necessary to reach maximum temperature t_{peak} versus strain amplitude for various gap thicknesses after the step motion. The time is equivalent for both bands. Red, blue, green and yellow points correspond to 100µm, 150µm, 200µm and 250µm gap thickness respectively.

We define a peak time as the time necessary for the liquid to reach the maximum temperature (hot and cold are similar). Figure 3.8 shows that the peak time is nearly constant: $t_{peak} \cong 0.19$s for most of the gap thickness and strain values probed. Except for 250µm, the peak time is about 0.15s, which is within the error bar of previously reported value ($t_{peak} \cong 0.19$s). Thus, this delay appears as an intrinsic property of the liquid and is not strongly dependent on the width of the bands (30 – 80µm), but only for the upper limit. This peak time may be connected with the minimization of energy process of the liquid. It shows that the time needed to assimilate the shear energy and convert it in two (for the cases studied here) thermodynamic regions is constant.

3.7 Comparison of shear stress, thermal variation and normal force variations

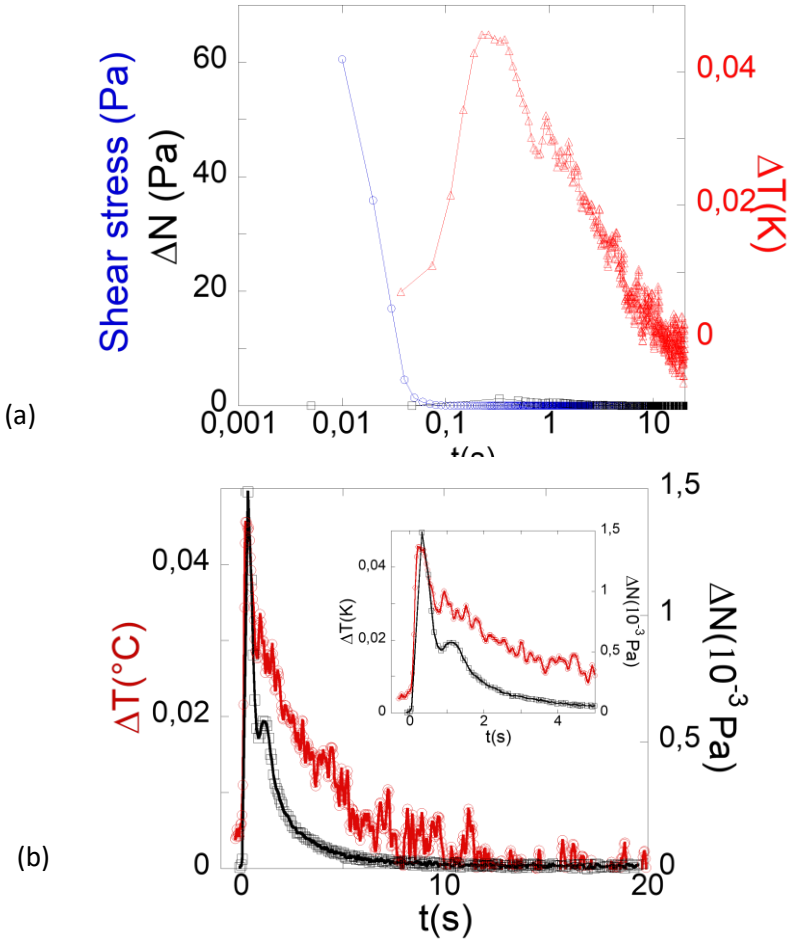

Figure 3.9: a) Measured shear stress (blue curve) and normal stress (ΔN) (black curve) during the step shear strain measurements (glycerol, 100µm, γ_0 = 9500%), in comparison with the thermal variation of thermal hot band. b) Detail of Figure 3.9a pointing out a similar relaxation of the temperature (hot band) and of the normal stress (showed in double scale). Inset: Same measurements focused on the early time of the thermo-mechanical response versus normal force.

Figure 3.9 compares the shear stress, normal stress variations and thermal variation of a 100µm glycerol layer to a step strain of 9500% (simultaneous measurements using three Keithley multimeters coupled to the rheometer and a microbolometer for the thermal acquisition). We observe a shear stress relaxation of the liquid of about 60Pa at maximum value that sharply decreases with time. A measurable shear stress relaxation might be surprising. However, similarly as for oscillatory measurements, the shear elastic component of fluids can be revealed by reinforcing wetting substrate (alumina). Shear stress moduli have been reported in liquid water and in glycerol at low gap thickness and applying small strain rate [22, 23].

An interesting observation in Figure 3.9 is the chronology of the events. We notice that the first response of the liquid is the shear stress relaxation, followed by the thermal relaxation. Therefore, the thermal relaxation is the product of the shear stress relaxation. Moreover, the

examination of the normal stress variation (shown in details in Figure 3.9b) shows a slight variation occurring at the same time as the thermal relaxation. This variation is about 2% of the shear stress value and is close to the limitations of the rheometer (lower limit about 1.5Pa), thus we cannot provide quantitative discussions on it. However, several similarities appear in the thermal and the normal stress behaviors.

Similarly to the temperature variation, the normal stress seems to exhibit an exponential relaxation to its equilibrium value after the overshoot. The similarity of the thermal and normal stress responses implies a connection between the quantities, even though the measured normal force is over the whole surface and thus is minimized integrating stresses related to both hot and cold thermal variations. Normal stress can be generated under pure shear for elastic systems [151, 152]. For the fixed volume case, shear forces lead to increase of the normal stresses in solids. Similar behaviour might be observed in our system, implying that the liquid strongly anchored to high-energy surfaces, exhibits via the normal stress, a typical solid-like feature when is subjected to high strain (non-linear region). The normal stress variation in liquid glycerol is an indirect confirmation of the exhibited shear elasticity. As argued in [152] for chemical elastic networks, a volumetric shear is created as an answer to the applied shear strain for the volume to remain constant, resulting to the observed normal stress. The existence of such shear could explain the compressed and stretched sub-volumes as demonstrated by the created thermal bands. Through the Grüneisen parameter, the volumetric strain relates to vibrational modes ω_n of the liquid [152]. The resulting volumetric strain causes the vibrational modes to shift and as these are related with the temperature from $T = h\omega_n/k_B$, the temperature where the volumetric strain is applied will change, as seen from the highlighting thermal bands. This process interprets the symmetry breaking in the temperature, while only the bottom plate is moved. The bottom region of the liquid is stretched by the fast step shear strain, while the top region is compressed from the resulting volumetric shear, leading to the observed temperature variations.

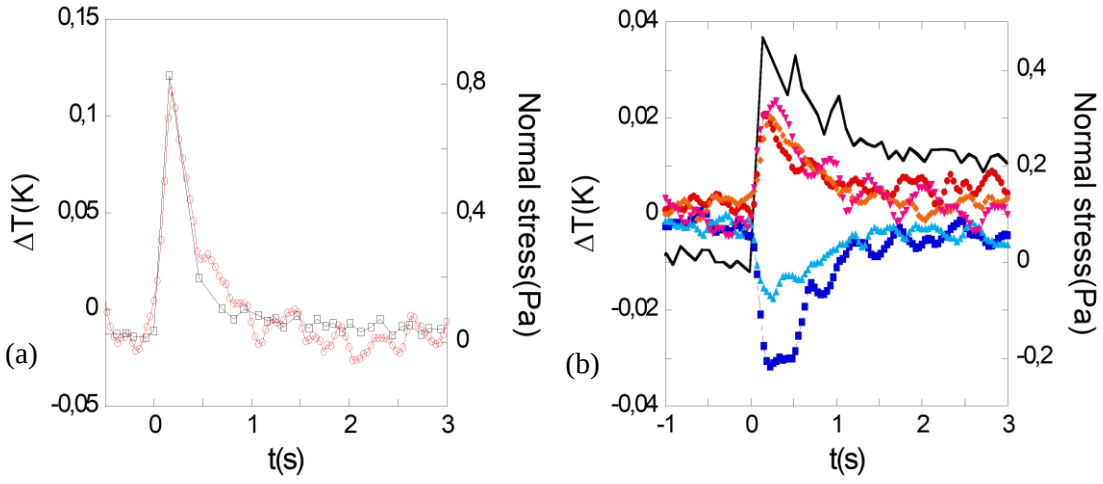

Figure 3.10: a) Measured normal stress variation (black line) during the step shear strain measurements (glycerol, 250μm, γ_0 = 3900%), in comparison with the thermal variation of thermal hot band. b) Same for glycerol, 500μm, γ_0 = 1500%. Graphical representation of Fig.1a. Bottom (closest to moving plate) band:■, intermediate between bottom and middle regions band: ●, middle band: ♦, intermediate between top and middle regions band: ▲ and top band: ▼. Black line is for normal stress variation.

In Figure 3.10, we show the normal stress in respect with the temperature for higher scale. The normal stress seems to share the same response as the temperature, but its variation is weaker

compared to lower gap thickness. An expected result as the elastic nature of liquid should be decreased as the scale increases.

3.8 Thermal response of glycerol at high gap thickness

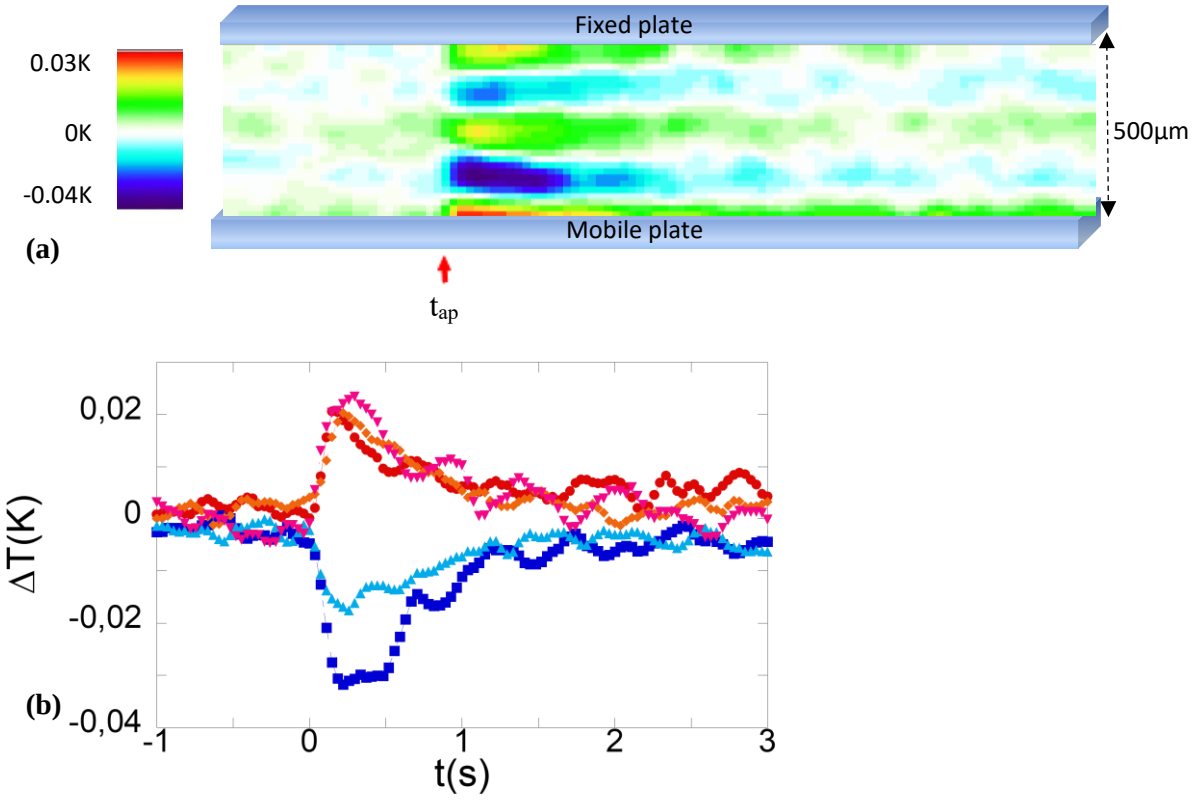

Figure 3.11: a) Thermal mapping at large liquid thickness (glycerol) under shear step strain of γ = 1500% applied at t_{ap} (room temperature measurements). Shear step was achieved in 0.03s by moving the bottom plate. X-axis is the time; z-axis is along the gap thickness (500μm). The colour index indicates the temperature variation with respect to the equilibrium temperature (at $t < t_{ap}$). **b)** Graphical representation of Fig.1a. Bottom (closest to moving plate) band:■, intermediate between bottom and middle regions band: ●, middle band: ♦, intermediate between top and middle regions band: ▲ and top band: ▼.

Next, we study the evolution of the effect for higher thickness. In Figure 3.11, the response of a 500μm layer thickness of glycerol is shown. It is seen that the thermal response differs in respect with the number of generated bands. Three hot and two cold bands alternate respectively. This may hint the existence of an upper limit width of a thermal band. For glycerol, the limit is about 100μm. The limit shows the maximum length over which the liquid molecules respond collectively (same temperature variation). If, we calculate the average temperature variation of the whole volume, it decreases during the initial thermal response right after the step strain (Figure 3.12). For the minimization of the internal energy, the liquid produces hot and cold bands which in total produce a decrease of the temperature (Figure 3.12) which indicates that the stretching effect dominates transiently. The temperature variation of the bands is estimated at $\Delta T \sim 0.02K$ for the hot bands and $\Delta T \sim -0.03K$ for the cold ones. Of course, the duration of the relaxation of the thermal bands is short and after a time of about a second, thermal equilibrium dominates again in the gap.

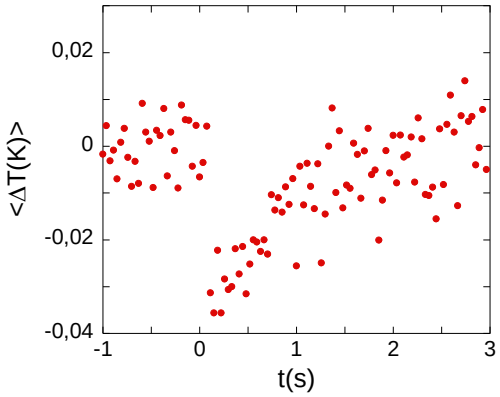

Figure 3.12: Average temperature variation integrated over the whole gap versus time during the step strain experiment at large gap (data of Figure 3.11a).

As the gap of the system is increased, the thermal response becomes weaker and fades faster (Figure 3.13). As seen for a system of 960μm, the thermal response is detectable only on the low half of the liquid close to the shear source, while the temperature variation resembles more to a fast flash before it returns to thermal equilibrium. The value of the temperature change is weaker and less than $\Delta T < 0.02K$. Thus, the influence of the elastic nature of the liquid fades with increased scale and tends to a conventional response, where shear energy is immediately dissipated in the liquid.

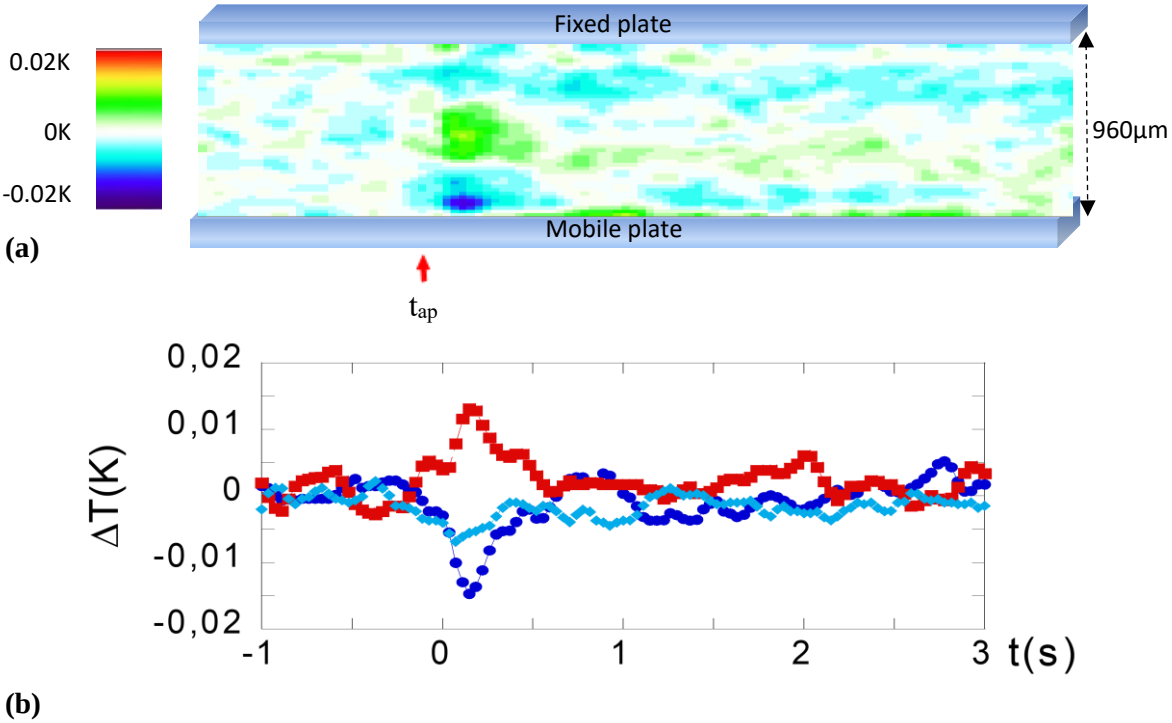

Figure 3.13: a) Thermal mapping of liquid glycerol under shear step strain at very large gap thickness (960μm), of γ = 1800% applied at t_{ap} (room temperature measurements). Shear step was achieved in 0.03s by moving the bottom plate. X-axis is the time; z-axis is along the gap thickness. The colour index indicates the temperature variation with respect to the equilibrium temperature (at $t < t_{ap}$). **b)** Graphical representation of Fig.1a. Bottom band: ●, middle band: ■ and top band: ♦.

In the previous sections, we studied the thermal response of glycerol to a sudden deformation (step shear strain), as well as its relaxation. Glycerol simplicity made this study possible. We also did a test with the 68 repetitive units PPG 4000 under the same mechanical conditions at 230µm. Its thermal behavior is more complex.

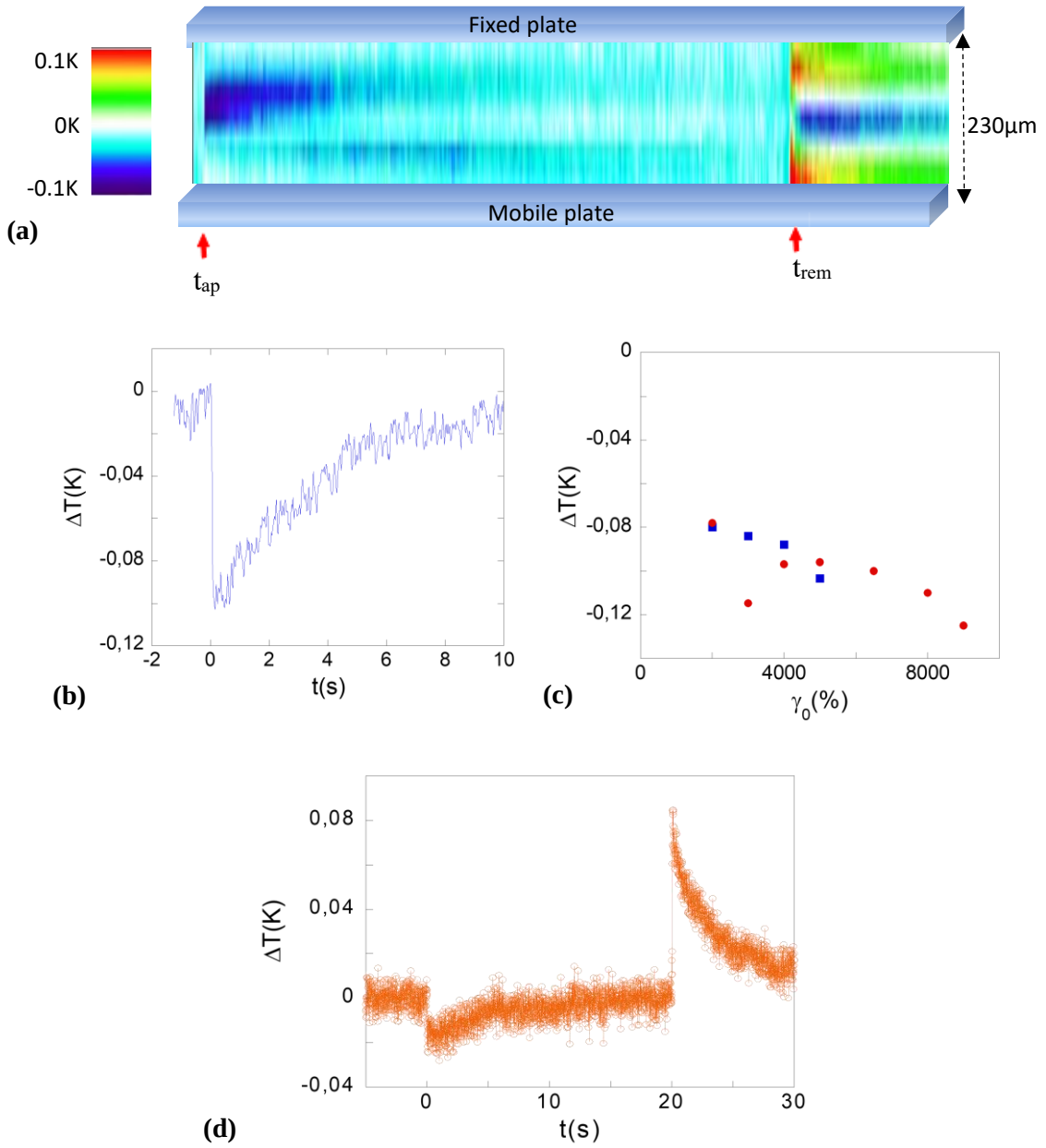

Figure 3.14: a) Thermal mapping of liquid PPG under shear step strain of γ = 5000% applied at t_{ap} (room temperature measurements). Shear step was achieved in 0.03s by moving the bottom plate. X-axis is the time; z-axis is along the gap thickness (230µm). The colour index indicates the temperature variation with respect to the equilibrium temperature (at $t < t_{ap}$). **b)** Graphical representation of cold band in during forward motion. **c)** Amplitude of the thermal overshoot variation versus strain of the cold band during forward motion for: 130µm: (●), 230µm: (■). **d)** Average thermal variation of the liquid gap (orange points) showing a rapid temperature drop at the onset of the relaxation. At t_{ap} = 0s, is the forward motion and at t_{rem} = 20s is the backward motion.

As seen in Figure 3.14a, right after the forward motion there is mainly only one cold band generated in the middle to top part of the liquid. As seen in Figure 3.14b, the resulting bulk evolution of thermal relaxation is similar to glycerol seems to be established after 20s (within the measurement accuracy). When the moving plate returns to its initial place (backward displacement), we observe a thermal response where three bands are generated. The two bands close to the surfaces are heated, while the middle one is cooling. In Figure 3.14c, we see the evolution of the temperature change of the cold band during the forward motion for two gap thicknesses. We observe that the thermal evolution is rather linear with strain, however the evolution does not tend to zero thermal variation for zero strain indicating that the liquid still stores some residual energy. The response of liquid PPG in stress relaxation measurement provides two different responses for excitations, opposite in their direction. A possible interpretation could lie in the in-between dynamics of the small polymer chains, meaning different ways of energy storage.

Chapter 4 Evidencing the interfacial liquid/solid coupling in the THz domain

In the previous chapters, we deal with a dynamic thermo-mechanical coupling in liquids. High wetting provided by the solid alumina surface played a crucial role to reveal this effect, as increased interaction between solid and liquid is required for maximum transmission of shear energy in the interface. What is the mechanism inducing an increased interaction? The interface is a specific zone where the energy is different from the bulk due to the imbalance between liquid molecule attraction and surface attraction. This transition zone where liquid-liquid and liquid-solid interactions compete, is intensively studied since decades and remains puzzling. In the specific case of alumina, it has been shown that this material has amphoteric properties, attracting both positively and negatively charges which is certainly an important parameter to explain its wetting properties (the isoelectric point being at pH = 8) [170]. The existence of an electric field produced by the oxide surface has been demonstrated inducing a local polarization of water dipoles in aqueous solutions extending up to several molecular layers [171].

These are known surface effects. Much less is known concerning thermal effects. The temperature is generally treated in terms of heat transport and the possibility of inducing different temperatures without transport is not addressed since theoretical and experimental developments suppose that density fluctuations in quiescent liquids guaranty uniform temperatures at solid-liquid interfaces. It was demonstrated that quiescent liquids close to high energy/wetting substrates exhibit non-uniform temperatures at the vicinity of the solid surface [172]. Thus, questions are born for a possible energy balance between the liquid and the solid surface-on the region. An investigation of the dynamics of solid substrate in interaction with a liquid has been carried out by inelastic x-ray scattering to probe the vibrational spectroscopy of the solid surface. Here, we present preliminary results from measurements conducted at the GALAXIES beamline at S.O.L.E.I.L (coll. J. Ablett, J.P. Rueff).

4.1 Basics of phonons

In crystalline materials, atoms or molecules exhibit a well-defined periodic structure, which made possible their in-depth study with the rise of quantum mechanics and statistical physics. The atoms are not steady in their equilibrium position, but oscillate around them, and propagate their vibrations from close-to-close neighbors. The resulting collective vibrations of the atoms are called phonons [173] and can be treated as propagating sound waves. A classical mechanics counterpart is the vibrational normal mode. Phonons play an important role for the interpretation of several thermal phenomena like, thermal conductivity, thermal expansion and specific heat. As a quantum mechanics entity, phonons have quantized energy $E = \hbar\omega$, where ω is the frequency of vibration and propagating waves that can be longitudinal (L) or transverse (T) ones. Based on the collective oscillation, a phonon is called acoustic (A) when the oscillation of the atoms is in-phase and optic (O), when it is out of phase. In a crystal lattice, a phonon can be any combination of LA, LO, TA and TO.

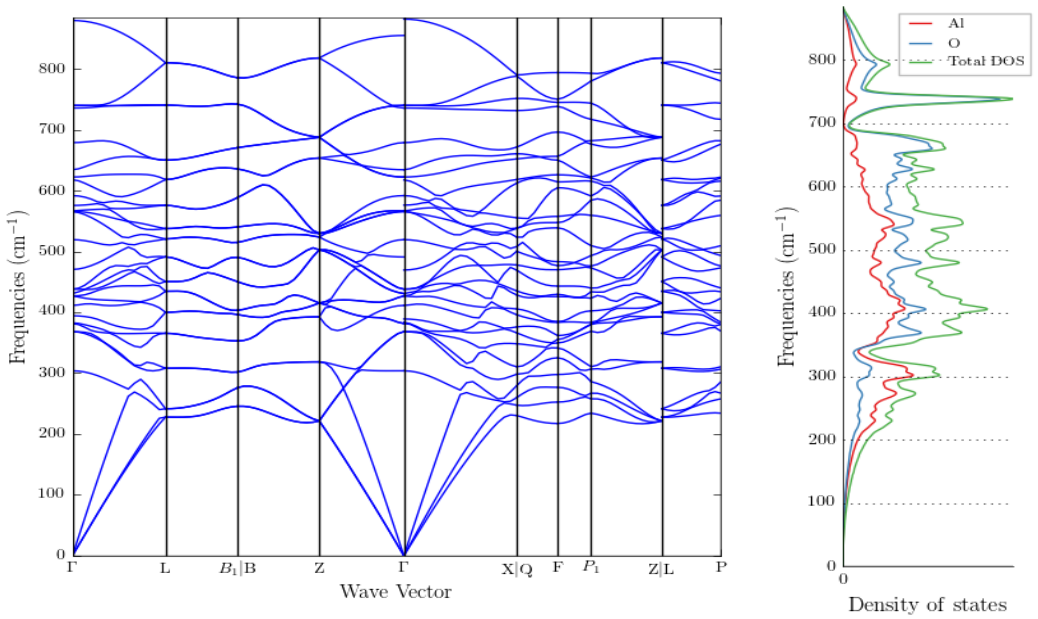

Figure 4.1: Phonon dispersion within the Brillouin zone (left graph) and vibration density of states (right graph) of Al_2O_3 [174].

Similar phonons do not interact and can be described by the Bose – Einstein statistics [173]:

$$\langle n \rangle = \frac{1}{e^{\frac{\hbar\omega}{k_B T}} - 1}$$

Following the Debye model, the phonon density of states increases in a parabolic manner with frequency, with a cutoff at Debye frequency ω_D, which is the highest frequency were the atoms can oscillate. However, this theory is an approximation where only three acoustic branches are considered. The density of states can be very complex as seen in Figure 4.1. The density of state $g(\omega)$ can be calculated for a three dimensional solid following the equation [175]:

$$g(\omega)d\omega = V\int_{S_\omega}\frac{dS_\omega}{\left|\frac{\partial}{\partial \boldsymbol{q}}\omega\right|}d\omega$$

with V the volume, S_ω the surface of constant energy and $\partial\omega/\partial\boldsymbol{q}$, the gradient of frequency in the reciprocal space. For the acoustic branch, we retrieve again a parabolic evolution of $g(\omega_{ac})\sim\omega^2$. Thermal properties of solids derive from phonon modes, thus measuring the phonon dispersion spectrum provides significant information on the dynamics of the system. At room temperature, phonon energy lies within the meV range, thus their frequency is of THz. The study of phonon spectrum provides immediate information on the dynamics (vibrational states) of a medium in the reciprocal space, while the infrared radiation is a consequence of the molecular motion. Accessing phonon dynamics is made possible with the development of inelastic x-ray scattering.

4.1.1 **Phonon theory of liquids**

While phonon lattice dynamics of crystalline materials is being just about 70 years old, studies of liquid phonons are rather scarce for liquid matter, with few exemptions [176]. From theoretical point of view, in the frame of an extension of the Frenkel's theory, Trachenko and Brazhkin developed a phonon theory suitable for liquids [30]. They proposed that the energy of the liquid is given as:

$$E = K_l + P_l + K_s(\omega > \omega_F) + P_s(\omega > \omega_F) + K_d + P_d$$

, meaning that the energy of the liquid is a sum of kinetic and potential components of longitudinal and transverse phonon energy, and energy of diffused molecules, as noted by Frenkel [5]. After ~~of~~ a series of calculation, where the authors utilize the virial theorem, the phonon free energy, the compressibility of the liquid and the Debye vibrational density of states, they concluded to a liquid energy:

$$E = NT\left(1+\frac{aT}{2}\right)\left(3D\left(\frac{\hbar\omega_D}{T}\right)-\left(\frac{\omega_F}{\omega_D}\right)^3 D\left(\frac{\hbar\omega_F}{T}\right)\right)$$

Where $D(x) = \frac{3}{x^3}\int_0^x \frac{z^3dz}{e^z-1}$, is the Debye function and ω_D the Debye frequency. The equation is valid in both classical and quantum regimes and results to the energy of solids $E = 3NT$, when $\omega_F = 0$ and thermal expansion coefficient is $a = 0$. They calculated the specific heat $c_v = \frac{1}{N}\frac{dE}{dT}$ for a variety of liquids, in classical and quantum regime for a wide range of temperature and reported close resemblance of the experimental results. They argue that the theory is a solid-like approach of liquid thermodynamics being possible through phonon theory, even though the liquid molecules interactions are not yet understood. In this chapter, we will not try to study the phonon spectrum of liquids but study the effect of a liquid layer on a solid surface dynamics.

4.2 Basics of inelastic x-ray scattering (IXS)

Inelastic x-ray scattering is an important tool for the display of atomic and molecular dynamics and structure. With the construction of high brilliance beam sources (3rd generation), highly resolved energy beams probing with high-energy x-ray provide the possibility to measure phonon dynamics.

In an inelastic x-ray scattering process, a well-defined incident photon with wave vector $\mathbf{k_i}$, energy E_i and a polarization $\boldsymbol{\varepsilon_i}$ hits the sample and results to a new scattered phonon of wave vector $\mathbf{k_f}$, energy E_f and polarization $\boldsymbol{\varepsilon_f}$. During the scattering process, energy and momentum ($\mathbf{q}$) are transferred to the sample electrons, as known conventionally [177, 178, 179]:

$$E = E_i - E_f = \hbar\omega_i - \hbar\omega_f = \hbar\omega \tag{5.1}$$

$$\boldsymbol{q} = \boldsymbol{k}_i - \boldsymbol{k}_f \tag{5.2}$$

$$q^2 = k_i^2 + k_f^2 - 2k_i k_f cos\,(2\theta) \tag{5.3}$$

where 2θ is the scattering angle (Figure 4.2).

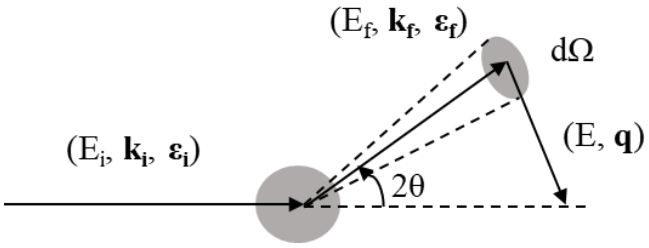

Figure 4.2: Representation of an inelastic scattering process in transmission geometry

For high energy x-ray scattering, $E<<E_i$, thus q from equation (5.3) is written

$$q = 2k_i \sin\theta \tag{5.4}$$

IXS is divided into two main categories. The resonant IXS (RIXS), where the incident photon energy is adjusted to be in resonance close to absorption edges or near to an atomic transition. In general, experiments using RIXS are considered to be difficult since it is harder to extract the results using conventional theory models [180]. The non-resonant IXS (NRIXS) is a better-suited method to extract atomic dynamics and structure, due to established theoretical knowledge. For a scattering event, the Hamiltonian of an electron system is:

$$H = H_0 + H_{int} \tag{5.5}$$

where, H_0 describes the kinetic and potential energy of the electron and H_{int} describes the interaction between the electron and the electromagnetic field (incident photon).

The non-relativistic interaction Hamiltonian is written [179, 181]:

$$H_{int} = \sum_j \frac{e^2}{2mc^2} \boldsymbol{A}_j^2 + \sum_j \frac{e}{mc} \boldsymbol{p}_j \cdot \boldsymbol{A}_j \tag{5.6}$$

where, j is the sum of electron, $\boldsymbol{p_j}$ the momentum and $\mathbf{A}_j$ is a vector potential of the field. The first term is associated with the Thomson scattering of the electromagnetic radiation (photon)

by the valence electron and is strongly connected with NRIXS. The second term involves electronic transition and is connected with absorption or emission phenomena and RIXS. In this chapter, resonance phenomena will be neglected as the results are detained from NRIXS.

The experimentally measured quantity is the double differential cross-section and for the IXS can be written as [178, 179]:

$$\frac{d^2\sigma}{d\Omega d\hbar\omega_f} = \left(\frac{d\sigma}{d\Omega}\right)_{Th} S(\boldsymbol{q},\omega) \tag{5.7}$$

where $(d\sigma/d\Omega)_{Th}$ is the Thomson scattering cross section, which describes the coupling between the photon and the electron. $S(\mathbf{q},\omega)$ is the dynamic structure factor which is the main quantity to describe the results from IXS and "describes the excitation strength of the scattering system from the initial state $|i\rangle$ to the final state $|f\rangle$" [177]. From first order perturbation theory, we can derive that

$$\left(\frac{d\sigma}{d\Omega}\right)_{Th} = r_0^2(\boldsymbol{\varepsilon}_i \cdot \boldsymbol{\varepsilon}_f)^2 \left(\frac{\omega_f}{\omega_i}\right) \tag{5.8}$$

where $r_0 = e^2/mc^2$ is the electron radius. For the NRIXS case, ω_f/ω_i equals to 1, since the energy loss E for phonons (10-200 meV) is much smaller than the incident beam energy E_i (~ 11 keV). Thus, IXS results to no correlation between momentum and energy transfer.

Based on Fermi's golden rule, the dynamical structure factor is written [178]:

$$S(\boldsymbol{q},\omega) = \sum_{i.f} \left|\langle f| \sum_j e^{i\boldsymbol{q}\boldsymbol{r}_j} |i\rangle\right|^2 \delta(\hbar\omega + E_i - E_f) \tag{5.9a}$$

$$= \frac{1}{2\pi}\int dt e^{-i\omega t}\langle f| \sum_{j,j'} e^{-i\boldsymbol{q}\boldsymbol{r}_{j'}(t)} e^{i\boldsymbol{q}\boldsymbol{r}_j(0)} |i\rangle \tag{5.9b}$$

First term of equation (5.9a) shows the possibility for an excitation to take place from the initial to a final state on the momentum level, while the Dirac function shows, when this excitation is possible on the energy level. The equations (5.9a & b) are based on first order perturbation theory, which IXS always satisfies [177, 182]. Depending on the value of the transferred momentum and energy, the dynamical structure factor can describe various scattering processes, from collective ones such as phonons, excitons and plasmons to single particle contributions such as Compton scattering [183]. For the study of collective scattering processes the dynamic structure factor is often written as a function of dynamic susceptibility $\chi(\mathbf{q},\omega)$ [178]:

$$S(\boldsymbol{q},\omega) = -\frac{1}{\pi}\frac{1}{1-e^{-\beta\hbar\omega}} Im\chi(\boldsymbol{q},\omega) \tag{5.10}$$

where $\beta = 1/k_BT$.

4.3 Experimental setup

The IXS measurements took place on the GALAXIES beamline at S.O.L.E.I.L. synchrotron centre. Next, some details of the beam line will be presented as found at [184, 185]. The beamline provides a high flux X-ray beam that ranges from 2.3 – 12 keV. The main components of the beamline's optical layout are depicted at Figure 4.3. The optical layout consist of an in-vaccum 20mm-period undulator U20 (Nd2Fe14B). The undulator serves the energy range (2.3 – 12 keV) with odd harmonics from 1 to 9 and reaches a maximum magnetic field of 1.04T at a minimmum gap of 5.5mm.

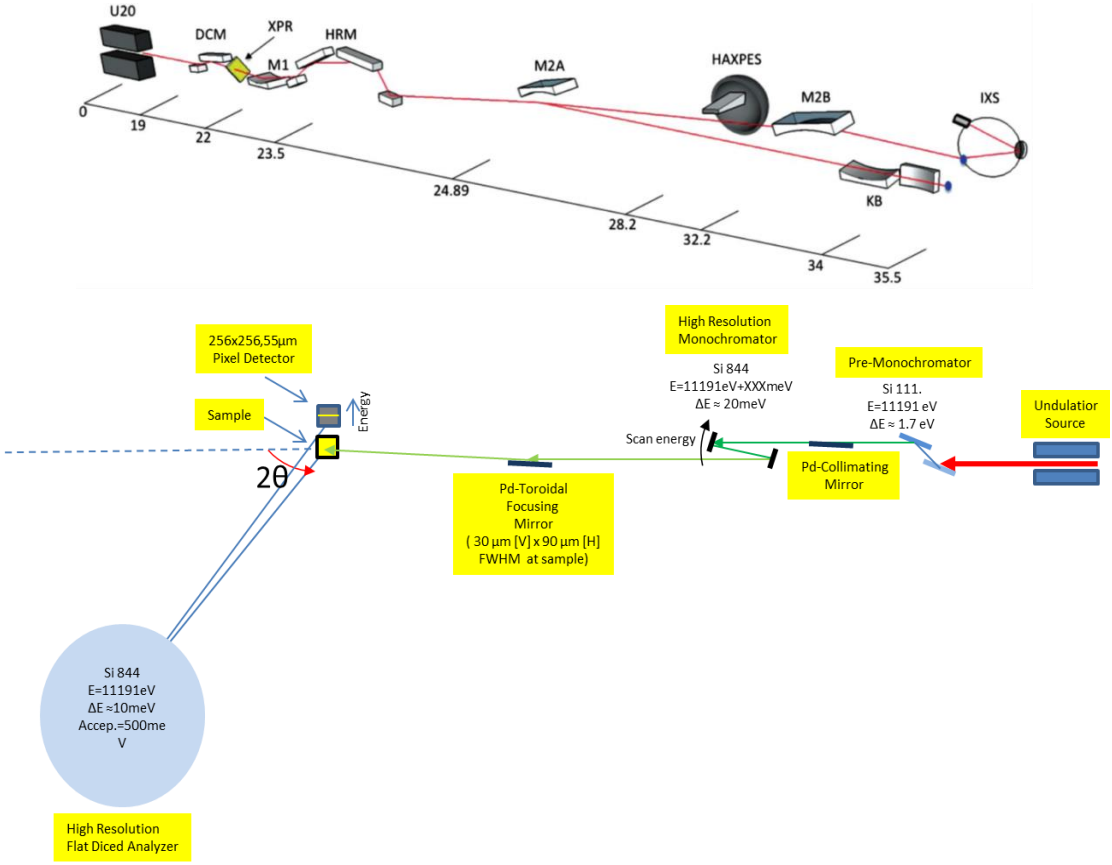

Figure 4.3: Top) Configuration of the optical layout of GALAXIES beamline that is used to create a highly focus x-ray beam at energy range 2.3 – 12 keV. The horizontal scale is the distance in meters. The sample is placed as shown by the blue point in the circle. Picture taken from [185]. **Bottom)** Technical characteristics of the experimental setup as provided by Dr J. Ablett.

The next optical component is the double-crystal monochromator (DCM). It is made out of silicon (1 1 1), which thermal expansion is low (1/3 of copper) and is cooled by liquid nitrogen. The cooling serves to dissipate the thermal power from the undulatory source. A second two-bounce high-resolution monochromator (HRM) is inserted in the beam and provides resolution $\delta E \sim 31$ meV FWHM for the experimental configuration of our measurements. The monochromator utilises backscattering geometry to satisfy higher angular acceptance [180]. The HRM gives energy resolution of $\delta E/E \sim 1.4 \times 10^{-4}$ FWHM.

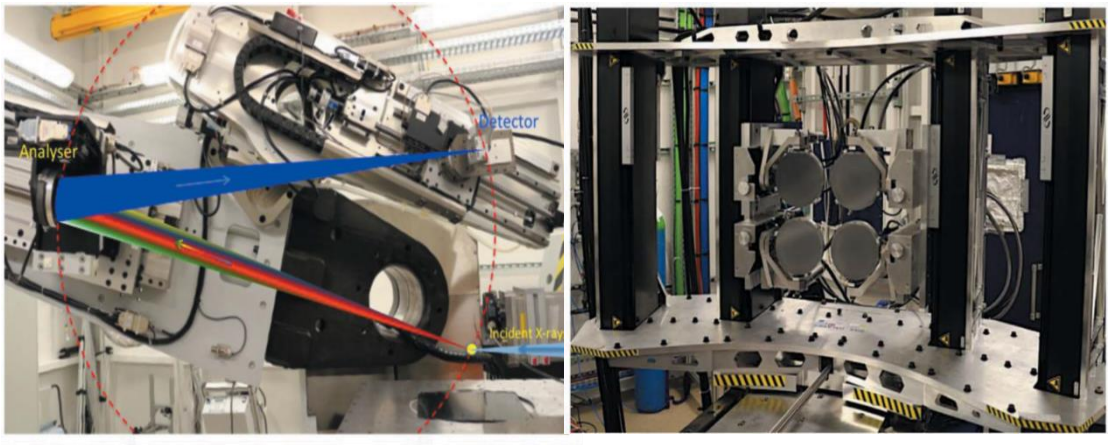

Figure 4.4: IXS spectrometer of GALAXIES beamline (left side). Typical geometry of spherical analyser arranged for IXS (right side) [185].

The sample is placed on the sample holder (yellow dot of the left side picture in Figure 4.4). Then, it is sealed in a cage filled with helium. The incident monochromatic beam hits the sample, and the scattered beam is collected by the multi-analyser configuration (right picture of Figure 4.4). Each crystal analyser has a diameter of 10 cm and radii of curvature of 0.5m to 1m. Each analyser is composed of various crystallites on a curved surface. The analysers are silicon-made and allows Bragg angle from 75.6º to 90º. For the present measurements, the analyser stays at fixed Bragg angle. For these set of IXS measurements, we utilize one analyser (Figure 4.4 right side) to ensure increased momentum resolution. The scattered beam is collected from the analyser to the detector. Between the sample, analyser and detector is placed a plastic bag filled with helium to reduce the absorption and the background noise from the air, since helium is x-ray transparent. The analyser and the detector are mounted to be in a Rowland circle geometry throughout the measurements (Figure 4.4 left side dotted red line). Each cube of the analyser serves as a dispersive optical element and the signal from the ~ 10000 cubes are combined into a single image on the detector. The image analysis provides a spectrum after calibration from pixel to meV.

Crystallographic description of the samples:

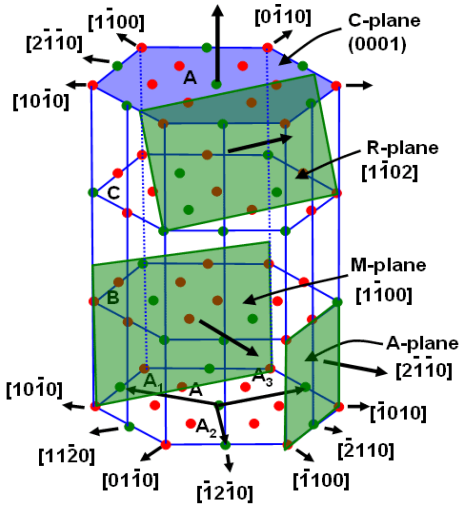

Figure 4.5: Different planes of Al_2O_3 structure. Figure taken from https://www.globalsino.com/EM/page2591.html.

In Figure 4.5, we show the structure of Al_2O_3. Green points represent the aluminium atoms, while red points the oxygen ones. For our measurement, we will use a monocrystalline α-alumina sample with c-plane orientation. More specifically, we will scan the sample from the reciprocal plane (0 0 6) to (0 0 7). The penetration length of the x-ray beam will be at about 80μm, meaning that we probe the bulk dynamics of the material.

4.4 Dynamic measurements

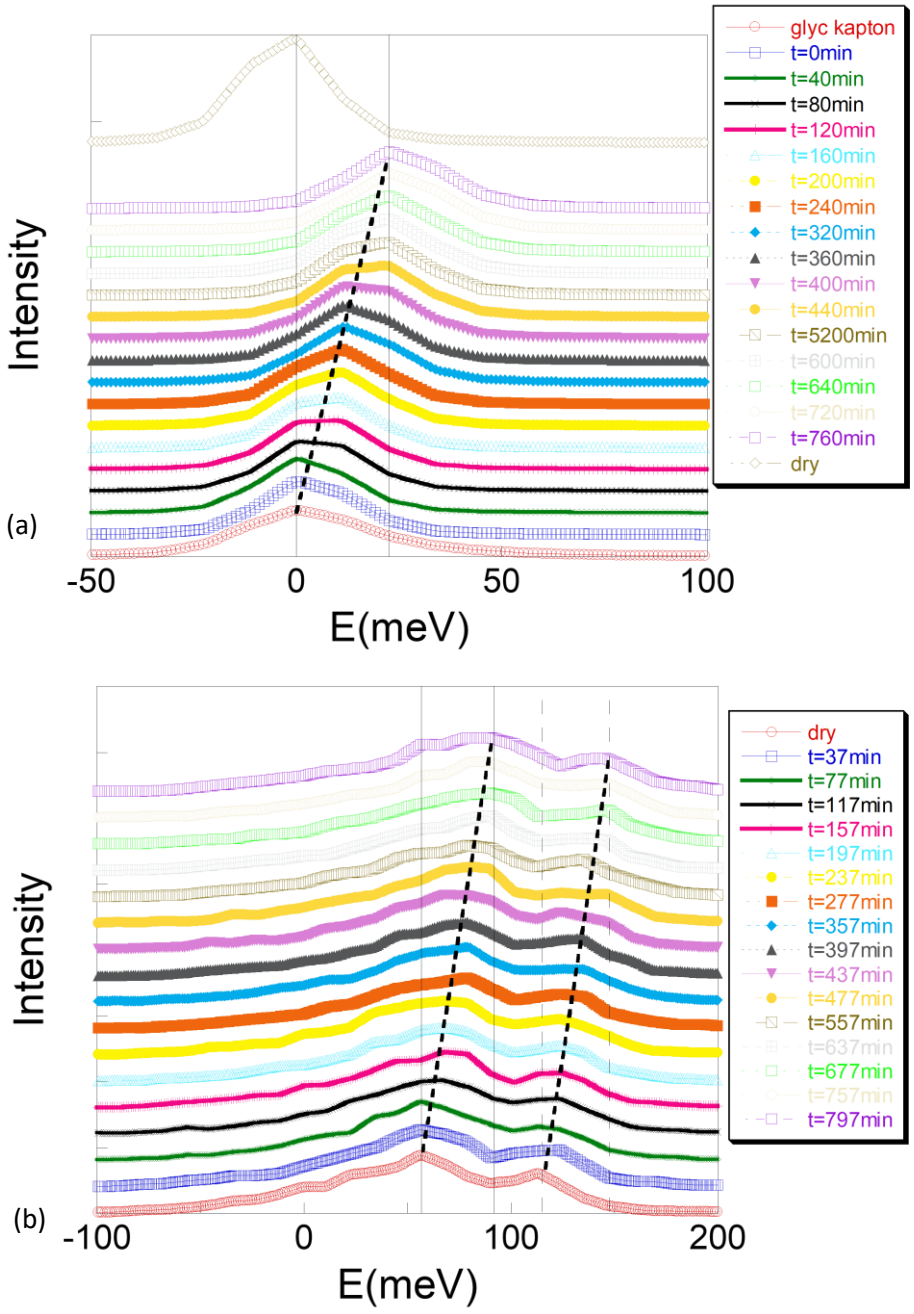

Figure 4.6: a) Inelastic x-ray scattering scan of monocrystal α-alumina sample, with c-plane orientation at the reciprocal plane (0 0 6.1) wetted by a layer of glycerol, where the intensities are shifted for sake of clarity. The legend includes different scans over the course of hours, with the t=0min measurement being the first one after the glycerol deposition on the surface, while t=760min being the time of the latest one after the glycerol deposition. Glycerol on Kapton is the reference inelastic scattering spectrum of glycerol, since Kapton is transparent to the x-ray beam. **b)** Same graph as (a), for (0 0 6.95). Black lines are used as eye guides.

In this section, we will show some preliminary results conducted on wetted α-alumina surfaces. Specifically, we will demonstrate the evolution of the phonon dynamics of the bulk alumina when the surface is wetted by glycerol over a long period of time (several hours) for different positions (q values) as we probe the dynamics from the (0 0 6) to (0 0 7) reciprocal plane.

In Figure 4.6, we observe the evolution of the alumina energy spectrum wetted by glycerol. Due to limited resolution (~ 31meV), we imposed that the highest intensity of the dry alumina close to 0 meV (quasi-elastic peak) as the plane (0 0 6) is a Bragg peak and thus would remain true for the selected q value (q = 0.1). The angle of the x-ray beam that hits the sample is sufficiently large to penetrate at 8μm inside the alumina surface, thus probing bulk response. Once glycerol is deposited on the surface (that is vertically mounted), we measure the IXS spectra for an extended time (time interval between same q value is about 40 minutes). We notice a gradual shift of the energy peaks over time for both q = 0.1 (Figure 4.6a) and q = 0.95 values (Figure 4.6b). For q = 0.1, the energy shift of the peaks is about 22.5meV, while for q = 0.95 the shift is about 35meV (Figure 4.7), hinting processes that took place due to the wetting of the alumina surface with glycerol. The results show that the wetting evolves with time for several hours, as the interactions between interfacial atoms and molecules is reinforced with the removal of bubble traps over a period of time. In the present measurement, we ensure pronounced interactions of the liquid glycerol with the monocrystal α-alumina surface since the current orientation (0 0 1) provides optimal wettability [186]. As seen from the previous reference, the wetting evolves with time, ensuring smaller contact angle over time. The different spectrum shift at different position of the Brillouin zone may hint an interfacial molecular orientation that is preferable, leading to orientation-based change of local dynamics. As the present measurements probe the bulk alumina, the newly established dynamics could not be ignored. An interpretation could be given on glycerol molecule polarization. Reports show that weak temperature gradients were identified at the vicinity of a wetting surface [172] indicating a polarization of the liquid molecules due to the surface (in absence of external thermal field), leading to induced electrostatic fields on the liquid [187] that substantially affect could affect the solid dynamics.

Except from the energy shift, the alumina energy spectra seem to be unchanged within the resolution. Based on Raman scattering reports [188], tensile stress on a material could lead to energy shift of about 0.54meV/GPa. Thus, for our case, the glycerol – sapphire interface could induce stresses leading to a gradual tensile stress in the bulk of solid close to the surface as the wetting is improved. However, these results are preliminary and for complete understanding of the state of the solid, complementary measurements at various penetration lengths (closer to the surface) are required. Moreover, measurements depicting a weaker energy shift for alumina wetted by water was also observed, but not depicted on the current manuscript. Nevertheless, a detailed study for different kinds of liquids is a necessity to properly understand the evolution of the interfacial energy in solid dynamics.

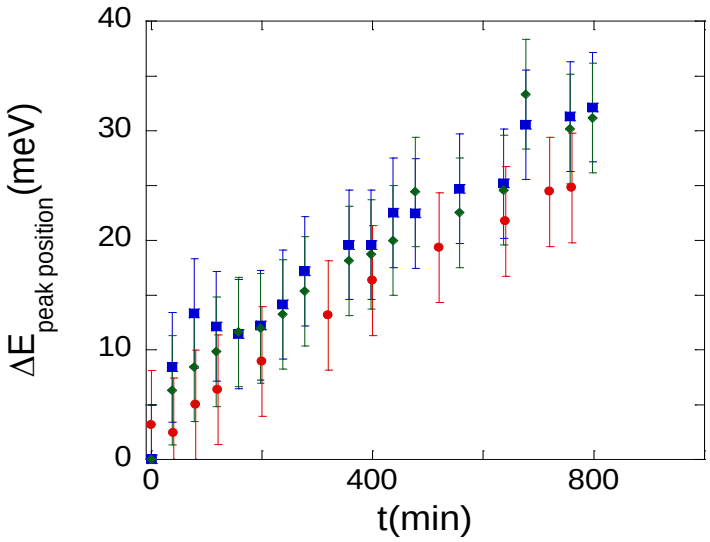

Figure 4.7: Red points represent the energy shift over time of the maximum peak of the energy spectrum of Figure 4.6a (vertical solid black line), while the blue and green points represent the energy shift over time of the maximum peaks of the energy spectrum of Figure 4.6b (vertical solid and dashed black line respectively). The peak position was identified by plotting a Gaussian function on the energy spectrum for the spectra of Figure 4.6a and several ones for Figure 4.6b.

General conclusion and perspectives

The recent identification of a finite shear elasticity in confined fluids (up to the sub-millimeter scale) has motivated the search for other solid-like properties. This is the aim of the present experimental PhD thesis, which uses the same experimental conditions to explore and identify new properties of confined liquids using mainly an innovative microthermal approach.

The access to the sub-millimeter shear elasticity was achieved by taking into account the fluid/substrate interfacial forces in the protocol of dynamic mechanical analysis. A strong liquid/substrate interaction amplifies the fluid response and reveals a mesoscopic liquid shear elasticity (0.1-10Hz). As a result, the viscoelastic response is not universal but can be modulated by the fluid/surface boundary conditions and by the scale at which the fluid response is measured. The mesoscopic shear elasticity concerns both simple liquids (Van der Waals and H-bond liquids), complex fluids (polymer melts, molecular glass formers, ionic liquids) and physiological fluids [18, 19, 20, 21, 22, 23, 26, 27]. The experimental identification of a "static" liquid shear elasticity at sub-millimeter scale is in agreement with recent theoretical predictions, foreseeing, that liquids can support the propagation of shear waves above nanoscopic scales. Thus, validating the measurement of a solid-like response extended up to a finite length scale of 1/k where k is the wavevector over which shear elastic waves can propagate (k-gap model [30, 77, 85, 86, 87, 88, 89, 28, 29, 90]). The liquid shear elasticity has independently established by both an experimental and theoretical approaches; that is the mesoscale liquid state is dominated by long-range elastic intermolecular interactions.

Because of the mesoscopic shear elasticity, fluids resist to flow below an elastic threshold whose resistance depends on the considered scale. The immediate consequence is that a thermo-elastic coupling becomes possible, challenging the assumption of an instant dissipation via the fast lifetime of the thermal fluctuations and justifying the search of another solid property: the thermoelasticity.

We have used the same experimental conditions (sub-millimeter scale, wetting substrate) to explore the stability of the thermal liquid equilibrium under a shear stress. Such a study has become possible due important recent instrumental progresses in the infrared detection that have enabled an accurate determination of the temperature in a wavelength range of 7-14μm. In accordance with the principle of viscoelastic measurements, we have applied a mechanical shear strain either oscillatory by modulating frequency and strain amplitudes or applying a step strain (Heaviside-like deformation). In both cases (low frequency oscillatory shear strain and step strain test), we have revealed a non-ambiguous dynamic thermal response of all tested liquids: PPG-4000, glycerol and liquid water (tested at one gap thickness).

In the case of oscillatory shear strain, we show that the shear strain generates a thermal wave synchronous with the applied strain within a wide range of strain amplitudes, different frequency and for gap thicknesses varying from 100μm up to the millimeter. The thermal waves are multiple forming hot and cold thermal shear bands filling the sub-millimeter liquid gap.

● Two strain regimes have been observed defining a linear and a non-linear behavior of the thermal waves.

- At low frequency and relatively low strain amplitude ($\gamma < 2000\%$), we observed that hot and cold thermal waves reproduce approximately the sin shape of the excitation and exhibit nearly a linear dependence to the mechanical shear strain.

The remarkable linear dependence of the thermal variation with respect to the strain amplitude indicates a direct thermo-strain coupling. Cold and hot wave amplitudes increase symmetrically with the strain rate obeying to the sin model oscillating around the equilibrium temperature defined by a zero-ΔT. The symmetric evolution of the cold and the warm branch of the thermal wave indicates a strict compensation in terms energy gain and loss that fits with a simple sin model $\Delta T(t) = \Delta T_A . sin(\omega.t + \Delta\phi)$ where $\Delta\phi$ is always found smaller than $\pi/4$. The quantity reported to the strain value $\Delta T_A(\gamma)/\gamma$ is thus a constant that can be considered as the thermal analogue of the shear stress σ reported to the shear strain, σ/γ which defines the shear elastic modulus following the Hooke's law. The liquid ability to convert the shear wave energy in local thermodynamic states exhibits the characteristics of a conservative mechanism that is:

- The linearity of the amplitude of the thermal wave as the shear strain increases (up to a shear strain value),
- A synchronous response with the applied excitation,
- A nearly instant thermal response to the strain,
- A rapid return to the equilibrium temperature at the strain stop,
- An absence of heat conduction between bands and with the environment.

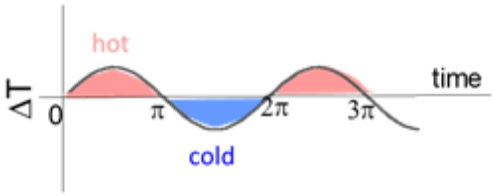

Simplified scheme illustrating a (simplified) behavior of the liquid thermal wave. The liquid is alternatively cold or hot with time. The thermal wave can be modelled by a sin wave whose amplitude is proportional to the applied strain, oscillating around the equilibrium temperature ensuring a global thermal balance (up to high strain amplitudes). The energy used to create a hot or cold band of similar temperature variations is equivalent.

Therefore, we have shown that while the viscoelastic measurement indicates a viscous behavior, the simultaneous recording of the thermal behavior that evolves nearly in phase with the strain wave, indicates a non-dissipative behavior. These thermal features are non-dissipative in nature indicating that the viscous (supposedly dissipative) behavior measured by stress measurements is incomplete and hides actually the complexity of the liquid dynamic.

- At larger strain values (typically above $\gamma > 2000\%$ at 240µm) or by increasing the frequency, the thermal signal is no more linear with the strain amplitude. The applied excitation no longer allows the relaxation of the thermal effect between two successive oscillations. The shape of thermal signal transits from an almost perfect sin wave to an anharmonic wave where higher harmonics affect greatly the thermal response [189]. The higher harmonics (second and third harmonics) indicate the occurrence of a dissipative process that might be attributed to flow instabilities, for example, increasing phase shift between thermal bands, compressibility limits, dynamic stick-slip friction, formation of slippage layer, autophobicity [71], generating distorted thermal waves with double frequency of the applied excitation.

● The thermal waves are also scale dependent. The study versus gap thickness indicates that the amplitude of the thermal wave increases with a decrease of the gap size. Of interest is the similar plateau value reached at large strain amplitudes by the thermal variation for each gap thickness (section 2.4.6). From the measurements, the value is constant no matter the gap thickness (at around 0.1K), showing an upper limit of temperature change. The increase of the

thermal effect with decreased scale is in agreement with the increasing shear elasticity of liquids $G' \sim L^{-3}$ [29]. The non-linear region ($\gamma_0 > 2000\%$) seems affected by the system scale (Figure 2.17a, Figure 2.22e & f, Figure 2.23b). As the gap decreases, the evolution changes from a constant profile to a decreasing one.

● The (shear) step strain study has also revealed that the confined liquid is able to respond thermally and nearly instantaneously to a step deformation. Both early time and relaxation of the studied thermal effect have been analyzed. The experiments show that, upon a shear step deformation at mesoscopic scale, the liquid loses its temperature stability, creates major hot and cold thermal bands, where the temperature deviates symmetrically from the equilibrium one. These mechanically induced thermodynamic rearrangements imply an ability of the liquid to store the strain energy. This process is adiabatic at small scale (100μm) for the glycerol as seen from the global temperature invariance while it generates a global cooling at larger thicknesses in agreement with an induced stretching state. The generated bands responded thermally similarly to a second order system like a RLC circuit to a sudden mechanical excitation, meaning that there is an exchange of energy between two storages. After the overshoot, the liquid loses the gain from the step shear strain, though constant strain is maintained. The thermal relaxation is described by a stretched exponential, behavior encountered on the dielectric response of glass formers (like glycerol). Thus, as a disordered system, the vibrational density of states of the liquids consists low-energy (frequency) modes greater than the Debye cut-off frequency [45].

● The examination of the shear stress wave confirms that from a viscoelastic point of view, the thermal waves are identified in a "viscous" regime which is in contradiction with the definition of a viscous flow supposed to be athermal and homogeneous. Therefore, the viscosity (and the viscoelastic) measurement is blind to adiabatic thermal changes occurring the liquid. The accurate examination of the normal force shows a weak variation of its value (2% of shear stress variation, close to the sensor limitations) but which nevertheless might be the stress signature of the thermal effect via another typical elastic effect which is shear dilatancy. This normal force variation is more pronounced in the case of the stress relaxation observed after a step strain test. The normal stress reproduces the shape of the thermal waves. In the case of thermal harmonics, the normal stress increased in amplitude and developed harmonics while being almost in-phase with the thermal waves. During step strain measurements, a clear second order response of the normal stress is evident at the same time as the thermal change occurs. All of the above results elucidate a direct connection of the normal stress rise with the studied temperature changes but stands a difficult topic for interpretation. Interpretation could be given in the frame of the shear elasticity [151, 152, 153] or vorticity banding [97, 98, 2]. Nevertheless, for the deeper understanding of the connection between normal stress rise and thermal effect, a quantitative experimental study of the normal stress would be of interest even if balance effects due to the antagonistic stresses (hot and cold waves balances in time or in the volume) lowers the impact.

In the frame of the study of the influence of the substrate (the alumina supports used are poor thermal conductors), we have also shown that it is possible to generate liquid thermal waves on aluminum surfaces such as those conventionally used in rheology. The aluminium surface is not a suitable substrate if the liquid thermal behaviour is the focus of the study. Due to its high thermal conductivity, a great part of the energy is conducted to the plates within the experimental time period of the measurements. Due to its high reflectivity and emissivity, an accurate determination of the liquid temperature can be hardly done. Alumina plates used in most of our measurements, do not exhibit these drawbacks and are adequately adapted to the present study. Studying the effect of surfaces of different conductivities would elucidate the limit where the thermal effect is greatly limited in the liquid.

To conclude, in the present thesis, we have revealed thermo-mechanical effects in mesoscale liquids, focusing on the origin of the effect, its mechanism and its scale dependence. The study of the effect in complete adiabatic conditions is of interest. From our measurements, we may deduce that the effect is adiabatic in nature, but it implies that the dynamics are faster than heat transfer/conduction, to ensure in-phase relation between mechanical deformation and thermal variation (zero phase shift). Another perspective worth studying is the evolution of the thermo-mechanical effect while a constant flow is applied, as it is the case in a microfluidic channel. Thermal study of various liquids (e.g., Van der Waals, etc.), polymers (different molecular weights), gels, and other soft materials would complete our understanding of the thermo-mechanical effect. However, for several cases even if the elasticity increases (e.g., polymer melts), the study stands different challenges and possibly elucidates effects like the so-called viscous heating friction.

Lastly, from theoretical perspective, the above results are not interpreted within the conventional Maxwell fluidic frame since the frequency of the external mechanical excitation do not couple with the molecular relaxation dynamics and thus only dissipation should occur. On the other hand, they demonstrate thermo-elastic effects in liquids, which can be explained in terms of the unsuspected ability of liquids to support low-frequency shear waves. The ability of liquids to propagate shear waves is described by the k-gap theory [79, 80, 81, 82, 83, 84, 10, 87, 28, 29]. The theory reconsiders the concept of short-range interaction and introduces the notion of propagating solid-like shear waves defining a k-gap dispersion relation. The dispersion law indicates that the propagation of solid-like shear waves is made possible for $k > k_g=1/(2c\cdot\tau)$ (real solutions). The present observations carried out at mesoscopic scale provide experimental evidence in this direction. As mentioned in [77], "we consider a liquid as collection of dynamical regions of characteristic size $c.\tau$ where the solid-like ability to support shear waves operate". These dynamical regions might coincide with the thermal bands. The quantity defined as propagation length of the shear waves $d_{el}=c\cdot\tau$ corresponds in the case of glycerol to $d_{el} \sim 3$ μm ($c=3000$ m/s and $\tau=10^{-9}$ s given for density fluctuations at equilibrium), and thus the shear wave (exponential in nature: $e^{-x/2d_{el}}$) should be dissipated at a distance of about 30μm. The predicted propagation length is of similar order to the width of the elementary bands (~ 25–80 μm), which might indicate the limit of the "correlated" interactions that lead to the generation of the thermal bands. The prediction of a finite propagation of the solid-like shear wave might explain why the liquid splits in several thermal bands, d_{el} being the ultimate liquid length supporting the shear wave. Over this limit, the conditions for a new shear mechanism take place and producing new (thermal) shear bands, each delimited by the finite propagation length.

Another approach on the existence of the bands is possible by utilizing the normal modes that exist in the system. The bands are macroscopically large since they contain a huge number of molecules, hence it makes sense to define long-wavelength phonon modes that live in these regions. In the hot/compressed regions the volume V of the region gets reduced, whereas in the cold/expanded regions the volume V is enlarged. Then, we may write the microscopic definition of the Grüneisen parameter:

$$\gamma = -\frac{d \ln \omega_n}{d \ln V}$$

Since the Grüneisen parameter γ is positive for liquids [167], this relation gives (upon integration) that the phonon frequency ω_n increases as the volume V decreases, whereas ω_n decreases as the volume V increases. Since the vibrational frequency is related to temperature, via $T = h\omega_n/k_B$, it is clear that T increases in the regions where V decreases ("compressed" regions), whereas T decreases in the regions where V increases ("expanded" regions), thus

leading to a hot and a cold band for the compressed and the expanded regions, respectively [190].

It is important to point out that thermal bands resemble also shear bands observed of soft matter flows, known as vorticity banding and for which the elastic origin remains unclear [97, 98]. The bands during vorticity banding exhibit different stress states for the same shear, which is similar with the case of the observed thermal bands.

Finally, from the preliminary IXS measurements on the GALAXIES beamline at S.O.L.E.I.L., we have demonstrated the evolution of the phonon dynamics of the bulk alumina when the surface is wetted by glycerol over a long period of time (several hours). It was known that the liquid molecule energy is modified at the vicinity of a solid wall (the surface molecules explore other neighborhood and are in another thermodynamic state with respect to the bulk molecules). It seems from these preliminary results that the dynamics (phonons) of the solid is also modified in the presence of a wetting liquid, creating a new interfacial solid/liquid equilibrium.

Liquid shear elasticity makes possible the identification of new non-equilibrium properties such as these strain-driven thermoelastic effects that we are just beginning to discover experimentally [191] and echo new theoretical predictions for liquid dynamics [29, 28, 93] and liquid thermal balance. The development of a thermoviscoelastic model, which considers viscous dissipation, scale dependent elastic storage of energy, and potentially solid-liquid interface would advance our understanding of liquids.

Résumé substantiel en français

L'état liquide est le plus répandu à la surface de la Terre, il y joue un rôle essentiel mais c'est aussi l'état de la matière le moins compris. L'échelle mésoscopique est certainement l'échelle à laquelle les limites de notre compréhension sont les plus visibles. Qu'il s'agisse de transitions de phase spectaculaires induites par cisaillement [1], d'apparitions de bandes de cisaillement [2], d'instabilités d'écoulement ou d'instabilités de surface mais aussi de contributions interfaciales subtiles (liquide/solide ou liquide/liquide), de la nature du substrat, ces effets remettent en cause une conception simple de l'état liquide et pointent les directions à prendre. Comprendre l'échelle mésoscopique est primordial, c'est également l'échelle de la microfluidique et des fluides physiologiques donc de la chaîne du vivant.

D'un point de vue théorique, l'état liquide ne permet pas une compréhension fine, contrairement aux solides et aux gaz. En raison du manque de périodicité entre les molécules liquides, une étude théorique similaire à celle des solides a été exclue, rendant l'approche fluidique de Maxwell (1876) [3] dominante. D'un point de point thermodynamique, les liquides sont supposés dissiper toute forme d'excitation mécanique à des échelles de temps supérieures à celles de leurs fluctuations thermiques (en accord avec le théorème de fluctuation-dissipation) [4]. Frenkel [5] a proposé que les liquides supportent les ondes de cisaillement si la dynamique de l'excitation est plus rapide que le temps de relaxation moléculaire, définissant le temps de relaxation de Maxwell comme le temps entre deux sauts d'une particule d'une position d'équilibre à la nouvelle position. Ainsi, la fréquence critique $\omega_F = 1/\tau_M$, est l'inverse d'un temps de relaxation moléculaire. Pour des fréquences plus petites ($\omega < \omega_F$), le liquide se comporte de manière dissipative, c'est le régime hydrodynamique. Tandis que pour $\omega > \omega_F$, la propagation des ondes de cisaillement conduit à une réponse de type solide haute fréquence. La vérification expérimentale de l'élasticité haute fréquence est arrivée plus tard avec les avancées technologiques, comme les grandes infrastructures de recherche [6, 7, 8, 9, 10].

Cependant, il existe une large gamme de matériaux qui présentent à l'échelle macroscopique une réponse intermédiaire entre le liquide visqueux et la réponse élastique comme les polymères, les gels, les solutions micellaires, etc. Des théories moléculaires ont été proposées [11, 12, 13, 14, 15, 16, 17], inspirées du modèle initial de Maxwell, où le temps de relaxation caractéristique n'est plus celui d'une particule mais celui associé à la relaxation de la macromolécule (en termes de temps de Rouse ou de reptation suivant la longueur de chaine considérée). Ce schéma qui est conventionnellement adopté en rhéologie des polymères a récemment été remis en question avec l'identification d'élasticité de cisaillement à basses fréquences à l'échelle mésoscopique notamment dans les fondus de polymères melts [18, 19], [20, 21, 22, 23, 24, 25]. En effet, l'existence d'élasticité « statique » montre qu'une description en termes de temps de relaxation n'est pas pertinente, mais qu'il convient de prendre en compte des corrélations élastiques, autrement dit l'émergence d'un comportement de type solide à l'échelle mésoscopique.

Divers travaux expérimentaux ont mis en évidence un comportement « statique » de type solide des liquides. Ces études ont été menées sur des liquides à différentes échelles, du nanomètre [26, 27], du micromètre [18, 19] au submillimétrique [20, 21, 22, 23]. Dans ces études, l'excitation mécanique de cisaillement est appliquée dans le domaine des basses fréquences (Hz), de plusieurs ordres plus lente que la dynamique moléculaire (GHz – THz pour les molécules simples). Dans ces conditions, il a été montré que le liquide résiste à l'écoulement avec une élasticité au cisaillement mesurable. Cette observation a été faite sur des échelles mésoscopiques relativement larges et sur une grande variété d'études dynamiques de liquides incluant la rhéologie des polymères. L'élasticité de cisaillement ne peut pas être décrit comme

une propriété induite par le substrat, mais comme une propriété intrinsèque. Cette notion s'oppose à la description viscoélastique classique, où l'élasticité de cisaillement s'évanouit dans les liquides à basse fréquence quelle que soit l'échelle (hypothèse du modèle de Frenkel). L'accès à l'élasticité de cisaillement submillimétrique a été réalisé en prenant en compte les forces interfaciales fluide/substrat dans le protocole d'analyse mécanique dynamique. Une forte interaction liquide/substrat amplifie la réponse fluide, et révèle l'élasticité de cisaillement mésoscopique (0.1-10Hz). De ce fait, la réponse viscoélastique n'est pas universelle mais modulée par les conditions aux limites fluide/surface et par l'échelle à laquelle la réponse fluide est mesurée. L'élasticité au cisaillement mésoscopique concerne à la fois les liquides simples (liquides de Van der Waals et H-bond), les fluides complexes (fondus de polymère, fondus de verre moléculaire, liquides ioniques) et les fluides physiologiques [18, 19, 20, 21, 22, 23, 26, 27]. L'élasticité basse fréquence montre l'existence de corrélations élastiques à longue distance entre les molécules liquides à l'échelle mésoscopique. A cette échelle, le comportement des liquides n'est plus celui du « bulk » bien que la dynamique concerne un grand nombre de molécules. Il y a donc urgence à revoir les modèles théoriques pour tenir compte de la réalité expérimentale.

Et de fait, d'un point de vue théorique, la théorie de Frenkel a été récemment révisée montrant que la propagation des ondes de cisaillement dans les liquides est possible mais sur une distance réduite 1/k définie par le temps de propagation de l'onde dans le milieu considéré ($\tau.c$ où τ est le temps de Maxwell et c la vitesse du son) [28], tandis que sur la base de la dynamique de réseau non affine, la dépendance à l'échelle de l'élasticité de cisaillement dans les liquides a également été récemment établie [29]. L'identification expérimentale d'une élasticité de cisaillement liquide « statique » à l'échelle submillimétrique est donc en accord avec les prédictions théoriques récentes, prévoyant que les liquides peuvent favoriser la propagation des ondes de cisaillement au-dessus des échelles nanoscopiques. Ainsi, valider la mesure d'une réponse de type solide étendue jusqu'à une échelle de longueur finie de 1/k où k est le vecteur d'onde sur lequel les ondes élastiques de cisaillement peuvent se propager (modèle k-gap model [30, 77, 85, 86, 87, 88, 89, 28, 29, 90]). L'élasticité de cisaillement liquide a été établie indépendamment par des approches expérimentales et théoriques, la dynamique des liquides est dominée par des interactions intermoléculaires élastiques à l'échelle mésoscopique.

Du fait de l'élasticité de cisaillement mésoscopique, les fluides résistent à l'écoulement en dessous d'un seuil élastique dont la résistance dépend de l'échelle considérée. La conséquence immédiate est qu'un couplage thermo-élastique devient possible, remettant en cause l'hypothèse d'une dissipation instantanée via la durée de vie rapide des fluctuations thermiques et justifiant la recherche d'une autre propriété du solide : la thermoélasticité. C'est l'objectif de la présente thèse expérimentale.

D'un point de vue thermique et sans apport de chaleur extérieure, les simulations moléculaires prévoient une augmentation de la température par friction visqueuse à la paroi dans les liquides nano-confinés sous cisaillement et pression [32, 33]. L'effet de paroi sur différents paramètres thermodynamiques a été largement étudié dans les liquides confinés [34, 35, 36, 37, 38, 39, 40, 41, 42, 43] tandis qu'à l'échelle macroscopique, l'approche théorique conventionnelle (Maxwell) prédit une augmentation de température par friction visqueuse générée lors d'un cisaillement oscillant à très grande amplitude de déformation et dans des conditions non-adiabatiques pour les polymères fondus [44]. Il n'y a pas à notre connaissance de données expérimentales validant les simulations en température.

Nous avons utilisé les mêmes conditions expérimentales (échelle submillimétrique, substrat mouillant) que celles utilisées pour accéder à l'élasticité de cisaillement et y avons couplé une

approche microthermique innovante. Une telle étude est devenue possible grâce à d'importants progrès instrumentaux récents dans la détection infrarouge qui ont permis une cartographie spatiale précise de la température dans une gamme de longueurs d'onde de 7 à 14 µm. Conformément au principe des mesures viscoélastiques, nous avons appliqué une déformation de cisaillement mécanique soit oscillatoire en modulant la fréquence et les amplitudes de déformation, soit en appliquant une déformation échelonnée (déformation de type Heaviside). Dans les deux cas (essai de contrainte de cisaillement oscillatoire à basse fréquence et essai de contrainte par étapes), nous avons révélé une réponse thermique dynamique non ambiguë de tous les liquides testés : PPG-4000, glycérol et eau liquide (testé à une épaisseur de fente).

Dans le cas de la déformation de cisaillement oscillante, nous montrons que la déformation de cisaillement génère une onde thermique synchrone avec la déformation appliquée dans une large gamme d'amplitudes de déformation, de fréquences et pour des épaisseurs d'entrefer variant de 100 µm jusqu'au millimètre. Les ondes thermiques sont multiples formant des bandes de cisaillement thermique chaudes et froides remplissant l'espace submillimétrique.

● Deux régimes de déformation ont été observés définissant un comportement linéaire et non linéaire des ondes thermiques.

- A basse fréquence et à amplitude de déformation relativement faible ($\gamma < 2000\%$), nous avons observé que les ondes thermiques chaudes et froides reproduisent approximativement la forme sinusoïdale de l'excitation mécanique et présentent une dépendance presque linéaire à l'amplitude de déformation.

La remarquable dépendance linéaire de la variation thermique par rapport à l'amplitude de déformation indique un couplage thermo-déformation direct. Les amplitudes des ondes froides et chaudes augmentent symétriquement avec l'amplitude de déformation oscillant autour de la température d'équilibre. L'évolution symétrique des bandes froides et chaudes de l'onde thermique indique une compensation stricte en termes de gain et de perte d'énergie qui correspond à un modèle sinusoïdal simple de type : $\Delta T(t) = \Delta T_A . sin(\omega.t + \Delta\phi)$ où le déphasage $\Delta\phi$ est toujours inférieur à $\pi/4$. La quantité rapportée au taux de déformation $\Delta T_A(\gamma)/\gamma$ est donc une constante qui caractérise le liquide et peut être considérée comme l'analogue thermique de la contrainte rapportée à la déformation de cisaillement, σ/γ qui définit le module élastique suivant la loi de Hooke . La capacité du liquide à convertir l'énergie des ondes de cisaillement dans des états thermodynamiques locaux présente les caractéristiques d'un mécanisme non-dissipatif qui sont :

- La dépendance linéaire de l'amplitude de l'onde thermique avec l'amplitude de la déformation de cisaillement,

- Une réponse synchrone avec l'excitation appliquée,

- Une réponse thermique quasi instantanée à la contrainte,

- Un retour rapide à la température d'équilibre à l'arrêt de la déformation (relaxation),

- Une absence de conduction thermique entre les bandes et avec l'environnement,

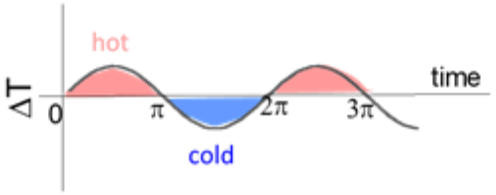

Schéma simplifié représentant le comportement (simplifié) de l'onde thermique liquide à l'échelle mésoscopique. Le liquide est alternativement froid ou chaud avec le temps (et dans le gap). L'onde thermique peut être modélisée par une onde sinusoïdale dont l'amplitude est proportionnelle à la déformation appliquée, oscillant autour de la température d'équilibre assurant un bilan thermique global (jusqu'à des amplitudes de déformation élevées). L'énergie utilisée pour créer une bande chaude ou froide de variations de température similaires est équivalente.

La comparaison avec les données rhéologiques a montré que si la mesure rhéologique indique un comportement visqueux, donc dissipatif, l'observation simultanée d'ondes chaudes et froides thermiques évoluant presque en phase avec la contrainte oscillante, indique que le comportement thermique est non dissipatif. Le comportement thermique indique que le comportement visqueux mesuré par les mesures dynamiques est incomplet et masque en fait la véritable complexité de la dynamique du liquide.

- A des valeurs de déformation plus élevées (typiquement au dessus de $\gamma_0 > 2000\%$) ou à des fréquences élevées, le signal thermique n'est plus linéaire avec l'amplitude de déformation. L'excitation appliquée ne permet plus la relaxation thermique entre deux oscillations successives. La forme du signal thermique passe d'une onde sinusoïdale presque parfaite à une onde anharmonique où les harmoniques plus élevées affectent grandement la réponse thermique [189]. Les harmoniques les plus élevées (deuxième et troisième harmoniques) indiquent l'apparition d'un processus dissipatif qui pourrait être attribué à des instabilités d'écoulement, par exemple, un déphasage croissant entre les bandes thermiques, des limites de compressibilité, un frottement dynamique de glissement, la formation d'une couche de glissement, l'autophobie [71], générant des ondes thermiques déformées à double fréquence de l'excitation appliquée.

● Les caractéristiques de l'onde thermique dépendent également de l'échelle. L'étude en fonction de l'épaisseur de l'échantillon indique que l'amplitude de l'onde thermique augmente avec une diminution de la taille de l'entrefer. Une même valeur asymptotique d'amplitude thermiques est atteinte à de grandes amplitudes de déformation pour chaque épaisseur (section 2.4.6). Cette valeur est constante quelle que soit l'épaisseur de l'échantillon (environ $\Delta T \cong 0{,}1$ K), montrant une limite supérieure de changement de température. L'augmentation de l'effet thermique avec la diminution de l'échelle est en accord avec l'augmentation de l'élasticité de cisaillement des liquides et est conforme au modèle théorique prévu par Zaccone et Trachenko en $G' \sim L^{-3}$ [29].La région non linéaire ($\gamma_0 > 2000\%$) semble également affectée par l'échelle du système (Figure 2.17a, Figure 2.22e & f, Figure 2.23b).

● L'étude de la réponse du liquide à un saut de déformation en cisaillement (fonction de Heaviside) a également révélé la capacité du liquide à répondre thermiquement et presque instantanément à ce type de déformation soudaine. Le temps court et la relaxation de l'effet thermique ont été analysés. Les expériences montrent que, lors d'une déformation de cisaillement soudaine, le liquide crée simultanément des bandes thermiques chaudes et froides importantes, où la température s'écarte symétriquement de celle d'équilibre. Ces réarrangements thermodynamiques induits mécaniquement démontrent la capacité du liquide à stocker l'énergie de déformation. Ce processus est adiabatique à petite échelle (100µm) pour le glycérol compte tenu de l'invariance globale de la température alors qu'il génère un refroidissement à des

épaisseurs plus importantes en accord avec un état d'étirement induit. La réponse thermique a les caractéristiques d'un système du second ordre (circuit RLC) à une excitation mécanique soudaine, ce qui signifie qu'il y a un échange d'énergie entre deux types de stockage. Après l'« overshoot », le liquide perd l'énergie de contrainte de cisaillement par paliers, sous déformation constante. La relaxation thermique est décrite par une exponentielle étirée, comportement observé en réponse diélectrique des « glass formers » (comme le glycérol), dont la densité d'état vibrationnel est constituée de modes de basse énergie (fréquence) supérieurs à la fréquence de coupure de Debye [45].

● Nous avons également examiné l'évolution de la contrainte de cisaillement simultanément à l'étude thermique. Cette étude confirme que les ondes thermiques sont identifiées dans un régime « visqueux » ce qui est en contradiction avec la définition d'un écoulement visqueux supposé dissipatif, athermique et homogène. Par conséquent, les mesure de viscosité (et de viscoélasticité sont aveugles aux changements thermiques adiabatiques se produisant au sein du liquide. L'examen précis de la force normale montre une faible variation de sa valeur (qui constitue 2% de variation de la contrainte de cisaillement et en dessous des limites de mesure indiquée par le fabricant) mais qui néanmoins pourrait être la signature de l'effet thermique via un autre effet élastique typique qui est la dilatance de cisaillement. Cette variation de force normale est plus prononcée dans le cas de la relaxation de contrainte observée après un saut de déformation. La contrainte normale reproduit en effet la forme des ondes thermiques. Dans le cas des harmoniques thermiques, la contrainte normale augmente en amplitude et développe des harmoniques tout en étant quasiment en phase avec les ondes thermiques. Pour les mesures en saut de déformation, une réponse claire de second ordre de la contrainte normale est mise en évidence en même temps que le changement thermique se produit. Tous les résultats ci-dessus élucident un lien direct entre l'augmentation normale de la contrainte et les changements de température étudiés, mais constituent un sujet difficile à interpréter. L'interprétation pourrait être donnée dans le cadre de l'élasticité de cisaillement [151, 152, 153] ou de la formation de bandes cisaillement, notamment de vorticité [97, 98, 2]. Néanmoins, pour une meilleure compréhension du lien entre l'élévation de la contrainte normale et l'effet thermique, une étude expérimentale quantitative de la contrainte normale serait intéressante même si les effets d'équilibre dus aux contraintes antagonistes (ré-équilibrage des ondes chaudes et froides dans le temps ou dans le volume) en réduisent l'impact.

Dans le cadre de l'étude de l'impact de la surface (les supports en alumine utilisés sont peu conducteurs thermique), nous avons également montré qu'il est possible de générer des ondes thermiques liquides sur des surfaces d'aluminium telles que celles conventionnellement utilisées en rhéologie. La surface en aluminium n'est pas un substrat approprié pour une étude du comportement thermique du liquide. En raison de sa conductivité thermique élevée, l'aluminium conduit une grande partie de l'énergie produite au cours de la déformation du liquide. Par ailleurs, en raison de sa réflectivité et de son émissivité élevées, la détermination précise de la température du liquide peut difficilement être effectuée. Les surface en alumine utilisées pour la grande majorité de cette étude, ne présentent pas ces inconvénients et sont adéquatement adaptées à la présente étude. L'étude de l'impact de la conductivité thermique des surfaces permettrait de déterminer les conditions pour lesquelles l'effet thermique serait fortement limité dans le liquide.

Pour conclure, dans la présente thèse, nous avons mis en évidence des effets thermomécaniques dans les liquides à l'échelle mésoscopique en nous concentrant sur l'origine de l'effet, son mécanisme et sa dépendance à l'échelle. L'étude de l'effet thermique dans des conditions adiabatiques est riche. De nos mesures, nous pouvons déduire que l'effet thermique est également de nature adiabatique, local, dynamique et élastique. Cela implique que l'effet

thermique apparait quasiment instantanément, le déphasage entre la déformation mécanique et la variation thermique est négligeable. Il ne peut donc pas être interprété en termes de transfert (conduction) de chaleur mais en termes de changement de température hors équilibre (équivalent à un déplacement dans le diagramme de phase pression-température). Une autre perspective à étudier est l'évolution de l'effet thermomécanique alors qu'un débit constant est appliqué, comme c'est le cas dans un canal microfluidique. L'étude thermique de divers liquides (par exemple, Van der Waals, etc.), des polymères (de différents poids moléculaires), des gels et d'autres matériaux mous compléterait notre compréhension de l'effet thermomécanique. Cependant, même si l'élasticité augmente (par exemple dans le cas d'un polymère fondu), l'étude relève de nouveaux différents défis comme l'occurrence de frictions visqueuses (ou non)

Enfin, d'un point de vue théorique, les résultats ci-dessus ne sont pas interprétés dans le cadre fluidique de Maxwell conventionnel car la fréquence de l'excitation mécanique externe ne se couple pas avec la dynamique de relaxation moléculaire et donc seule la dissipation devrait se produire. D'autre part, les effets thermoélastiques ne peuvent s'expliquer que par la capacité des liquides à supporter des ondes de cisaillement à basse fréquence. La capacité des liquides à propager des ondes de cisaillement est décrite par la théorie du k-gap [79, 80, 81, 82, 83, 84, 10, 87, 28, 29]. La théorie reconsidère le concept d'interaction à courte portée et introduit la notion de propagation d'ondes de cisaillement de type solide définissant une relation de dispersion k-gap. La loi de dispersion indique que la propagation des ondes de cisaillement de type solide est rendue possible pour $k > k_g = 1/(2c \cdot \tau)$ (solutions réelles). Les présentes observations réalisées à l'échelle mésoscopique fournissent des preuves expérimentales qui vont dans ce sens. Comme mentionné dans [77], « nous considérons un liquide comme une collection de régions dynamiques de taille caractéristique $c.\tau$ où opère la capacité de type solide à supporter les ondes de cisaillement ». Ces régions dynamiques pourraient coïncider avec les bandes thermiques. La longueur de propagation des ondes de cisaillement $d_{el}=c \cdot \tau$ correspond dans le cas du glycérol à $d_{el} \sim 3$ µm ($c=3000$ m/s et $\tau=10^{-9}$s donnés pour des fluctuations de densité à l'équilibre), et ainsi l'onde de cisaillement (de nature exponentielle : $e^{-x/2d_{el}}$) doit être dissipée à une distance d'environ 30µm. La longueur de propagation prédite est d'ordre similaire à la largeur des bandes élémentaires (~ 25–80 µm), ce qui pourrait indiquer la limite des interactions « corrélées » qui conduisent à la génération des bandes thermiques. La prédiction d'une propagation finie de l'onde de cisaillement de type solide pourrait expliquer pourquoi le liquide se divise en plusieurs bandes thermiques, d_{el} étant la longueur ultime de liquide supportant l'onde de cisaillement. Au-delà de cette limite, les conditions d'un nouveau mécanisme de cisaillement se produisent et produisent de nouvelles bandes de cisaillement (thermiques), chacune délimitée par la longueur de propagation finie.

Une autre approche sur l'existence des bandes thermiques est possible en utilisant les modes normaux qui existent dans le système. Les bandes sont macroscopiquement grandes car elles contiennent un grand nombre de molécules, il est donc logique de définir des modes de phonons à grande longueur d'onde dans ces régions. Dans les régions chaudes/comprimées, le volume V de la région est réduit, tandis que dans les régions froides/dilatées, le volume V est agrandi. Ensuite, nous pouvons écrire la définition microscopique du paramètre de Grüneisen :

$$\gamma = -\frac{d \ln \omega_n}{d \ln V}$$

Puisque le paramètre de Grüneisen γ est positif pour les liquides [167], cette relation donne (après intégration) que la fréquence des phonons ω_n augmente lorsque le volume V diminue, alors que ω_n diminue lorsque le volume V augmente. La fréquence vibrationnelle étant liée à la température, via $T = h\omega_n/k_B$, il est clair que la température augmente dans les régions où le volume diminue (régions « compressées »), alors qu'elle diminue dans les régions où le

volume augmente (régions « dilatées »), conduisant ainsi à une bande chaude et une bande froide pour les régions comprimées et expansées, respectivement [190].

L'observation de bandes thermiques pourrait par ailleurs être associée aux bandes de cisaillement observées dans les fluides complexes sous cisaillement continu, appelées bandes de vorticité et dont l'origine reste discutée [97, 98]. Les bandes de vorticité présentent des états de contraintes différents pour le même cisaillement, ce qui est similaire à l'alternance des bandes thermiques froides et chaudes observées.

Enfin, à partir des mesures préliminaires IXS sur la ligne GALAXIES à S.O.L.E.I.L., nous avons démontré que la dynamique des phonons du support solide (alumine) est modifiée lorsque la surface est en contact avec un liquide sur une longue période de temps (plusieurs heures). On savait que l'énergie des molécules liquides est modifiée au voisinage d'une paroi solide (les molécules de surface explorent d'autres voisinages et sont dans un autre état thermodynamique par rapport aux molécules en vrac). Il ressort de ces premiers résultats que la dynamique (phonons) du solide est également impactée en présence d'un liquide mouillant, créant un nouvel équilibre solide/liquide de part et d'autre de l'interface.

Nous avons donc montré dans cette thèse que la prise en compte de l'élasticité de cisaillement des liquides permet l'identification de nouvelles propriétés à l'échelle mésoscopique telles que ces effets thermoélastiques induits par la déformation que nous commençons tout juste à découvrir expérimentalement et qui font écho à de nouvelles prédictions théoriques pour la dynamique [29, 28, 93]. Le développement d'un modèle dynamique, qui prend en compte la dissipation visqueuse et la conversion de l'énergie élastique, dépendantes de l'échelle et de l'environnement (interface solide-liquide), ferait progresser notre compréhension des propriétés liquides, mais aussi de l'interface solide.

Appendix A: Parallelism considerations

An important factor in our measurements is the correct positioning of the alumina plates on the fixtures that connect them with the rheometer's motor and sensor. The ideal geometry for the rheometer is the one depicted in Figure App. 1a. The plates should be mounted on the fixtures and been adjusted in a manner where when they touch each other at a zero-gap test, their total surface area touch the other. Then, the plates are parallel and ready for correct rheological measurements (Figure App. 1a). Practically, the perfect parallelism is not possible, but the plates are tilted in respect with each other. This leads to different values of the gap in the system. On the one side, we get the apparent gap H and the actual one H+ε (Figure App. 1b & c). The misaligned plates cause problems on rheological measurements and do not allow for reliable measurements [192, 193, 102, 194]. In this geometry, the strain is related with the distance from the centre of the surface. The non-parallelism causes non-homogeneous strain for points that have the same distance from the centre r < R.

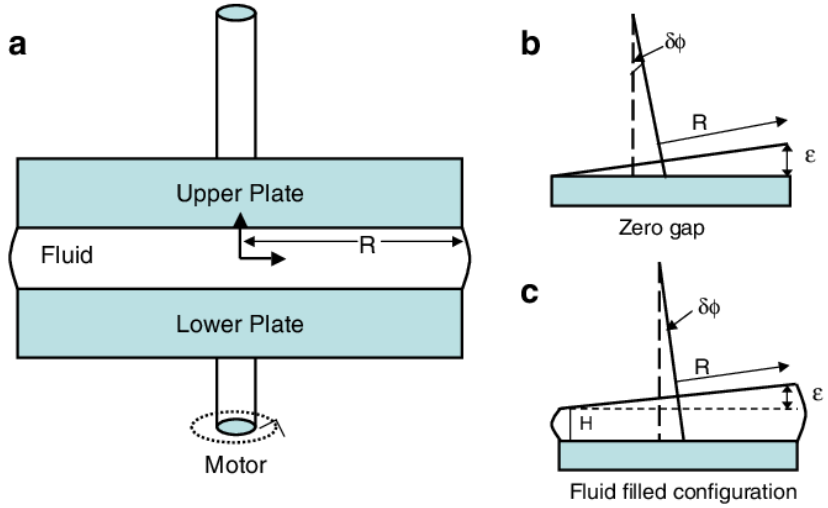

Figure App. 1: a) Diagram of typical geometry of a rheometer. The plates are placed parallel to each other. **b)** When the plates are non-parallel, at zero gap they will touch only on one side. **c)** Scheme of the geometry when the liquid is placed. The lack of parallelism will lead to non-homogeneous height of the gap. Scheme taken from *[139].*

To make sure that the effect of non-parallelism is not important for our measurements, we use the IR sensor as follows. We mount one surface on its fixture and place the fixture on the recess that is connected with the motor. Then, we command the motor to rotate at fast rotation and with the IR camera, we capture this rotation on video. From the video, we deduce if there is any perpendicular motion of the plate, due to the placement of the IR sensor in respect with the plates (Figure 2.2 bottom scheme). We repeat the procedure until both plates do not move perpendicularly on the IR sensor. With this method, we can significantly reduce the gap error to $\varepsilon < 8$ μm. This value corresponds to the size of each pixel. However, a secondary possible source of error that we should take account is the mount of each fixture to the rheometer's sensor or motor respectively. The fixtures are made to perfectly fit and stand perpendicular. Thus, we should assure that the best connection by cleaning the connection area from dirt.

Appendix A: Parallelism considerations

Appendix B: Data treatment

Each raw video captured during the measurements is treated to extract the information needed in a clear and easily understandable presentation. The quantity, measured from these measurements, is the omitted radiation in the form of intensity. The selected video was input in the software in grayscale mode and the liquid region at the centre of the video and part of the plates were selected from the rest. The exclusion of parts on the edges was made due to the radial geometry of the plates. The surface of the plates is a circle, meaning that the focus of the camera in the centre causes distortion on the edges. The determination of the bands is possible by utilizing the previous method (2D mapping) first. The method also acts as a median to check any reflectivity issues related with the background.

Another challenge is the connection of thermal and mechanical measurements. The measurements are independent and thus they do not share a common time start. A connection will allow to compare those measurements together. To achieve that we used the time where the measurements end. For the thermal measurement, the end can be seen on the video and the exact time can be allocated with an error of two slides, meaning ~ 0.07s. This error arises problems for the determination of the phase shift between the thermal and mechanical measurements. To understand if this error is significant, we should compare it with the period of the mechanical measurement. If the period is 1.25s (ω = 5rad/s), then the error to period rate is 5.6%. If the period is 12.56s (ω = 0.5rad/s), then the error to period rate is 0.56% and an evaluation of the phase shift is acceptable.

Appendix B: Data treatment

Appendix C: Specific features of the infrared emissivity – importance of the choice of the substrate

In this appendix, we describe the studied system (aluminium/alumina plates + liquid) at rest, where the equilibrium has been established.

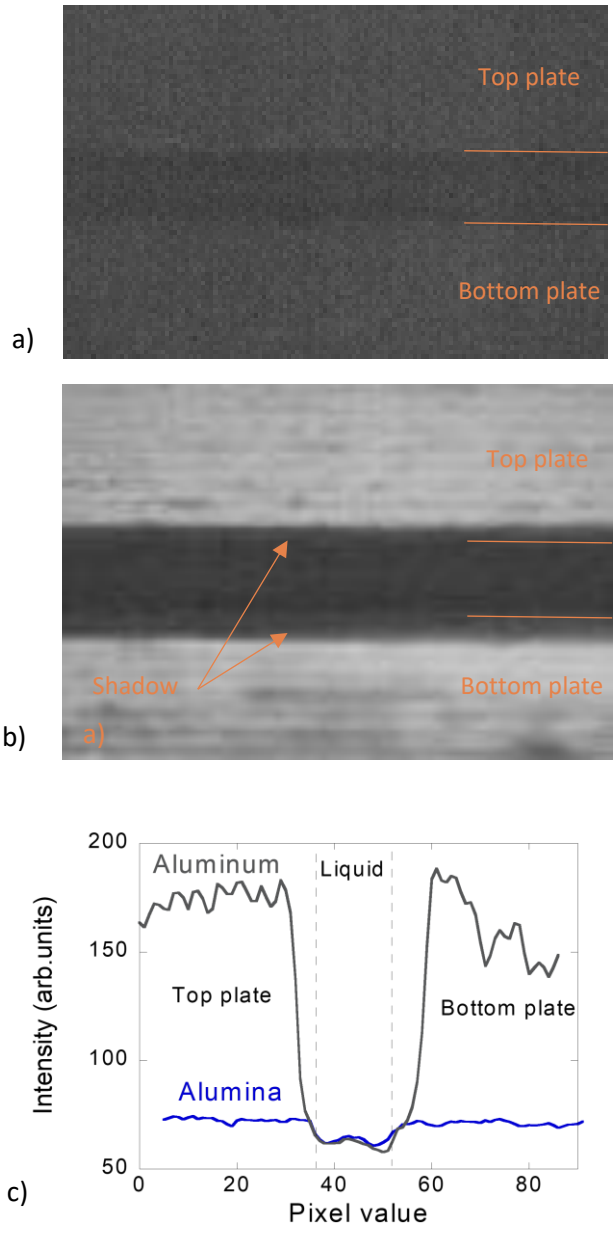

Figure App. 2: a) Raw infra-red snapshot of the alumina plate-liquid- alumina plate system at rest. **b)** Raw infra-red snapshot of the aluminium plate-liquid- aluminium plate system at rest. **c)** Comparison of the emissivity profiles (vertical cut) of the gap of the alumina plate-liquid- alumina plate and aluminium plate-liquid- aluminium plate system at rest. Gap value 250µm.

In Figure App. 2a, we observe a raw IR image recorded by the sensor of the alumina/liquid system at rest. Figure App. 2b is the raw IR image in the case of a liquid confined between aluminum plates. Figure App. 2c shows a vertical cut of the images. The difference between the two profiles is due to their difference in emissivity. In the case of aluminium plates (Figure App. 2b), the difference of intensity between the plates and liquid is much higher due to the reflective nature of the aluminium surface. Thermal measurements with the use of standard aluminium substrates, instead of the high-energy alumina ones, stand as a great challenge. Aluminium and alumina plates have different properties, such as the thermal conductivity (k_{Al} = 237W/m*K, k_{Al2O3} = 30 W/m*K), emissivity and reflectivity. Particularly, aluminium substrates conduct heat rapidly and reflect greatly heat from a nearby heat source.

A careful examination of the liquid profile (Figure App. 2c) indicates that a slight variation of the temperature (< 0.005°C/mm) can be detected near the walls. This static wall effect is a physical effect due to the energy imbalance of the liquid molecules at the vicinity of the surface that exerts an attractive field as precisely described in [172]. This small effect has been nevertheless systematically taken into account in the data treatment by recording a series of images at rest, prior each series of dynamic measurements.

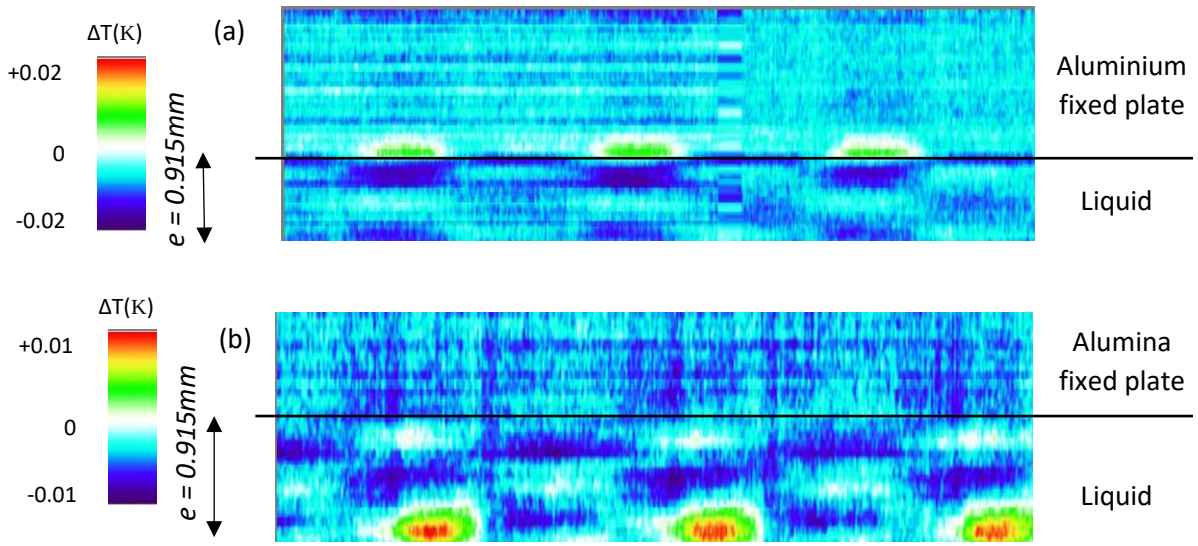

Figure App. 3: a) 2D thermal mapping of top fixed aluminium plate and PPG-4000 during oscillatory strain measurements (e = 915µm, ω = 1 rad/s, γ_0 = 800 – 1000%). **b)** Same for alumina substrate. 2D mappings not on the same colour scale.

The properties of aluminium stand troublesome for the study of any thermal effect in the confined liquid. For the aluminium plate case, we must also consider the conduction between the plates and the liquid, in the time scale of the measurements. In Figure App. 3, we show the evolution of the fixed top plate and the liquid over the course of an oscillatory measurement. We observe that for the aluminium case (Figure App. 3a), the top plate close to the liquid oscillates thermally over time. For alumina (Figure App. 3b), no thermal change is visible in the plate within the experimental error bar. The various lines of slightly different, but constant temperature in the area of the top plate, is due to roughness effect. As the plates are not perfectly smooth, the roughness causes different reflection values and thus changing the emissivity of the area, making it to appear as slightly cooler or hotter than the neighbour regions. The (moving) bottom plate is not depicted. We observe from the 2D mapping that for the aluminium

case, the liquid thermal bands changes can be spotted without severe shadow effects from the plate. The bulk behaviour appears to be comparable for the two different substrates, with the aluminium case to appear slightly stronger, but deviates greatly from a sin wave response, with the appearance of second harmonics leading to double the frequency of the thermal wave, hinting viscous heating effects. For the alumina case, the bulk response remains as a simple sin wave.

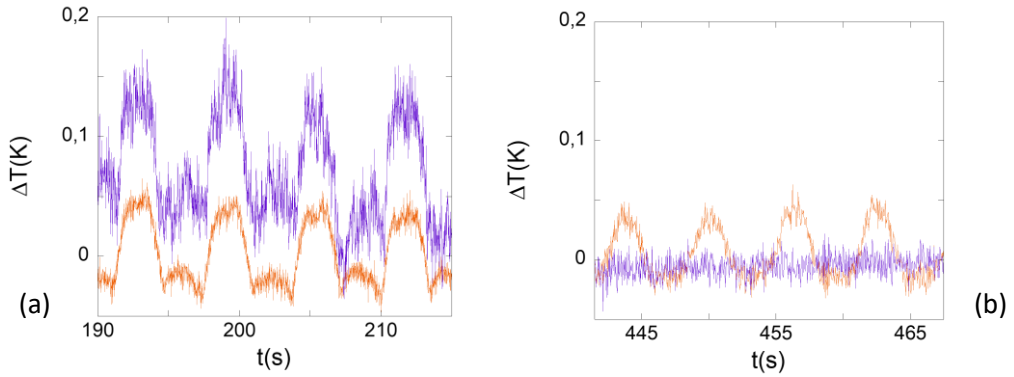

Figure App. 4: a) Emissivity variation of top fixed aluminium plate and PPG-4000 during oscillatory strain measurements (e = 260µm, ω = 1 rad/s, γ_0 = 3150 - 4000%). **b)** Same for alumina substrate (e = 240µm). The solid and liquid temperatures are not comparable due to the different emissivity coefficients.

In Figure App. 4, we show the response of the system to an oscillatory excitation, with the liquid thickness of around 250µm.

For the aluminium case (Figure App. 4a), we notice a similar behaviour of the top plate as for 920µm. The thermal response of the liquid is more difficult to be studied. We notice shadow of the aluminium plates to the edges of the liquid, due to the high reflectivity. We are unable to study in detail the liquid response and we are restricted to limited (to the centre) space of the liquid. As seen in Figure App. 4a, the thermal response of the top plate is simultaneous with the bulk liquid temperature. Such behaviour further strengthens conduction effect and reflectivity of the plate.

The alumina plate (Figure App. 4b), about seven times less thermally conductive, does not respond thermally to the excitations (purple line). As seen in Figure App. 4b, the portion of the plate closest to the liquid exhibits steady temperature while the liquid thermally oscillates. For both substrates, the bulk liquid changes its temperature based on the applied excitation. For the aluminium case, this change deviates greatly from a sin wave than the alumina counterpart.

From the presented figures, we conclude that we can generate a thermal response on a confined liquid (here PPG-4000) independently of the substrate (aluminium or alumina). However, aluminium plates hinder the in-depth study of the desired liquid due to its great conductivity and reflectivity. Its large conductivity results to energy exchange between the plate and the liquid, meaning that it should be considered during the thermal study of the liquid. Its great reflectivity results to shadowing of the nearby areas, such as the edges of the confined liquid (Figure App. 4a) and makes difficult the evaluation of its actual thermal change. Finally, the liquid-solid interfacial forces being different, the conditions of slippage and liquid/solid friction are different.

Appendix C: Specific features of the infrared emissivity – importance of the choice of the substrate

Annex A: Published articles and conference participations

In the frame of the current PhD thesis, four articles are published in scientific journals. In detail these scientific papers are:

1) Kume, E., Baroni, P. & Noirez, L. Strain-induced violation of temperature uniformity in mesoscale liquids. *Sci Rep* **10**, 13340 (2020). https://doi.org/10.1038/s41598-020-69404-1.

2) Eni Kume, Alessio Zaccone, Laurence Noirez. Unexpected thermo-elastic effects in liquid glycerol by mechanical deformation. *Physics of Fluids* **33**, 072007 (2021); https://doi.org/10.1063/5.0051587.

3) Kume, E., Noirez, L. Identification of Mechanical-stimuli Thermal Response in Mesoscopic Liquids: from Harmonic to non-Harmonic Thermal Wave. *J. Phys. Chem. B* 2021, **125**, 30, 8652–8658. https://doi.org/10.1021/acs.jpcb.1c04362.

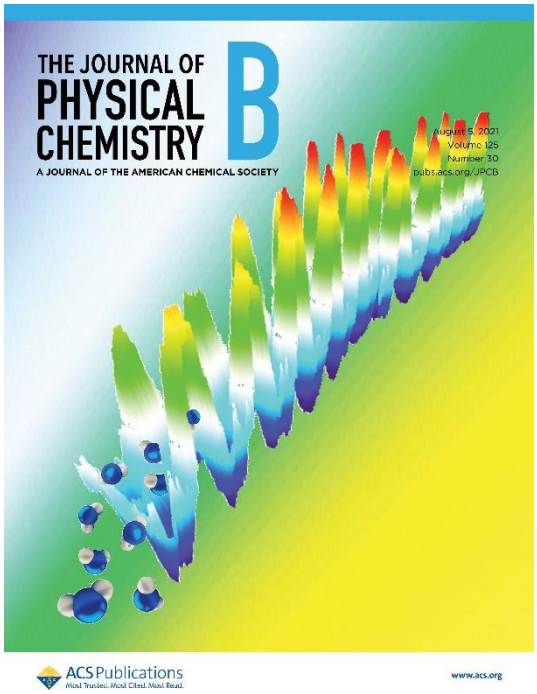

The paper was chosen as the cover art of Volume 125, Issue 30 of J. Chem. Phys. B.

4) Eni Kume, Patrick Baroni, Laurence Noirez. Highlighting Thermo-Elastic effects in Confined Fluids. *Polymers* **2021**, *13*(14), 2378; https://doi.org/10.3390/polym13142378.

Below the list of conference participations where work related with this manuscript was presented:

1) European Polymer Congress (EPF2019), Crete, Greece, *oral communication*.

2) European/Japanese Molecular Liquid Group Conference (EMLG/JMLG 2019), Kutna Hora, Czech Republic, *oral communication*.

3) Annual European Rheology Conference (AERC2021), virtual, *oral communication*.

4) Liquid Matter Conference (LMC2021), virtual, *poster presentation*.

Annex A: Published articles and conference participations

References

[1] Pujolle-Robic, C., Noirez, L. , “Observation of shear-induced nematic–isotropic transition in side-chain liquid crystal polymers,” *Nature 409, 167–171 (2001).*

[2] Olmsted, P.D. , “Perspectives on shear banding in complex fluids.,” *Rheol Acta 47, 283–300 (2008)..*

[3] J. Clerk Maxwell, “On the Dynamical Theory of Gases”.*Philosophical Transactions of the Royal Society of London, Vol. 157 (1867), pp. 49-88.*

[4] Herbert B. Callen and Theodore A. Welton, “Irreversibility and Generalized Noise”.*Phys. Rev. 83, 34 (1951).*

[5] J. Frenkel, Kinetic theory of liquids, Dover Publications, 1947.

[6] Robert Zwanzig and Raymond D. Mountain, “High-Frequency Elastic Moduli of Simple Fluids,” *J. Chem. Phys. 43, 4464 (1965).*

[7] Robert Piccirelli, and T. A. Litovitz, “Ultrasonic Shear and Compressional Relaxation in Liquid Glycerol,” *The Journal of the Acoustical Society of America 29, 1009 (1957).*

[8] Thomas Pezeril, “Laser generation and detection of ultrafast shear acoustic waves in solids and liquids,” *Optics & Laser Technology, 83 (2016), 177–188.*

[9] W. P. Mason, et al., “Measurement of Shear Elasticity and Viscosity of Liquids at Ultrasonic Frequencies”.*Phys. Rev. 75, 936 (1949).*

[10] Filippo Scarponi et al., “Brillouin light scattering from transverse and longitudinal acoustic waves in glycerol,” *Phys. Rev. B 70, 054203 (2004).*

[11] Walter Kauzmann and Henry Eyring, “The Viscous Flow of Large Molecules,” *J. Am. Chem. Soc. 1940, 62, 11, 3113–3125.*

[12] P. Rouse, “A Theory of the Linear Viscoelastic Properties of Dilute Solutions of Coiling Polymers,” *J. Chem. Phys. 21, 1272 (1953).*

[13] Bruno H. Zimm, “Dynamics of Polymer Molecules in Dilute Solution: Viscoelasticity, Flow Birefringence and Dielectric Loss,” *J. Chem. Phys. 24, 269 (1956).*

[14] P. G. de Gennes, “Reptation of a Polymer Chain in the Presence of Fixed Obstacles,” *J. Chem. Phys. 55, 572 (1971).*

[15] Masao Doi and S. F. Edwards , “Dynamics of concentrated polymer systems. Part 1.—Brownian motion in the equilibrium state,” *J. Chem. Soc., Faraday Trans. 2, 1978,74, 1789-1801.*

[16] Masao Doi and S. F. Edwards, The Theory of Polymer Dynamics, Clarendon Press, Oxford, 1986.

[17] Christoph A Weber et al, "Physics of active emulsions," *2019 Rep. Prog. Phys. 82 064601.*

[18] B. V. Derjaguin, et al., "Shear elasticity of low-viscosity liquids at low frequencies," *Phys Rev A 42(4):2255–2258. (1990).*

[19] B. V. Derjaguin, et al., "The complex shear modulus of polymeric and small-molecule liquids," *Polymer 30(1):97–103. (1989) .*

[20] H. Mendil et al , "Unexpected giant elasticity in side-chain liquid-crystal polymer melts: A new approach for the understanding of shear-induced phase transitions," *2005 EPL 72 983.*

[21] L. Noirez et al., "Richness of Side-Chain Liquid-Crystal Polymers: From Isotropic Phase towards the Identification of Neglected Solid-Like Properties in Liquids," *Polymers 2012, 4(2), 1109-1124.*

[22] L. Noirez, P. Baroni, "Identification of a low-frequency elastic behaviour in liquid water," *J Phys Condens Matter 24 (37): 372101. (2012).*

[23] L. Noirez, P. Baroni, "Revealing the solid-like nature of glycerol at ambient temperature," *Journal of Molecular Structure, Vol. 972, Issues 1–3, Pages 16-21 (2010).*

[24] H. Mendil, P. Baroni & L. Noirez, "Solid-like rheological response of non-entangled polymers in the molten state," *The European Physical Journal E volume 19, pages77–85 (2006).*

[25] L. Noirez et al., "The missing parameter in rheology: hidden solid-like correlations in viscous liquids, polymer melts and glass formers," *Polymer International 58 (2009) 962.*

[26] Hsuan-Wei Hu, George A. Carson, and Steve Granick, "Relaxation time of confined liquids under shear," *Phys. Rev. Lett. 66, 2758 (1991).*

[27] A. Levent Demirel and Steve Granick, "Glasslike Transition of a Confined Simple Fluid," *Phys. Rev. Lett. 77, 2261 (1996).*

[28] M. Baggioli, et al., "Field theory of dissipative systems with gapped momentum states," *Phys. Rev. D 102, 025012 (2020).*

[29] Alessio Zaccone and Kostya Trachenko, "Explaining the low-frequency shear elasticity of confined liquids," *PNAS August 18, 2020 117 (33) 19653-19655.*

[30] D. Bolmatov, V. V. Brazhkin & K. Trachenko, "The phonon theory of liquid thermodynamics," *Sci Rep, 2, 421 (2012).*

[31] A. Z. a. M. Baggioli, “Universal law for the vibrational density of states of liquids,” *PNAS February 2, 2021 118 (5) e2022303118.*

[32] Hassan Berro, et al., “Energy dissipation in non-isothermal molecular dynamics simulations of confined liquids under shear,” *J. Chem. Phys. 135, 134708 (2011).*

[33] Bo Hung Kim, et al., “Viscous heating in nanoscale shear driven liquid flows,” *Microfluid Nanofluid (2010) 9:31–40.*

[34] D. M. Heyes, et al., “Pressure dependence of confined liquid behavior subjected to boundary-driven shear,” *J. Chem. Phys. 136, 134705 (2012).*

[35] Christopher Monahan et al., “Hydrodynamic fluctuation-induced forces in confined fluids,” *Soft Matter, 2016,12, 441-459.*

[36] Ketzasmin A. Terron-Mejia et al., “Mesoscopic modeling of structural and thermodynamic properties of fluids confined by rough surfaces,” *Phys.Chem.Chem.Phys., 2015, 17, 26403.*

[37] Steve Granick, “Motions and Relaxations of Confined Liquids,” *Science, 253, 5026, 1374-1379 (1991).*

[38] M. Morciano, et al., “Nonequilibrium molecular dynamics simulations of nanoconfined fluids at solid-liquid interfaces,” *J. Chem. Phys. 146, 244507 (2017).*

[39] Hsuan-Wei Hu. et al., “Relaxation time of confined liquids under shear,” *Phys. Rev. Lett. 66, 2758 (1991).*

[40] Tatiana Schmatko, Hubert Hervet, and Liliane Leger, “Friction and Slip at Simple Fluid-Solid Interfaces: The Roles of the Molecular Shape and the Solid-Liquid Interaction,” *Phys. Rev. Lett. 94, 244501 (2005).*

[41] Ken-ichiro Murata and Hajime Tanaka, “Impact of surface roughness on liquid-liquid transition,” *Sci. Adv. 2017;3: e1602209.*

[42] Rong-Guang Xu and Yongsheng Leng, “Squeezing and stick–slip friction behaviors of lubricants in boundary lubrication,” *PNAS June 26, 2018 115 (26) 6560-6565.*

[43] Yue Zhang, et al., “Effect of substrate interactions on the glass transition and length-scale of correlated dynamics in ultra-thin molecular glass films,” *J. Chem. Phys. 149, 184902 (2018).*

[44] A. J. Giacomin, et al., “Large-amplitude oscillatory shear flow from the corotational Maxwell model,” *Journal of Non-Newtonian Fluid Mechanics Volume 166, Issues 19–20, October 2011, Pages 1081-1099.*

[45] B. Cui, R. Milkus, A. Zaccone, “Direct link between boson-peak modes and dielectric α-relaxation in glasses,” *Phys. Rev. E 95, 022603 (2017).*

[46] D.W.A. Rees, Basic Engineering Plasticity, Elsevier, (2006).

[47] Nicholas W. Tschoegl, The Phenomenological Theory of Linear Viscoelastic Behavior, Springer-Verlag Berlin Heidelberg, 1989.

[48] W.N. Findley et al., Creep And Relaxation Of Nonlinear Viscoelastic Materials With An Introduction To Linear Viscoelasticity, Elsevier, 1976.

[49] Little D.N., Allen D.H., Bhasin A., "(2018) Viscoelasticity and Thermoviscoelasticity. In: Modeling and Design of Flexible Pavements and Materials.," *Springer, Cham..*

[50] J.Peirs et al., "Determining the stress–strain behaviour at large strains from high strain rate tensile and shear experiments," *International Journal of Impact Engineering, 38, 5, 406-415 (2011).*

[51] Qin Xu et al., "Direct measurement of strain-dependent solid surface stress," *Nat Commun. 2017; 8: 555..*

[52] Biroli, G., Urbani, P. , "Breakdown of elasticity in amorphous solids," *Nature Phys 12, 1130–1133 (2016).*

[53] Bingyu Cui et al., "Theory of elastic constants of athermal amorphous solids with internal stresses," *Granular Matter (2019) 21:69.*

[54] Alessio Zaccone and Enzo Scossa-Romano, "Approximate analytical description of the nonaffine response of amorphous solids," *Phys. Rev. B 83, 184205 (2011).*

[55] Vladimir V. Palyulin et al., "Parameter-free predictions of the viscoelastic response of glassy polymers from non-affine lattice dynamics," *Soft Matter, 2018, 14, 8475-8482.*

[56] John G. Curro and Philip Pincus, "A theoretical basis for viscoelastic relaxation of elastomers in the long-time limit," *Macromolecules 1983, 16, 4, 559–562.*

[57] J.A.Epaarachchi, 17 - The effect of viscoelasticity on fatigue behaviour of polymer matrix composites, Creep and Fatigue in Polymer Matrix Composites, Woodhead Publishing Series in Composites Science and Engineering.

[58] J.K.Li et al., "7.19 - Polymer Nanomechanics," *Polymer Science: A Comprehensive Reference, Volume 7, 2012, Pages 377-404.*

[59] A.L.Kwansa, J.W.Freeman, Chapter 7 - Ligament tissue engineering, Regenerative Engineering of Musculoskeletal Tissues and Interfaces, 2015.

[60] Zhijie Wang, Mark J. Golob and Naomi C. Chesler, "Viscoelastic Properties of Cardiovascular Tissues, Viscoelastic and Viscoplastic Materials," *Mohamed Fathy El-Amin, IntechOpen (2016).*

[61] Malvern, L., Introduction to the mechanics of a continuous medium, Prentice-Hall, (1969).

[62] Pitarresi, Giuseppe & Patterson, EA., "A review of the general theory of thermoelastic effect," *Journal of Strain Analysis for Engineering Design, 38, 405-417 (2003).*

[63] William N. Sharpe, Jr., Chapter 26, Springer Handbook of Experimental Solid Mechanics, Springer US, 2008.

[64] “https://waves.neocities.org/shape.html,” [Online].

[65] David Roylance, ENGINEERING VISCOELASTICITY, M.I.T., 2001.

[66] Ravinder Bansal, “Maxwell relaxation time for the transverse mode in simple liquids,” *Phys. Rev. A 16, 2191 (1977).*

[67] Oldroyd, James, On the Formulation of Rheological Equations of State, Proceedings of the Royal Society of London. Series A, Mathematical and Physical Sciences. 200 (1063): 523–541 (1950).

[68] Per Gradin et al., “16 - Dynamic-mechanical Properties,” in *Comprehensive Polymer Science and Supplements*, 1989, pp. Volume 2, Pages 533-569.

[69] M. Reiner, “The Deborah Number Physics Today 17, 1, 62 (1964)”.

[70] James Peachey, John Van Alsten, and Steve Granick, “Design of an apparatus to measure the shear response of ultrathin liquid films,” *Review of Scientific Instruments 62, 463 (1991).*

[71] G. Reiter, et al., “Stick to slip transition and adhesion of lubricated surfaces in moving contact,” *J. Chem. Phys. 101, 2606 (1994).*

[72] J. L. Gallani et al., “Abnormal viscoelastic behavior of side-chain liquid-crystal polymers,” *Phys. Rev. Lett. 72, 2109 (1994).*

[73] D.Collin, P.Martinoty, “Dynamic macroscopic heterogeneities in a flexible linear polymer melt,” *Physica A: Statistical Mechanics and its Applications, 320, 235-248 (2003).*

[74] Laurence Noirez, “Origin of shear-induced phase transitions in melts of liquid-crystal polymers,” *Phys. Rev. E 72, 051701 (2005).*

[75] P. Kahl, P. Baroni, and L. Noirez, “Harmonic strain-optical response revealed in the isotropic (liquid) phase of liquid crystals,” *Appl. Phys. Lett. 107, 084101 (2015).*

[76] H. Mendil-Jakani et al., “Shear-Induced Isotropic to Nematic Transition of Liquid-Crystal Polymers: Identification of Gap Thickness and Slipping Effects,” *Langmuir 2009, 25, 9, 5248–5252*.

[77] M. Baggioli, V. Brazhkin, K. Trachenko, M. Vasin, “Gapped momentum states,” *Physics Reports ,Vol. 865, 1-44 (2020).*

[78] Stillinger F H and Weber T A , “Dynamics of structural transitions in liquids,” *Phys. Rev. A 28 2408 (1983).*

[79] S. Hosokawa et al., “Transverse Acoustic Excitations in Liquid Ga,” *Phys. Rev. Lett. 102, 105502 (2009).*

[80] Valentina M. Giordano and Giulio Monaco, “Inelastic x-ray scattering study of liquid Ga: Implications for the short-range order,” *Phys. Rev. B 84, 052201 (2011).*

[81] J. R. D. Copley and J. M. Rowe, “Short-Wavelength Collective Excitations in Liquid Rubidium Observed by Coherent Neutron Scattering,” *Phys. Rev. Lett. 32, 49 (1974).*

[82] Valentina M. Giordano and Giulio Monaco, “Fingerprints of order and disorder on the high-frequency dynamics of liquids,” *PNAS, 2010 107 (51) 21985-21989.*

[83] S Hosokawa et al., “Transverse excitations in liquid Sn,” *2013 J. Phys.: Condens. Matter 25 112101.*

[84] Tullio Scopigno, et al., “Microscopic dynamics in liquid metals: The experimental point of view,” *Rev. Mod. Phys. 77, 881 (2005).*

[85] K. Trachenko, “Quantum dissipation in a scalar field theory with gapped momentum states,” *Scientific Reports 9, 6766 (2019).*

[86] Yu D Fomin et al , “Dynamics, thermodynamics and structure of liquids and supercritical fluids: crossover at the Frenkel line,” *2018 J. Phys.: Condens. Matter 30 134003.*

[87] K. Trachenko, “Lagrangian formulation and symmetrical description of liquid dynamics,” *Phys. Rev. E 96, 062134 (2017).*

[88] C. Yang, “Emergence and Evolution of the k-Gap in Spectra of Liquid and Supercritical States,” *Phys. Rev. Lett. 118, 215502 (2017).*

[89] K Trachenko and V V Brazhkin , “Collective modes and thermodynamics of the liquid state,” *2016 Rep. Prog. Phys. 79 016502.*

[90] Alessio Zaccone and Laurence Noirez, “Universal G’ ∼ L–3 Law for the Low-Frequency Shear Modulus of Confined Liquids,” *J. Phys. Chem. Lett. 2021, 12, 1, 650–657.*

[91] Lematre, A et al., “Sum Rules for the Quasi-Static and Visco-Elastic Response of Disordered Solids at Zero Temperature,” *Journal of Statistical Physics 2006, 123, 415.*

[92] Palyulin, V. V et al., “Palyulin, V. V.; Ness, C.; Milkus, R.; Elder, R. M.; Sirk, T. W.; Zaccone, A. Parameterfree,” *Soft Matter 2018, 14, 8475-8482.*

[93] Matteo Baggioli, Michael Landry, Alessio Zaccone, “Deformations, relaxation and broken symmetries in liquids, solids and glasses: a unified topological field theory,” *arXiv:2101.05015.*

[94] U Windberger, Laurence Noirez, “Human Blood Plasma in Capillary-size Flow: Revealing Hidden Elasticity and Scale Dependence,” *2020. (hal-02513618).*

[95] Noirez, L., Baroni, P., “Identification of thermal shear bands in a low molecular weight polymer melt under oscillatory strain field,” *Colloid Polym Sci 296, 713–720 (2018).*

[96] L. Noirez et al., “Highlighting non-uniform temperatures close to liquid/solid surfaces,” *Appl. Phys. Lett. 110, 213904 (2017).*

[97] Dhont, J.K.G., Briels, W.J., “Gradient and vorticity banding,” *Rheol Acta 47, 257–281 (2008).*

[98] Kyongok Kang et al., “Vorticity banding in rodlike virus suspensions,” *Phys. Rev. E 74, 026307 (2006).*

[99] L. Noirez & P. Baroni, “Identification of thermal shear bands in a low molecular weight polymer melt under oscillatory strain field,” *Colloid and Polymer Science (2018) 296:713–720.*

[100] A. Kate Gurnon and Norman J. Wagner, “Large amplitude oscillatory shear (LAOS) measurements to obtain constitutive equation model parameters: Giesekus model of banding and nonbanding wormlike micelles,” *Journal of Rheology 56, 333 (2012).*

[101] Kyu Hyun et al., “A review of nonlinear oscillatory shear tests: Analysis and application of large amplitude oscillatory shear (LAOS),” *Progress in Polymer Science 36,12, 2011, Pages 1697-1753.*

[102] Ewoldt R.H., Johnston M.T., Caretta L.M. (2015), “Experimental Challenges of Shear Rheology: How to Avoid Bad Data. In: Spagnolie S. (eds) Complex Fluids in Biological Systems.,” *Biological and Medical Physics, Biomedical Engineering. Springer, New York, NY..*

[103] Groisman, A., Steinberg, V. , “Elastic turbulence in a polymer solution flow,” *Nature 405, 53–55 (2000).*

[104] Joseph A. Yosick, et al., “Fluid inertia in large amplitude oscillatory shear,” *Rheol Acta 37:365–373 (1998).*

[105] M.Müller, “1.15 - Polymers at Interfaces and Surfaces and in Confined Geometries,” in *Polymer Science: A Comprehensive Reference*, Elsevier, 2012, pp. Volume 1, Pages 387-416.

[106] David Quéré, “Wetting and Roughness,” *Annual Review of Materials Research Vol. 38:71-99 (2008).*

[107] Roman S. Voronov et al., “Boundary slip and wetting properties of interfaces: Correlation of the contact angle with the slip length,” *J. Chem. Phys. 124, 204701 (2006).*

[108] Daniel Bonn et al., “Wetting and spreading,” *Rev. Mod. Phys. 81, 739 (2009).*

[109] Granick, S., Zhu, Y. & Lee, H. , “Slippery questions about complex fluids flowing past solids,” *Nature Mater 2, 221–227 (2003).*

[110] P. G. de Gennes, “Wetting: statics and dynamics,” *Rev. Mod. Phys. 57, 827 (1985).*

[111] Philipp Kahl, “Identification of long-range solid-like correlations in liquids and role of the interaction fluid-substrate,” 2016.

[112] S. Granick, Y. Zhu & H. Lee, “Slippery questions about complex fluids flowing past solids,” *Nature Materials Vol. 2, pages 221-227 (2003).*

[113] L Noirez and P Baroni, “Wall Effects induced by Ceramic in Quiescent Liquids,” *J. Phys.: Conf. Ser. 790 012024 (2017).*

[114] Michael Vollmer, Klaus-Peter Möllmann, Infrared Thermal Imaging: Fundamentals, Research and Applications, John Wiley & Sons, 2017.

[115] Planck, M. , The Theory of Heat Radiation. Translated by Masius, M. (2nd ed.)., P. Blakiston's Son & Co., 1914.

[116] Wien, W., “On the division of energy in the emission-spectrum of a black body,” *Philosophical Magazine. Series 5. 43 (262): 214–220 (1897).*

[117] “https://webbook.nist.gov/cgi/cbook.cgi?ID=C56815&Type=IR-SPEC&Index=1”.

[118] “https://webbook.nist.gov/cgi/cbook.cgi?ID=C57556&Type=IR-SPEC&Index=1”.

[119] R Kubo , “The fluctuation-dissipation theorem,” *1966 Rep. Prog. Phys. 29 255.*

[120] T. Kume, M. Daimon, S. Sasaki, and H. Shimizu, “High-pressure elastic properties of liquid and solid ammonia,” *Phys. Rev. B 57, 13347 (1998).*

[121] E. L. Gromnitskaya et al., *Phys. Chem. Chem. Phys., 2019,21, 2665-2672.*

[122] Franco-Gómez, A., Onuki, H., Yokoyama, Y. et al., “Effect of liquid elasticity on the behaviour of high-speed focused jets,” *Exp Fluids 62, 41 (2021).*

[123] R. M. Power et al., “The transition from liquid to solid-like behaviour in ultrahigh viscosity aerosol particles,” *Chem. Sci., 2013,4, 2597-2604.*

[124] M. A. Biot, “Theory of Propagation of Elastic Waves in a Fluid-Saturated Porous Solid. II. Higher Frequency Range,” *The Journal of the Acoustical Society of America 28, 179 (1956).*

[125] P. Lv, et al., “Measurement of viscosity of liquid in micro-crevice,” *Flow Measurement and Instrumentation 46 (2015) 72–79..*

[126] Yahsi U., Coskun B., Yumak A., Boubaker K., Tav C., “Relaxation time of polypropylene glycol and polypropylene glycol dimethylether-like polymers in terms of fluid-phase

temperature and pressure dependent hole fraction," *European Polymer Journal, 68 226 (2015).*

[127] Gustavo A. Schwartz, et al., "Relaxation dynamics of a polymer in a 2D confinement," *J. Chem. Phys. 120, 5736 (2004).*

[128] J. R. T. Seddon, et al., "A deliberation on nanobubbles at surfaces and in bulk," *ChemPhysChem, 13:2179, 2012.*

[129] K. Lum, D. Chandler, and J. D. Weeks, "Hydrophobicity at small and large length scales," *J. Phys. Chem. B, 103(22):4570, 1999.*

[130] Nicholas W. Tschoegl, The Phenomenological Theory of Linear Viscoelastic Behavior, Springer-Verlag Berlin Heidelberg, 1989.

[131] Basic Elasticity and Viscoelasticity, Princeton University Press.

[132] Jiho Choi, Florian Nettesheim, and Simon A. , "The unification of disparate rheological measures in oscillatory shearing," *Phys. Fluids 31, 073107 (2019).*

[133] Manfred Wilhelm et al., "Fourier-transform rheology," *Rheol Acta 37:399–405 (1998).*

[134] Manfred Wilhelm et al., "High sensitivity Fourier-transform rheology," *Rheol Acta 38: 349±356 (1999).*

[135] Randy H. Ewoldt, et al., "Experimental Challenges of Shear Rheology: How to Avoid Bad Data," *Complex Fluids in Biological Systems pp 207-241 (2014).*

[136] Peter C. Sukanek Robert L. Laurence, "An experimental investigation of viscous heating in some simple shear flows," *20, 3, 474-484 (1974).*

[137] P.C. Sukanek, R.L. Laurence , "An Experimental Investigation of Viscous Heating in Some Simple Shear Flows," *AlChE J. 20 (1974).*

[138] Winter HH. , "Viscous dissipation in shear flows of molten polymers," *Advances in Heat Transfer;13:205–67 (1977)..*

[139] C. J. Pipe et al., "High shear rate viscometry," *Rheol Acta (2008) 47:621–642.*

[140] A. J. Giacomin, et al., "Viscous heating in large-amplitude oscillatory shear flow," *Phys. Fluids 24, 103101 (2012).*

[141] Munier, R., Doudard, C., Calloch, S., Weber, B., "Determination of high cycle fatigue properties of a wide range of steelsheet grades from self-heating measurement.," *Inter. J. Fatigue, 63, 46-61 (2014)..*

[142] Boley, B. A. and Weiner, J. H., "Theory of Thermal Stresses," *(1960), John Wiley, London.*

[143] W. H. J. a. Y. A. S. S. Q. Zhou, “Nonlinear bulk acoustic waves in anisotropic solids: Propagation, generation and reflection,” *J. Appl. Phys., vol. 78, pp. 39–46, 1995.*

[144] Wenhua Jiang; Wenwu Cao, “Second harmonic generation of shear waves in crystals,” *IEEE Transactions on Ultrasonics,Ferroelectrics, and Frequency Control, 51, 2, 2004.*

[145] Muhammad Hassani et al., “Long-range strain correlations in 3D quiescent glass forming liquids,” *2018 EPL 124 18003.*

[146] Scarponi F., Comez L., Fioretto D., and Palmieri L, “Brillouin light scattering from transverse and longitudinal acoustic waves in glycerol,,” *Phys. Rev. B 2004, 70, 054203..*

[147] A. Anopchenko, et al., “Dielectric study of the antiplasticization of trehalose by glycerol,” *Phys. Rev. E 74, 031501 (2006).*

[148] L. Korson, et al., “Viscosity of water at various temperatures,” *J. Phys. Chem. 1969, 73, 1, 34–39 .*

[149] Udo Kaatze, “Reference liquids for the calibration of dielectric sensors and measurement instruments,” *2007 Meas. Sci. Technol. 18 967.*

[150] P. Baroni, P. Bouchet, and L. Noirez, “Highlighting a Cooling Regime in Liquids under Submillimeter Flows,” *J. Phys. Chem. Lett. 2013, 4, 12, 2026–2029.*

[151] B. P. Tighe, “Shear dilatancy in marginal solids,” *Granular Matter. 16:203–208 (2014).*

[152] Karsten Baumgarten and Brian P. Tighe, “Normal Stresses, Contraction, and Stiffening in Sheared Elastic Networks,” *Phys. Rev. Let.t 120, 148004 (2018).*

[153] J. Poynting, “On pressure perpendicular to the shear planes in finite pure shears , and on the lengthening of loaded wires when twisted,” *Proc. R. Soc. A 82, 546 (1909)..*

[154] Janmey, P., McCormick, M., Rammensee, S. et al., “Negative normal stress in semiflexible biopolymer gels,” *Nature Mater 6, 48–51 (2007).*

[155] A. Pommella, L. Cipelletti, and L. Ramos, “Role of Normal Stress in the Creep Dynamics and Failure of a Biopolymer Gel,” *Phys. Rev. Lett. 125, 268006 (2020).*

[156] Xianzhong Xu, Jinping Hou, “A stress relaxation model for the viscoelastic solids based on the steady-state creep equation,” *Mechanics of Time-Dependent Materials 15(1):29-39 (2010).*

[157] T.M. Junisbekov et al., "Stress Relaxation in Viscoelastic Materials" (2003), Science Publishers.

[158] Zhang, H., Lamnawar, K., Maazouz, A. et al. , “Experimental considerations on the step shear strain in polymer melts: sources of error and windows of confidence,” *Rheol Acta 54, 121–138 (2015).*

[159] M.T. Thompson, “Chapter 2 - Review of Signal Processing Basics,” *Intuitive Analog Circuit Design. Elsevier (2014).*

[160] Nicolae Lobontiu, System Dynamics for Engineering Students,, Pages 151-203, Elsevier (2010).

[161] Mark A.Haidekker, Linear Feedback Controls The Essentials, Pages 27-56, Elsevier (2013).

[162] W. Bolton, “Control Systems,” *Elsevier (2002).*

[163] D. C. Johnston, “Stretched exponential relaxation arising from a continuous sum of exponential decays,” *Phys. Rev. B 74, 184430 (2006).*

[164] B. Cui, R. Milkus, A. Zaccone, “The relation between stretched-exponential relaxation and the vibrational density of states in glassy disordered systems,” *Phys. Lett. A 381, 446–451 (2017).*

[165] A. Zaccone, “Relaxation and vibrational properties in metal alloys and other disordered systems,” *J. Phys.: Cond. Matter 32, 203001 (2020).*

[166] O. L. Anderson, “The Grüneisen Parameter for the Last 30 Years,” *Geophys. J. Int. 143, 279 (2000).*

[167] L. Knopoff and J. N. Shapiro, “Pseudo-Grüneisen Parameter for Liquids,” *Phys. Rev. B 1, 3893 (1970)..*

[168] Prasannarao Dontula, et al., “Does the Viscosity of Glycerin Fall at High Shear Rates?,” *Ind. Eng. Chem. Res., 38, 1729-1735 (1999).*

[169] Winter HH. , “Viscous dissipation in shear flows of molten polymers,” *Advancesin Heat Transfer;13:205–67 (1977)..*

[170] M. S. Yeganeh, S. M. Dougal, and H. S. Pink, “Vibrational Spectroscopy of Water at Liquid/Solid Interfaces: Crossing the Isoelectric Point of a Solid Surface,” *Phys. Rev. Lett. 83, 1179 (1999).*

[171] Toney, M., Howard, J., Richer, J. et al., “Voltage-dependent ordering of water molecules at an electrode–electrolyte interface,” *Nature 368, 444–446 (1994).*

[172] L. Noirez, P. Baroni, and J. F. Bardeau, *Appl. Phys. Lett. 110, 213904 (2017).*

[173] Razeghi M., Phonons and Thermal Properties. In: Fundamentals of Solid State Engineering., Springer, Cham., 2019.

[174] Persson, Kristin, “Materials Data on Al2O3 (SG:167) by Materials Project. Computed materials data using density functional theory calculations. These calculations determine the electronic structure of bulk materials by solving approximations to the Schrodinger equation. For,” doi: 10.17188/1187823, 2014. [Online]. Available: https://materialsproject.org/materials/mp-1143/.

[175] Böer, Karl W., Pohl, Udo, Semiconductor Physics, Springer International Publishing, 2018.

[176] T. Scopigno et al. , "Phonon-like and single-particle dynamics in liquid lithium," *2000 EPL 50 189.*

[177] S. Wang, and L. Zhu, "Non-resonant inelastic X-ray scattering spectroscopy: A momentum probe to detect the electronic structures of atoms and molecules," *Matter Radiat. Extremes 5, 054201 (2020).*

[178] E. Burkel, "Phonon spectroscopy by inelastic x-ray scattering," *Rep. Prog. Phys. 63 171 (2000).*

[179] J-P. Rueff, "An Introduction to Inelastic X-Ray Scattering," *Magnetism and Synchrotron Radiation pp 263-277 (2010).*

[180] Baron A.Q.R., "High-Resolution Inelastic X-Ray Scattering II: Scattering Theory, Harmonic Phonons, and Calculations.," *In: Jaeschke E., Khan S., Schneider J., Hastings J. (eds) Synchrotron Light Sources and Free-Electron Lasers. Springer, Cham. (2016).*

[181] K Hämäläinen and S Manninen , *2001 J. Phys.: Condens. Matter 13 7539.*

[182] W. Schulke, "Electron Dynamics by Inelastic X-Ray Scattering," *(Oxford University Press, 2007).*

[183] Platzman P M , "Elementary Excitations in Solids, Molecules and Atoms Part A ed J T Devreese et al," *(Nato Advanced Study Institute Series (Series B Physics)) (New York: Plenum) (1974).*

[184] J.-P. Rueff, et al., "The galaxies beamline at soleil synchrotron: Inelastic x-ray scattering and photoelectron spectroscopy in the hard x-ray range," *J. Synchrotron Rad. 22, 175 (2015).*

[185] Ablett, J. M., et al., *J. Synchrotron Rad. 26, 263-271. (2019).*

[186] Chengyu He et al., "Effect of crystal orientation on droplet wetting behavior on single-crystal Al2O3 substrates: An experimental study," *Phys. Fluids 32, 127110 (2020).*

[187] Fernando Bresme et al., "Water Polarization under Thermal Gradients," *Phys. Rev. Lett. 101, 020602 (2008).*

[188] Duan Huantao et al, "Characterization of GaN grown on 4H-SiC and sapphire by Raman spectroscopy and high resolution XRD," *2009 J. Semicond. 30 073001.*

[189] Kume, E., Noirez, L., "Identification of Mechanical-stimuli Thermal Response in Mesoscopic Liquids: from Harmonic to non-Harmonic Thermal Wave.," *J. Phys. Chem. B 2021, 125, 30, 8652–8658..*

[190] Eni Kume, Alessio Zaccone, Laurence Noirez. , "Unexpected thermo-elastic effects in liquid glycerol by mechanical deformation.," *Physics of Fluids 33, 072007 (2021)..*

[191] Kume, E., Baroni, P. & Noirez, L. , “Strain-induced violation of temperature uniformity in mesoscale liquids.,” *Sci Rep 10, 13340 (2020)..*

[192] Leo H O Hellström et al. , *2015 Meas. Sci. Technol. 26 015301.*

[193] Clasen, C. , “A self-aligning parallel plate (SAPP) fixture for tribology and high shear rheometry,” *Rheol Acta 52, 191–200 (2013).*

[194] Efrén Andablo-Reyes, et al., “A method for the estimation of the film thickness and plate tilt angle in thin film misaligned plate–plate rheometry,” *J. Non-Newtonian Fluid Mech. 165 (2010) 1419–1421.*

[195] Kunt Atalık, Roland Keunings, “On the occurrence of even harmonics in the shear stress response of viscoelastic fluids in large amplitude oscillatory shear,” *J. Non-Newtonian Fluid Mech. 122 (2004) 107–116.*

[196] Shah H. Khan et al., “Dynamic Solidification in Nanoconfined Water Films,” *Phys. Rev. Lett. 105, 106101 (2010).*

[197] Shivprasad Patil et al., “Solid or Liquid? Solidification of a Nanoconfined Liquid under Nonequilibrium Conditions,” *Langmuir 2006, 22, 15, 6485–6488.*

[198] Kazuhide Ueno et al., “Resonance shear measurement of nanoconfined ionic liquids,” *Phys. Chem. Chem. Phys., 2010, 12, 4066-4071.*

[199] Ingo F. C. Naue et al., “High sensitivity measurements of normal force under large amplitude oscillatory shear,” *Rheologica Acta volume 57, pages757–770 (2018).*

[200] T. B. Liverpool and F. C. MacKintosh, “Inertial Effects in the Response of Viscous and Viscoelastic Fluids,” *Phys. Rev. Lett. 95, 208303 (2005).*

[201] Tarc´ısio N. Teles, et al., “Temperature inversion in long-range interacting systems,” *Phys. Rev. E 92, 020101(R) (2015).*

[202] Shamik Gupta and Lapo Casetti, “Surprises from quenches in long-range-interacting systems: temperature inversion and cooling,” *New J. Phys. 18 (2016) 103051.*

[203] Lapo Casetti and Shamik Gupta, “Velocity filtration and temperature inversion in a system with long-range interactions,” *Eur. Phys. J. B (2014) 87: 91.*

université PARIS-SACLAY

ÉCOLE DOCTORALE
Physique en l'Île-de-France (PIF)

Titre : Mise en évidence de l'effet thermoélastique induit par déformation de cisaillement dans les liquides mésoscopiques

Mots clés : liquides confinés, élasticité de cisaillement, couplage thermomécanique, ondes thermiques, loi d'échelle

Résumé : La compréhension approfondie des liquides constitue un grand défi. Leur dynamique moléculaire rapide conduit à l'incapacité de supporter les ondes transversales (cisaillement) de basses fréquences qui se dissipent dans le milieu. Cependant, des rapports expérimentaux et théoriques récents semblent s'opposer à cette notion et mettent en évidence une élasticité de cisaillement finie dans les liquides à l'échelle mésoscopique. Dans le cadre de cette élasticité de cisaillement, nous étudions la réponse thermique à une déformation en cisaillement. Les liquides sont confinés à des épaisseurs variantes entre 100 et 1000 µm entre des surfaces à haute énergie et sollicités dans une gamme de fréquences de 0,5 à 5 rad/s (0,08 à 0,8 Hz). Nous montrons que l'onde de cisaillement génère des ondes thermiques froides et chaudes quasi instantanées et réversibles dont l'amplitude et la forme sont modulées par la déformation de cisaillement, conduisant à la génération d'un signal thermique non linéaire (harmoniques) à grande amplitude ou fréquence. Nous mettons également en évidence une relaxation thermique exponentielle étirée lors de la déformation-échelle ainsi qu'une dépendance d'échelle similaire à celle de l'élasticité de cisaillement. Les effets thermiques observés indiquent que les liquides mésoscopiques sont capables de convertir l'énergie de cisaillement mécanique dans des états thermodynamiques non uniformes, et sont donc dotés de thermoélasticité, une propriété identifiée jusqu'à présent dans les solides. Enfin, dans le cadre de l'étude dynamique de l'interface solide-liquide, nous révélons par diffusion inélastique de rayons X, l'impact du mouillage sur la dynamique de surface solide.

Title : Highlighting strain-induced thermoelastic effect in mesoscopic liquids

Keywords : confined liquids, shear elasticity, thermo-mechanical coupling, thermal waves, scale dependence

Abstract : In depth understanding of liquids stand as a great challenge. Their fast molecular dynamics lead to inability of supporting transverse (shear) waves, which energy should dissipate in a liquid medium. However, recent experimental and theoretical reports argue against this notion and highlight finite shear elasticity in mesoscale (semi-confined) liquids. In the frame of finite shear elasticity in mesoscopic liquids, we probe the thermal response under mechanical oscillatory shear excitation within the conventional viscous regime for a frequency range of 0.5 – 5 rad/s (0.08 – 0.8 Hz). The studied liquids (glycerol, polypropylene glycol and water) are confined between high-energy surfaces with thickness gap varying between 100 – 1000µm. We show that the applied shear strain generates nearly instant and reversible (hot and cold) thermal waves, whose amplitude and shape are linearly modulated by the shear strain at moderate shear strain and frequency, while leading to the generation of a non-linear thermal signal (harmonics) at large amplitude or larger frequency. We also examine the stability of the thermal equilibrium while the liquid is submitted to a sudden step shear strain. We evidence fast thermal changes reaching +0.04°C and -0.04°C amplitude that relax following a stretched-exponential while keeping the global temperature unchanged. Finally, we highlight a scale dependence of the thermal wave similar to that of the shear elasticity. The observed thermal effects indicate that mesoscopic liquids are able to convert (partly) the mechanical shear energy in non-uniform and non-equilibrium thermodynamic states, thus are endowed with thermoelasticity, a property so far identified in solids. Finally, in the frame of the dynamic study of the solid-liquid interface, we reveal via inelastic x-ray scattering, the impact of wetting on the solid surface dynamics.